THE DYNAMIC BEHAVIOR OF TRANSFORMER CORES

A Thesis

Presented to the Faculty of Graduate Studies and Research

University of Manitoba

In partial fulfillment of the requirements for the degree

MASTER OF SCIENCE IN ELECTRICAL ENGINEERING

---

by

John Douglas Poustie

May , 1970

ABSTRACT

This investigation was concerned initially with comparing the dynamic, or time varying, behaviour of two very different transformer cores. The various electrical characteristics of a core-winding assembly sometimes used as a "current transformer", and known as a bushing type C.T., were compared with the responses of a modified core and coil assembly taken from a power distribution transformer.

The relevant measurement techniques were thoroughly analyzed and are shown in the Appendix.

It was demonstrated that binomial equations; in one case a quintic, in the other a septic; are a fairly good representation for the average of the flux density vs magnetic field intensity, or B-H, characteristics. For certain situations, the average of the B-H curve may be represented by three segment straight line approximations.

The availability of a reliable two term equation is potentially very useful in harmonic or ferroresonant studies. Recent work has indicated that, for the investigation of the latter, loss representation is not of prime importance to the transformer model.

Using the binomial equations to model the core characteristics, the relationship between applied RMS voltage and resulting RMS current was developed.

A second prime concern of this investigation was the attempt to demonstrate that, for a series circuit containing linear resistance and capacitance as well as non-linear inductance, the analytical prediction of various aspects of ferroresonant behaviour was relatively straightforward

if the above binomial approximations are used, and that the agreement with test results was quite reasonable. Certain generalizations were made in regard to the "incremental describing function" for an odd powered polynomial relationship between current and flux linkages.

Finally, the excitation of the second and third subharmonics was accomplished and recorded, although no mathematical analysis was attempted in this area.

ACKNOWLEDGEMENT

The author wishes to thank Dr. G. W. Swift for suggesting the topic, arranging financial assistance through the National Research Council of Canada, and for his helpful suggestions during work on this thesis.

In addition, the help obtained from E. A. Dillon of Pioneer Electric Co. to obtain suitable core and coil samples is much appreciated.

John Poustie, B.Sc.(E.E.)

TABLE OF CONTENTS

CHAPTER CONTENTS PAGE

CONTENTS

LIST OF ILLUSTRATIONS

ILLUSTRATIONS

ILLUSTRATIONS

INTRODUCTION

The first real objective of this thesis, which is an offshoot of the Doctoral Dissertation presented to Illinois Institute of Technology by G. W. Swift, was to obtain accurate flux density vs magnetic field intensity curves. These curves, also called B-H curves, were obtained by operational simplifier techniques and allow several electrical characteristics to be deduced regarding the sample, if frequency, flux density and time of switching are the experimental variables. Of most interest was the binomial equation, $i = C_1 \ell + C_n \ell^n$ which was proposed as the arithmetic average of the ℓ/i relationship, which is directly proportional to the B/H relationship.

In the previously mentioned Ph.D. thesis, the equation:

$$i = \ell + 4\ell^5$$

was presented as the per unit binomial best fitting the core and coils of a 5 kva distribution transformer manufactured by the Commonwealth Edison Co. of Chicago. Although the details of the core's construction were not known to the present author, it was of interest to compare the same results to the two cores of this thesis, for which constructional details were known.

It was also of interest to derive the theoretical "magnetization curve", that is, the I(RMS) vs E(RMS) relationship, using the binomial i/ℓ equation as the starting point, and then to compare the results with the actual magnetization test on the same core. Since agreement was not too close, presumably due to the inadequate modelling of iron losses, no

attempt was made to obtain the i/ℓ curve from the actual magnetization test results. The latter procedure would have been very useful, since to date, transformer manufacturers are not obliged to furnish B-H curves, but normally provide the magnetization data obtained from the acceptance tests.

While examining the ferroresonant response of a series R-L-C circuit, the author was able to measure the second and third subharmonics, and also became interested in the methods available for predicting ferroresonance analytically, and Chapter Seven represents an attempt to reconcile a mathematical prediction based on an approximate model to the measurements made on the circuit in the laboratory situation.

CHAPTER I

CONSTRUCTION OF CORE-COIL SAMPLES

The object of this Chapter is to compare physically the available test samples. The abbreviations C.T. and P.T. shall be used for "current transformers" and "power transformers" respectively.

Figure 1 gives physical details of the C.T. core, while in Figure 2, the P.T. is detailed.

Since the cores were available initially without windings, it was necessary to determine the number of turns to wind in order to accomplish further testing. In general, this is determined by applying the equation

$$E = \frac{4.44\, fN\, (B_m A_n)}{10^8}$$

where E = RMS voltage [usually called "rated" voltage],

f = frequency

N = number of turns (to be found)

B_m = peak flux density (to be chosen)

A_n = net steel cross sectional area.

If E is chosen, and since in this instance A_n is fixed, B_m is then chosen to restrict exciting current, as well as total core loss. Depending on steel type and treatment, and core construction, B_m may vary over a wide range.

For the C.T., E was chosen for convenience in testing to be 50 v RMS, and a figure of $B_m = 100$ kilolines/in^2 was thought to be

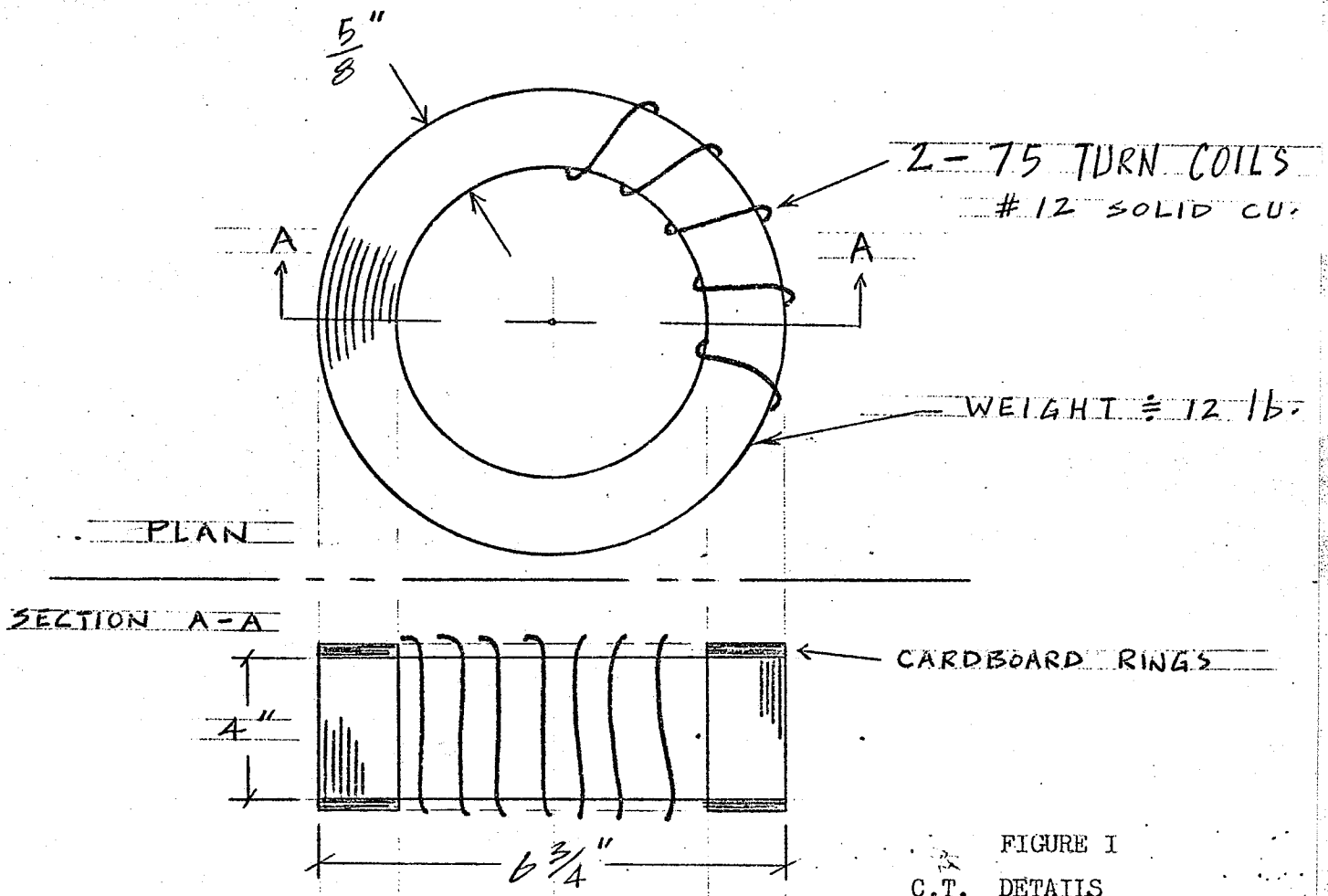

FIGURE 1
C.T. DETAILS

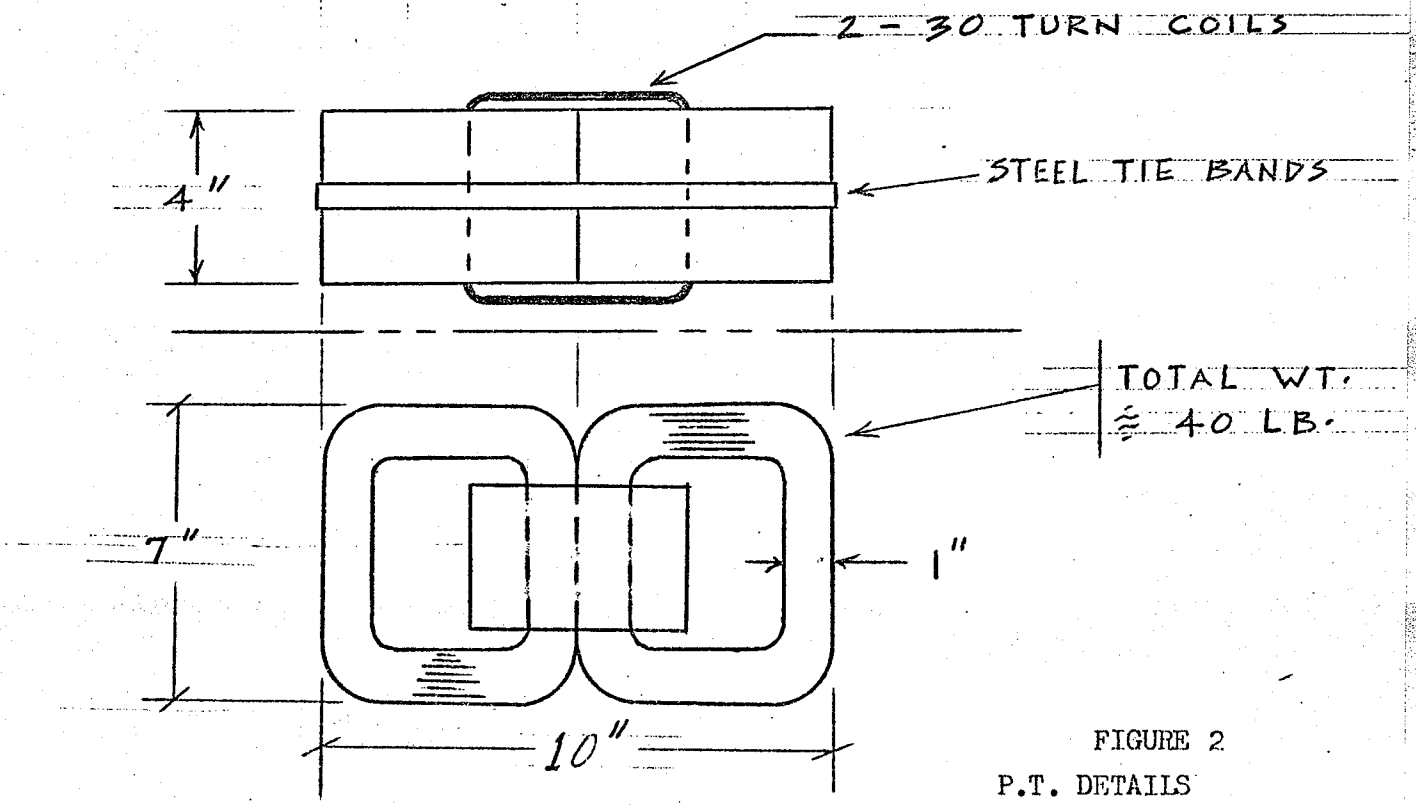

FIGURE 2
P.T. DETAILS

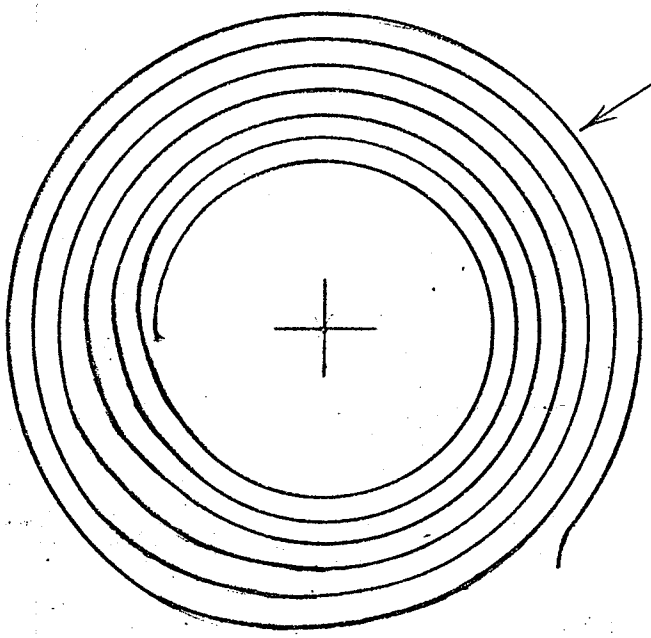

FIGURE 3
CT CORE CONSTRUCTION

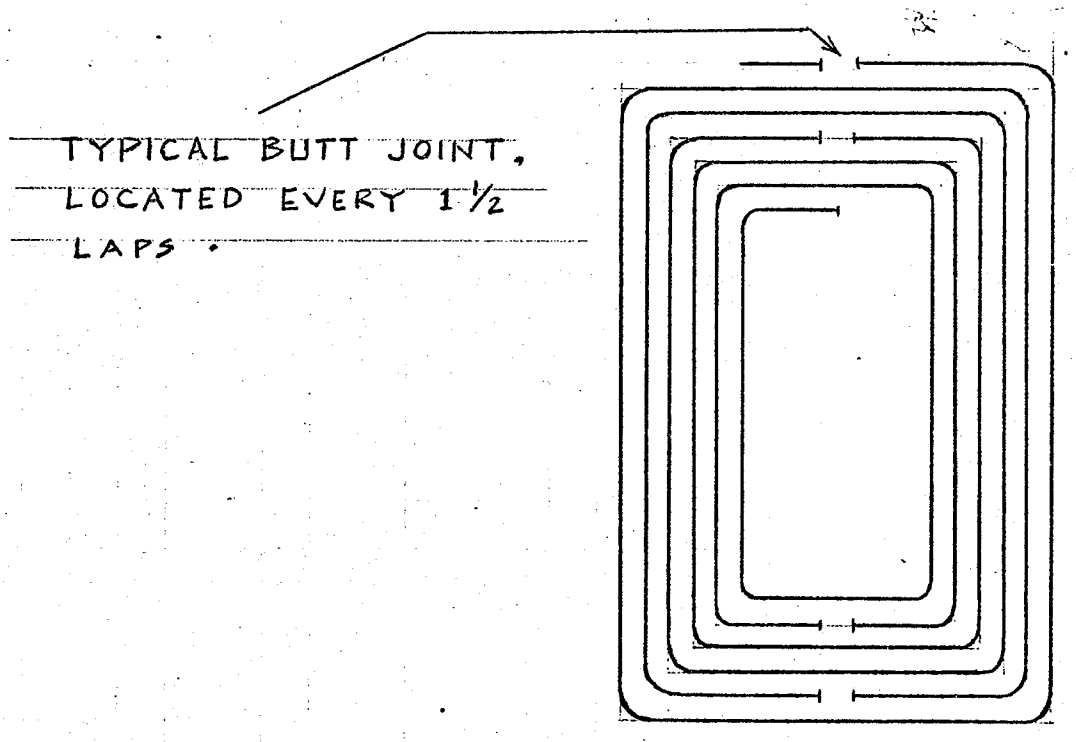

FIGURE 4
PT CORE CONSTRUCTION

satisfactory. This determined N = 75 turns. Two identical windings, of 75 turns and using #12 Heavy Formel solid copper were wound to allow the measurement of B-H curves, using an operational amplifier technique which will be explained later. The wire gauge was heavy enough to prevent winding overheating under all anticipated test conditions.

In the case of the P.T., E was also chosen to be 50 v RMS, while B_m = 83 kilolines/in^2 was used to restrict excitation current. Available test data on cores of similar construction indicated that excitation current would be much higher for the P.T. than for the C.T. core. Calculations indicated that 30 turns should be satisfactory, and two identical, 30 turn, #12 HF copper windings were wound as shown in Figure 2.

The material used in both cores was a modern, grain oriented transformer steel of approximately 11 mils thickness. The objective at this point was to emphasize differences in core cutting and assembly, rather than to discuss manufacturing specifications for the steel. To this end, Figures 3 and 4 illustrate core construction. It was felt that these samples represented extreme cases. The C.T. core could be said to approach the ideal, that is, fairly tightly wound on a machine, employing high grade steel, with no air gaps in the magnetic circuit, and no small radius bends in the steel. The P.T., on the other hand, which in this instance was salvaged, had air gaps (which tended to cause flux concentration) at 4 points on its periphery. It was assembled by hand onto the coil, and could have been mishandled, thus causing increased eddy current losses where interlayer insulation was scraped off, in addition to introducing metallic stresses which could not be relieved by "soaking" in a high temperature oven after the coil had been assembled on the core.

It is held by the author that the core of a large power transformer would lie in between the P.T. and the C.T. as far as the number and size of air gaps in the core, and relative amount of human handling goes.

This fact, then, might permit the application to large power transformers of some of the conclusions drawn in this thesis.

The author makes the presumption here of some prior knowledge of power transformer core assembly by his examiners.

CHAPTER II

RMS VOLTAGE AND CURRENT CHARACTERISTICS

The object of this Chapter is, at the same time as presenting comparative measurements of magnetization or open circuit data, including harmonic component determination, to examine the techniques used to obtain these characteristics.

Also, an attempt is made employing graphical analysis to show the influence of the shape of the B-H curve on the excitation current waveform.

Finally, an explanation for the shape of the actual magnetization curve is attempted, based on the B-H curve measurements to be presented in future chapters.

2.1 RMS responding meters.

Proper measurement of power frequency voltage and current was complicated by the following. While many types of meters, including Volt-Ohm Meters, Vacuum Tube Voltmeters, and moving iron instruments will read perfectly sinusoidal voltages accurately (assuming proper calibration), the source impedance may, in some instances, be sufficiently high to cause the terminal voltage to be distorted, expecially when currents flowing to the transformer on open circuit are not perfectly sinusoidal. Figure 5 depicts this circuit in a very general way, while Figure 6 shows what type of distortion could occur in the terminal voltage for an assumed current waveform. For an inductive source impedance, the harmonic distortion is intensified, since the current, the waveform of which is said to contain "harmonics", or higher frequency components, causes a relatively

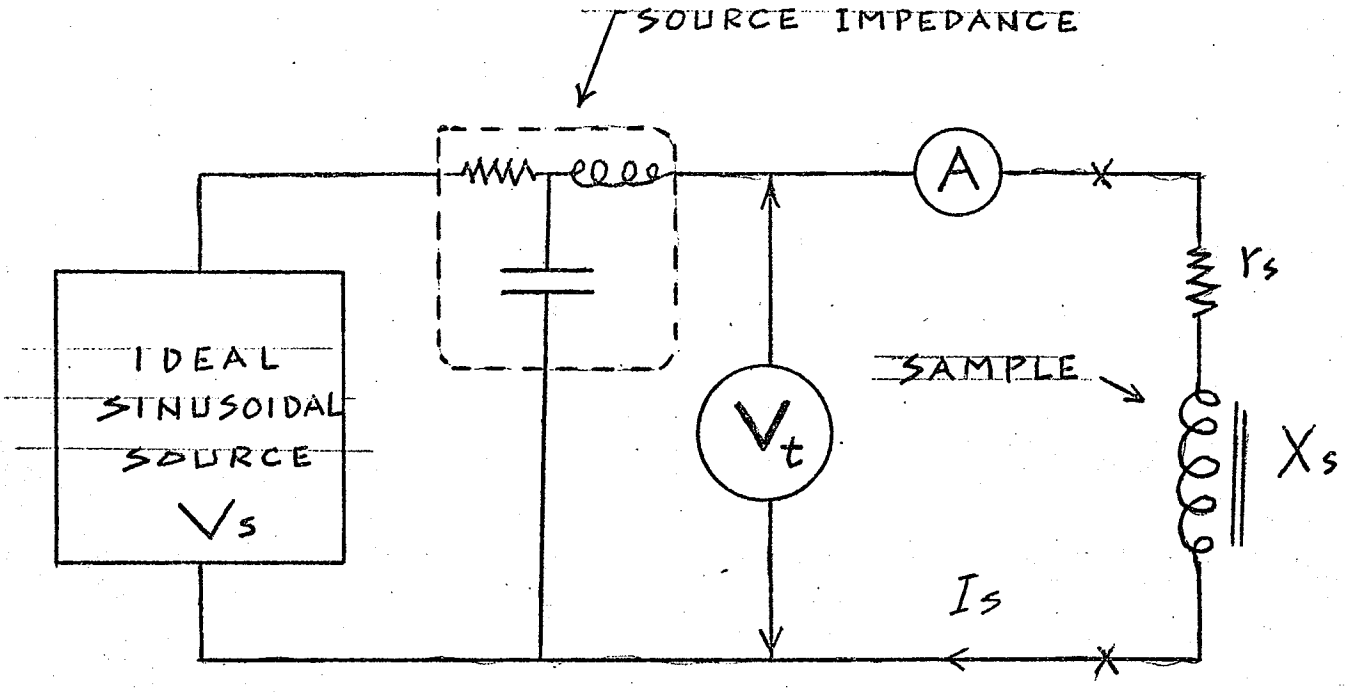

FIGURE 5

THE CIRCUIT USED TO MEASURE MAGNETIZATION CHARACTERISTICS

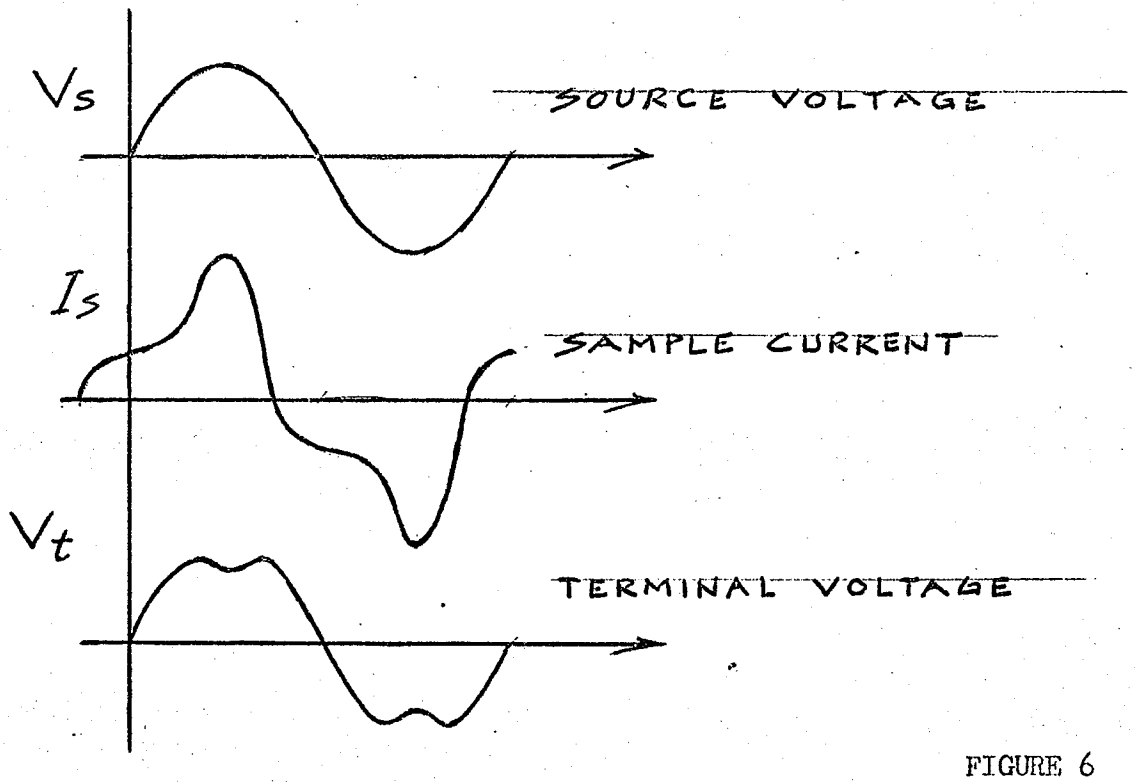

FIGURE 6

SHOWING POSSIBLE DISTORTION OF V_t & I_s

larger harmonic voltage drop across this same inductive source reactance. In transformer test installations, tooth ripple in the supply generator might cause unwanted (higher frequency) peaks in the test voltage.

It must be remembered that a VTVM, depending on the manufacturer, might respond either to the 0-peak or the peak-peak of a rectified sine wave. It is to be stressed that the VTVM is calibrated on a sinusoidal waveshape and will be in error for any distortion in the measured voltage. Similarly, a VOM will respond accurately to a sinusoidal voltage only; its movement being of the d'Arsonval type, fed from either a full wave or half wave rectifier unit.

In a meter having the moving iron type of construction, angular deflection is proportional to the square of the operating current and the rate of change of inductance with respect to angular deflection , so that calibration may be accomplished in terms of effective [RMS] voltage or current. According to Harris, "The waveform error of a modern instrument with short vanes is negligible for the third harmonic at power frequencies".

During the magnetization current measurements associated with this thesis, the author checked the applied voltage waveform with an oscilloscope to ensure that no distortion occurred. In this instance, the currents encountered were not larger than 3% of the source RMS current rating. Voltage magnitude was measured with a 75 volt range moving iron meter, while RMS currents were determined with a moving iron meter rated 1 amp RMS.

In a situation where source voltage distortion exists, the conversion of results back to an equivalent sine wave basis is exceedingly complicated. The interested reader is referred to Chapter II of reference # 3 in the bibliography .

2.2 Comparison of Magnetization Characteristics.

The characteristics are presented in Figure 7 A and 7 B . Certain similarities between the curves of 7 A deserve comments. Current increased with voltage, but not in a linear fashion, even for lower values of voltage. In both cases, as expected, $\Delta I/\Delta V$ becomes very large for larger voltages. On the other hand, the basic curve shapes are dissimilar, that is, the curves could not be superimposed in a per unit sense, even if different base quantities were chosen.

A transformer designer might point out that 83 kilolines per square inch was a poor choice for the design figure for the P.T., since the magnetization curve indicates that the core is into the saturation region at 50 volts RMS applied. The curve shows that 30 to 35 volts would have been a better choice for the "rating", now that the core is assembled. The C.T. design, however, worked out quite well for the assumptions made.

In Figure 8, tracings of the photographs of the actual current waveforms are shown. The large amount of distortion present in the C.T. current waveform is contrasted to the P.T. waveform at the chosen "rated" voltages.

It is to be stressed that the P.T. has, overall, a much more linear magnetization characteristic than does the C.T.

2.3 Harmonics in the Excitation Current.

It is of interest to analyze the excitation current waveform for both the C.T. and the P.T. The measurement technique used to accomplish this is analyzed in Appendix A. The results of these measurements are shown in Figure 9. The following calculations demonstrate the

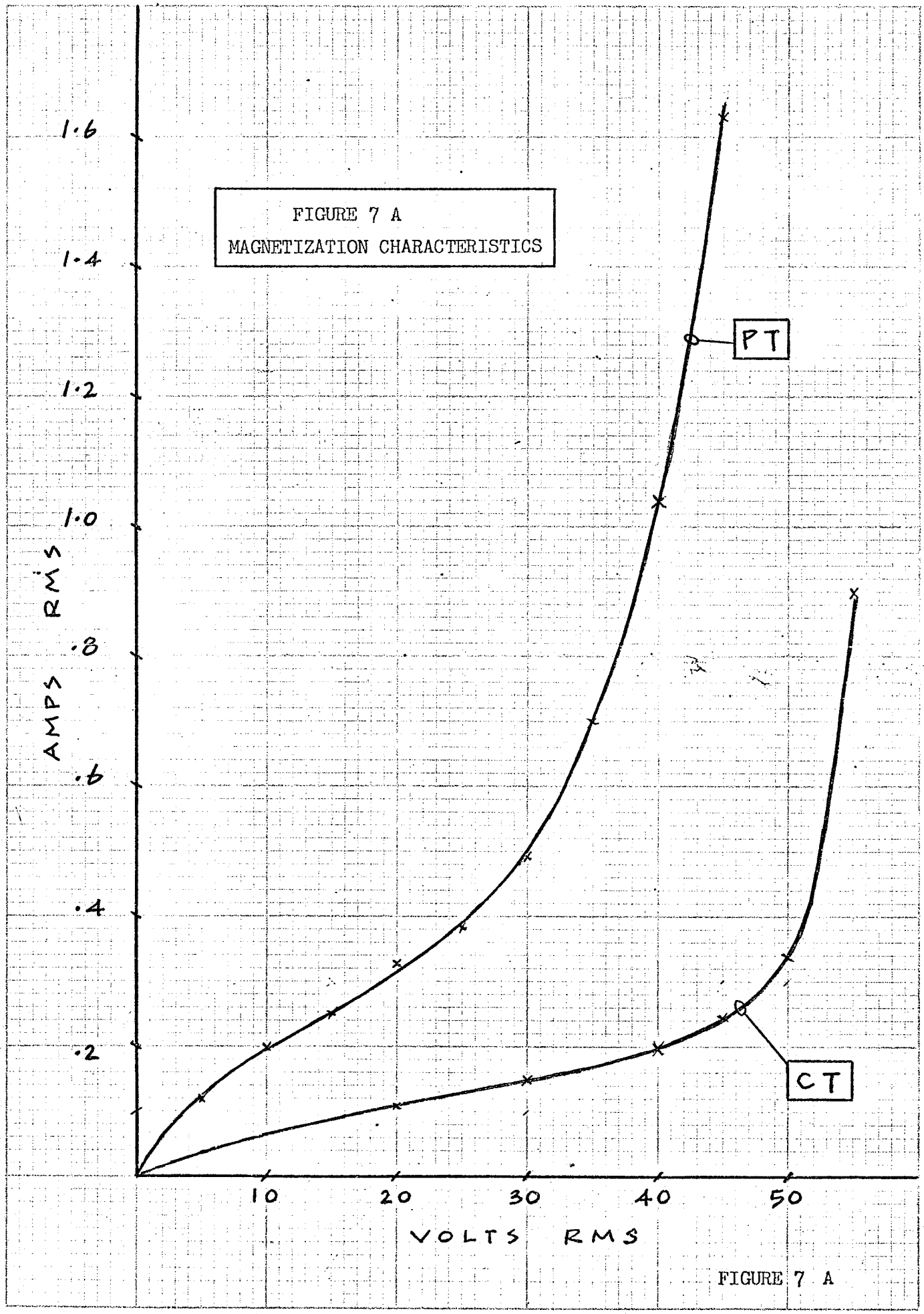
FIGURE 7 A
MAGNETIZATION CHARACTERISTICS
1.6
1.4
1.2
1.0
.8
.6
.4
.2
AMPS RMS
PT
CT
10
20
30
40
50
VOLTS RMS

FIGURE 7 A

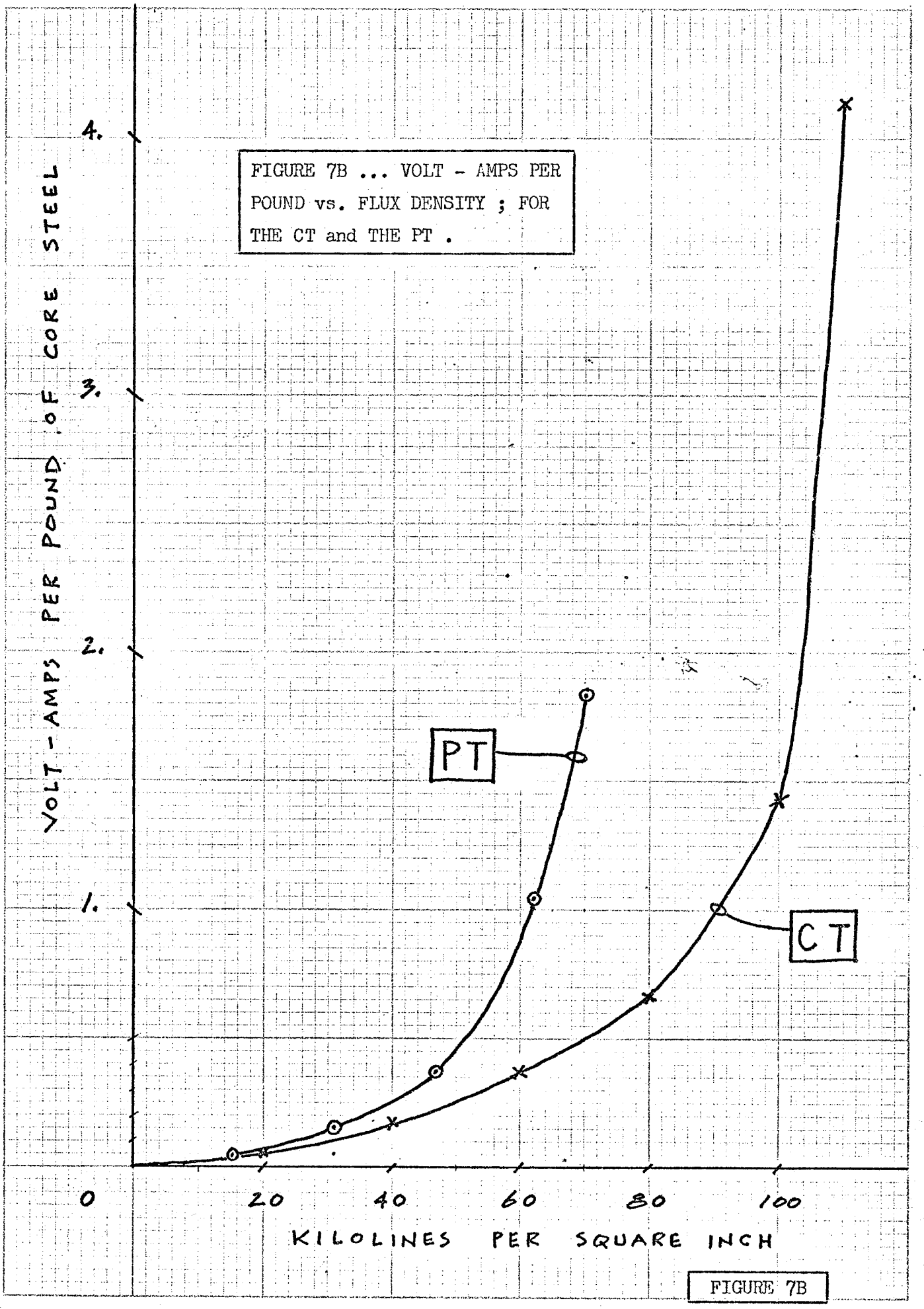
FIGURE 7B ... VOLT - AMPS PER POUND vs. FLUX DENSITY ; FOR THE CT and THE PT .
VOLT - AMPS PER POUND OF CORE STEEL
4.
3.
2.
1.
0
20
40
60
80
100
KILOLINES PER SQUARE INCH
PT
CT

FIGURE 7B

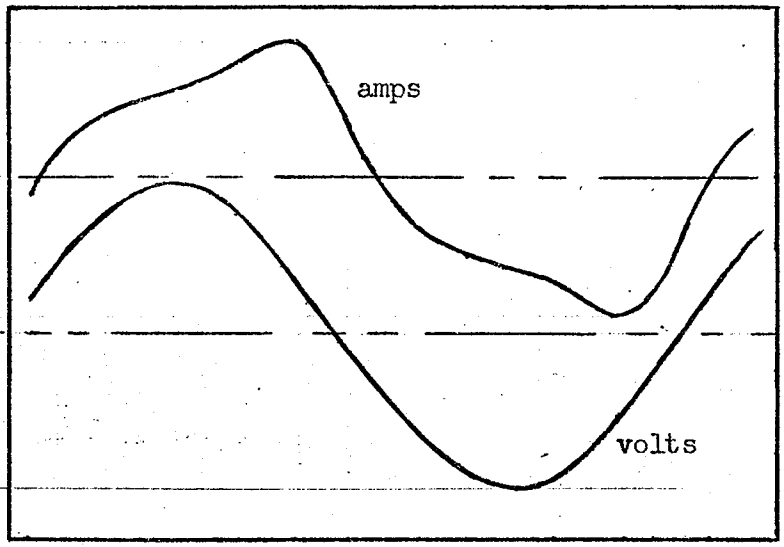

POWER
TRANSFORMER
(P.T.)

V = 30 (RMS)

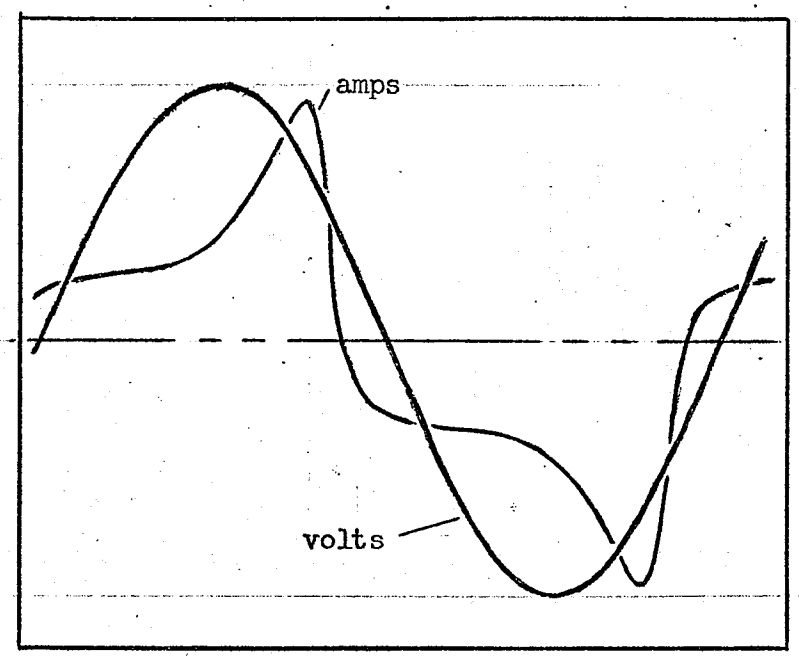

CURRENT
TRANSFORMER
(C.T.)

V = 50 (RMS)

TRACINGS OF VOLTAGE AND CURRENT WAVEFORMS FOR THE CT AND THE PT , UNDER OPEN CIRCUIT CONDITIONS

FIGURE 8
PHOTO TRACINGS

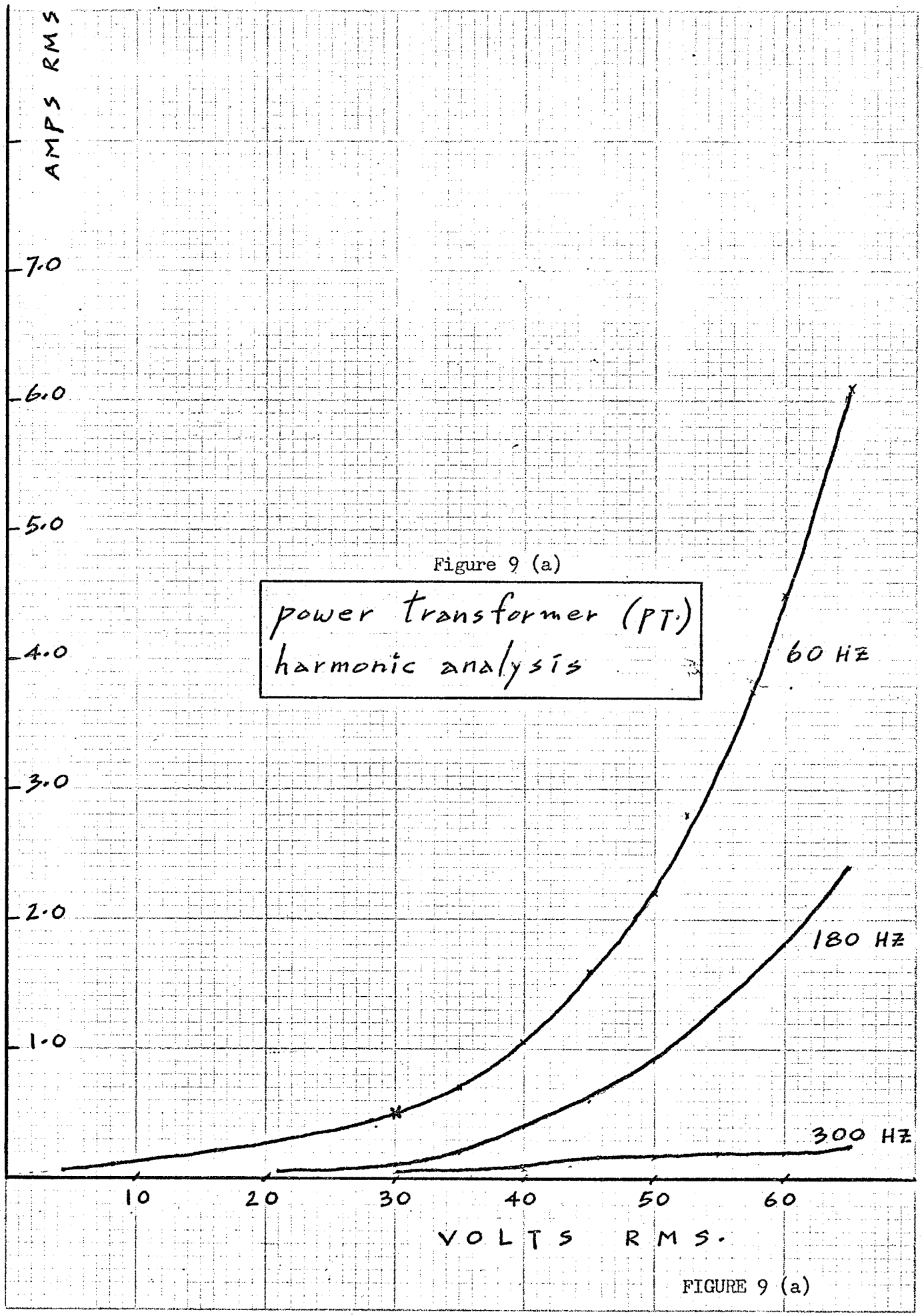

Figure 9 (a)

FIGURE 9 (a)

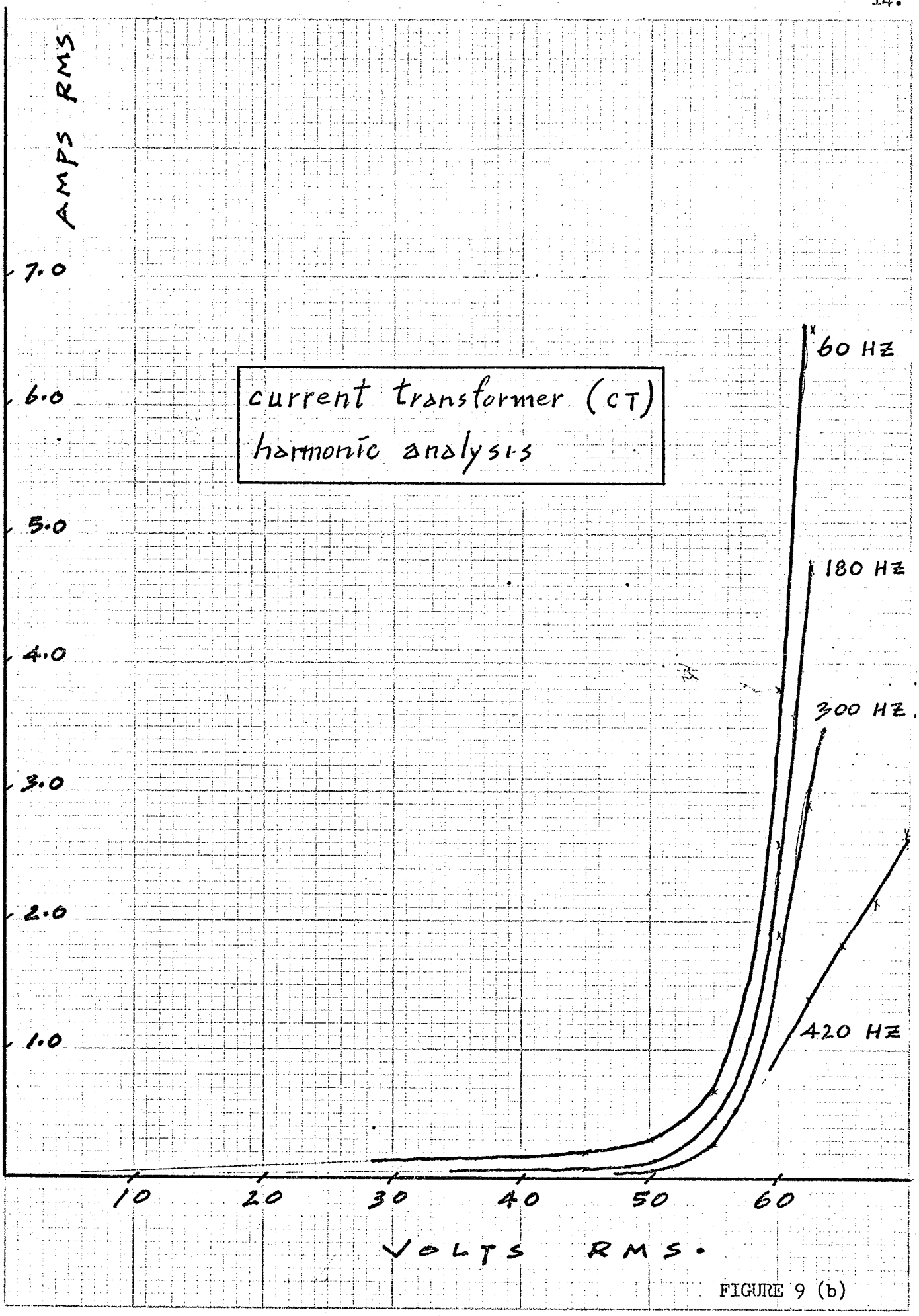
AMPS RMS
7.0
6.0
5.0
4.0
3.0
2.0
1.0
current transformer (CT)
harmonic analysis
60 HZ
180 HZ
300 HZ
420 HZ
10
20
30
40
50
60
VOLTS RMS.

FIGURE 9 (b)

excellent agreement between the two methods of measuring exciting current.

$$I_T = \sqrt{(I_1)^2 + (I_3)^2 + (I_5)^2}$$

where I_1, I_3, I_5 are the RMS values of the harmonic components, and I_T is the total RMS harmonic current. Seventh and higher harmonics are neglected. For the P.T., at 50 volts RMS:

$$I_T = \sqrt{(2.2)^2 + (.9)^2 + (.2)^2} = 2.39 \text{ amps.}$$

Direct measurement, that is, the magnetization curve, yielded $I_T = 2.45$ amps at this voltage, a 2.5% difference. For the C.T., at 50 volts RMS

$$I_T = \sqrt{(.3)^2 + (.12)^2 + (.05)^2} = .33 \text{ amps.}$$

Here direct measurement yielded .34 amps = I_T.

It is significant to note that, for the CT, at 50 volts, the third harmonic was 36% of the total current, while the fifth harmonic was 15% of the total.

But for the P.T., at 30 volts the third harmonic was 24% and the fifth harmonic 6% of the total current.

In other words, at voltages which would be "rated" values, based on the magnetization curves, the percent harmonics in the C.T. exciting current were higher than those in the P.T.

It is, perhaps, more meaningful to find percent harmonics at, say, 10% above the assigned rated value.

When the C.T. voltage was increased by 10%, total current rose

from .34 to .90 amps, a 165% increase, while the third harmonic increased to 55% and the fifth to 29% of the total.

When the P.T. voltage was raised 10%, total current rose from .5 to .6 amps, a 20% increase, while the third harmonic increased to 27% from 24% and the fifth to 7% from 6% of the total.

In other words, the C.T. core went into saturation much more rapidly than the P.T. core, for increasing voltages.

2.4 Relationship of Magnetization Current to the B-H curve - Graphical.

To derive the waveshape of the "magnetic field intensity" (H) when a sinusoidal flux (B) is caused to exist in a closed magnetic circuit by the application of a sinusoidal voltage, a graphical technique is employed. In Figure 10 is shown a "typical" B-H curve. Although its significance and methods of determination will be more fully discussed in later chapters, it must be stated at the outset that, in the sinusoidal steady state, a traverse is made around this curve on the boundary contour sketched, and in the direction shown by arrows.

Figure 11 indicates the waveform of H(t), which is directly proportional to the current flow to a coil on a transformer core, when the saturation effect is the only one represented by the BH curve.

Figure 12 shows the effect on the current of introducing the hysteresis effect, and Figure 13 shows the current when saturation, hysteresis, and eddy currents are all represented.

Also in Figure 13, the currents from Figures 11, 12 and 13 are superimposed to emphasize differences.

It may be noted that it is the hysteresis effect which introduced phase shift. Recent research by Swift has shown that eddy current effects

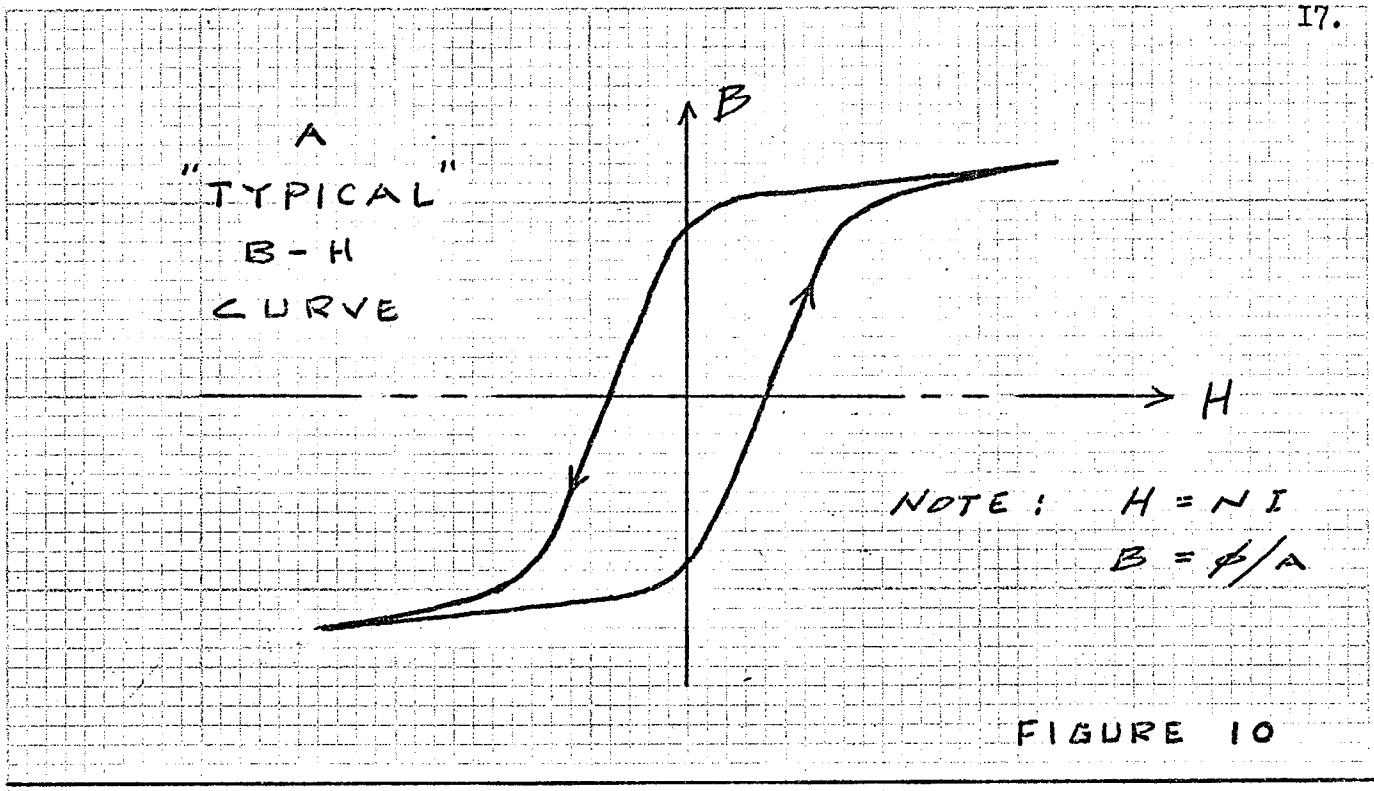

FIGURE 10

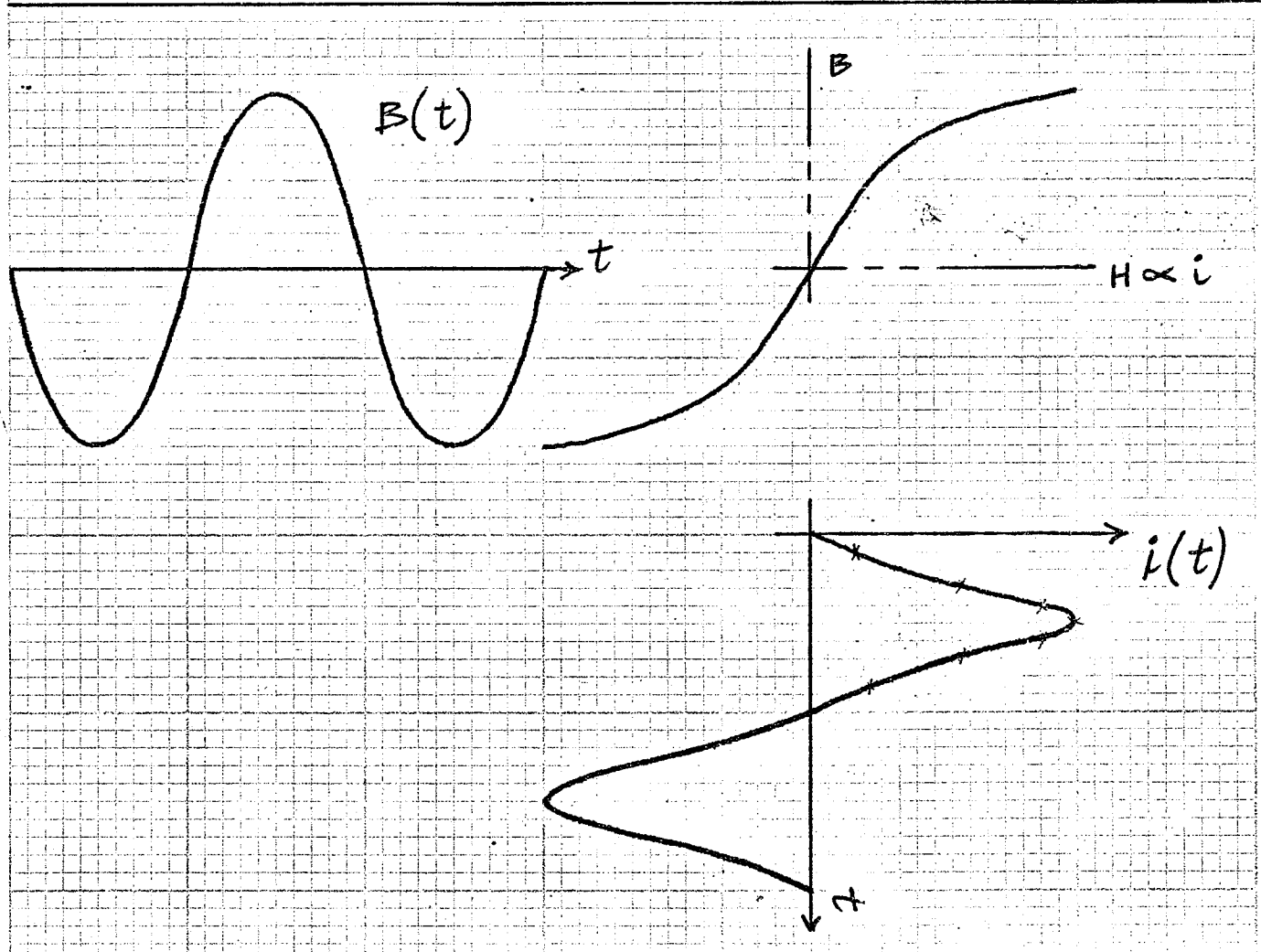

FIGURE 11
CURRENT RESULTING WHEN SATURATION ONLY IS REPRESENTED

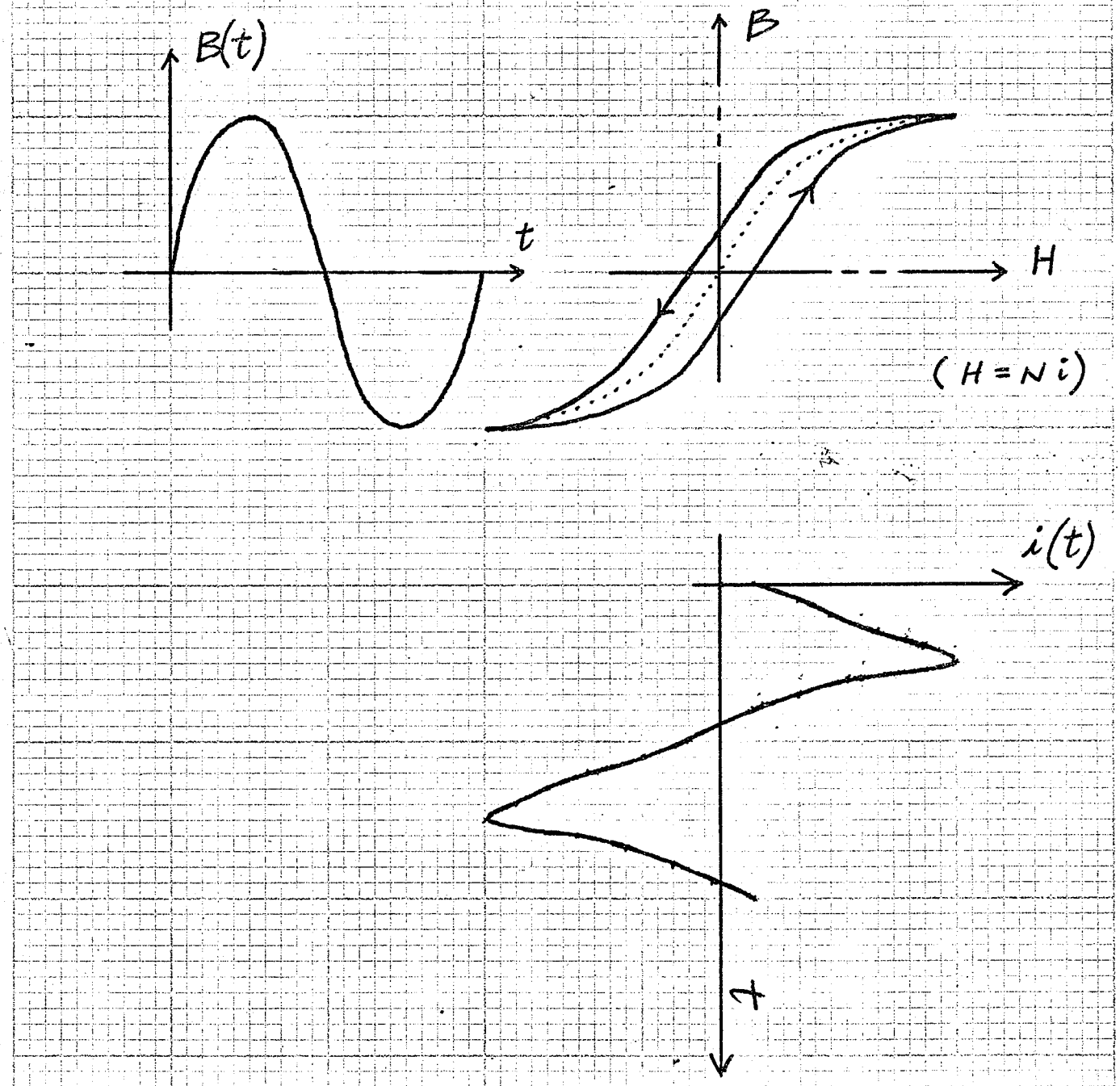

FIGURE 12
CURRENT RESULTING WHEN SATURATION AND HYSTERESIS ARE BOTH REPRESENTED.

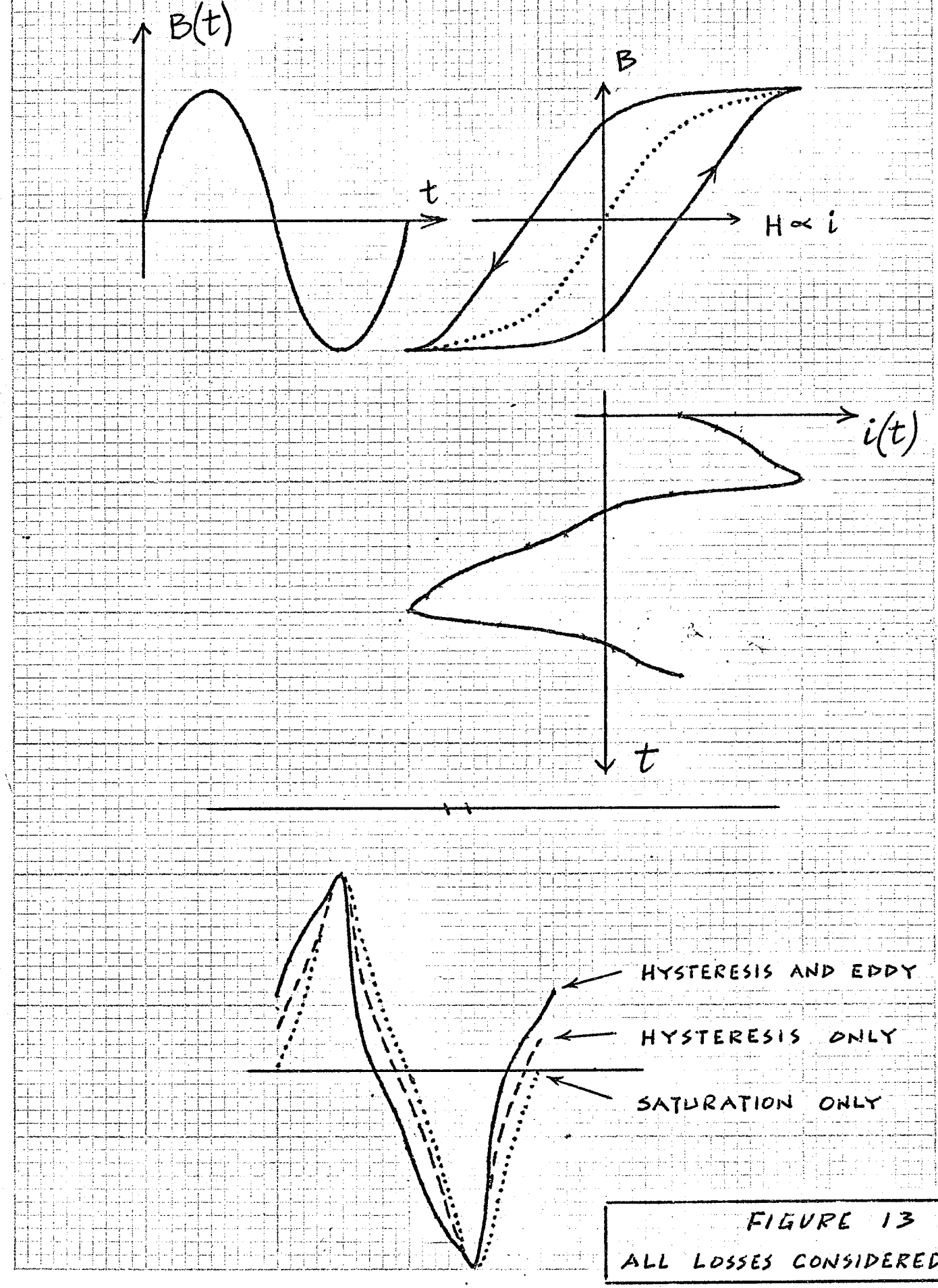

FIGURE 13
ALL LOSSES CONSIDERED

may be represented by a simple linear resistor placed in parallel with the core model which, if it is a proper model, will exhibit saturation and hysteresis. Eddy currents, then, should not contribute to the phase shift between applied voltage and excitation current.

2.5 A Physical Explanation for Magnetization Characteristics.

A discussion of the RMS volt-ampere characteristics must ultimately evolve from energy considerations. Although a more comprehensive discussion of iron losses will be deferred until Chapter III, the marked non-linearity evidenced at lower voltages, especially for the P.T., was deserving of comment.

Figure 14 is a tracing of the photograph of the B-H curves for the P.T. sample at voltages of 10, 20 and 30 volts RMS, at 60 hz. As the ratio of (trace width along the x axis)/(trace height along the y axis) was examined, it was seen that this ratio decreased for increased flux density. Recalling the proportionality of flux density to voltage, and magnetic field intensity to current, it was implied at this point that the curve was "relatively fatter" for lower voltages, hence current was relatively higher. This general behaviour was borne out by magnetization data.

At higher voltages, the magnetization curve swung upwards due to the appearance in the current waveform of a peaked distortion, mathematically described as being comprised of harmonics, and which are more easily explained after the discussion of losses and the B-H curve.

(PHOTO TRACING)

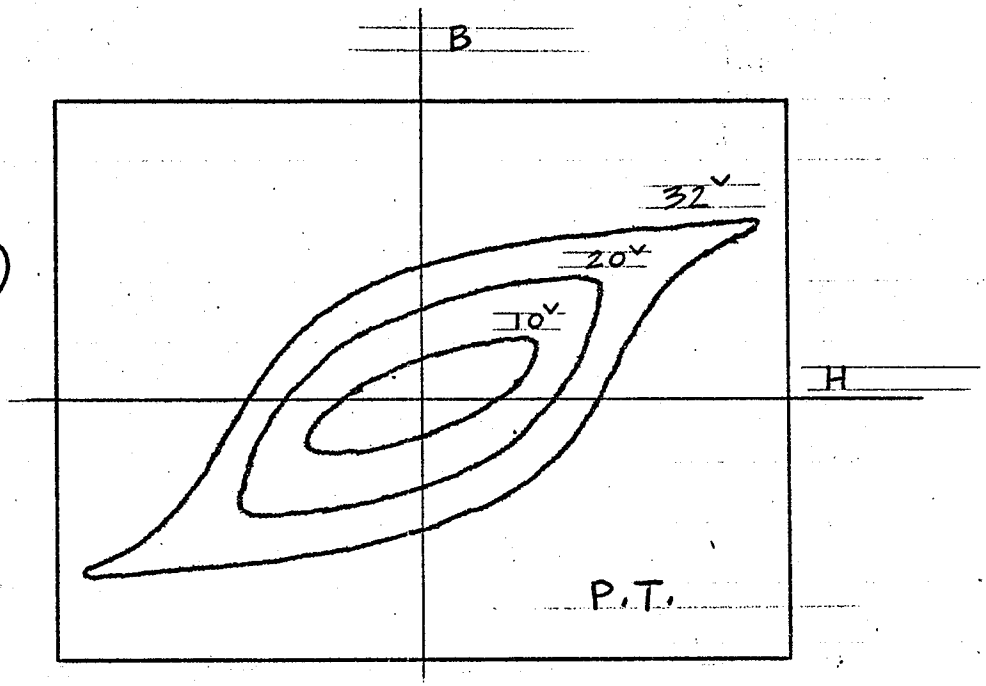

(FREQUENCY IS FIXED AT 60 HZ.)

FIGURE 14

B - H CURVE FOR DIFFERENT VOLTAGES

CHAPTER III

RMS VOLTAGE vs WATTS CHARACTERISTICS

The purpose of this chapter is, initially, to discuss the measurement of power to an iron core using a wattmeter, then to discuss core loss curves from the C.T. and P.T. samples. A resumé of the theory behind core losses, both mathematical and physical, is also presented.

Further references are made to B-H curve measurements in order to determine the "Steinmetz exponent" occurring in the mathematical expression for core loss. Also, total losses are broken down into components using B-H curves.

3.1 Power Measurement: The Wattmeter.

Figure 15 shows the circuit used to measure power flow to the sample, while Figure 16 illustrates the details of the electrodynamometer movement used in the wattmeter. Coils 'F' were fixed in space, of wire heavy enough to carry the line current, and wound on a non ferrous form. Coil M is a very light coil mounted as shown between the fixed coils and also on a non ferrous form, but arranged to carry a small current proportional to the line voltage by employing a wire wound series resistor. Ideally, it is considered that current in the coil M is in phase with load voltage, and that the magnitude of the line current is not influenced by the low impedance fixed coils F. It may be shown that instantaneous torque is proportional to the product of the line current i_L and current flow in the moving coils i_v. Since i_L and i_v are sinusoidal variables, it may be shown further that the <u>average</u> torque is proportional to

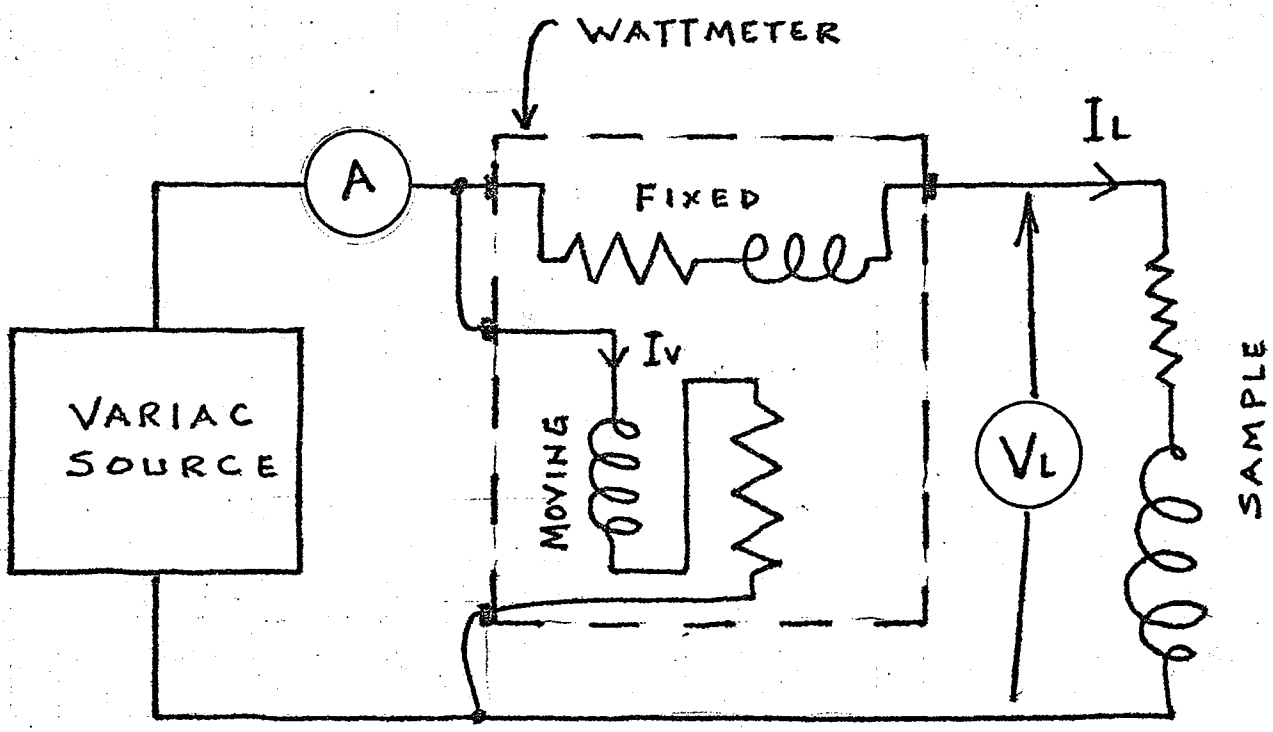

FIGURE I5

CIRCUIT USED FOR POWER MEASUREMENT

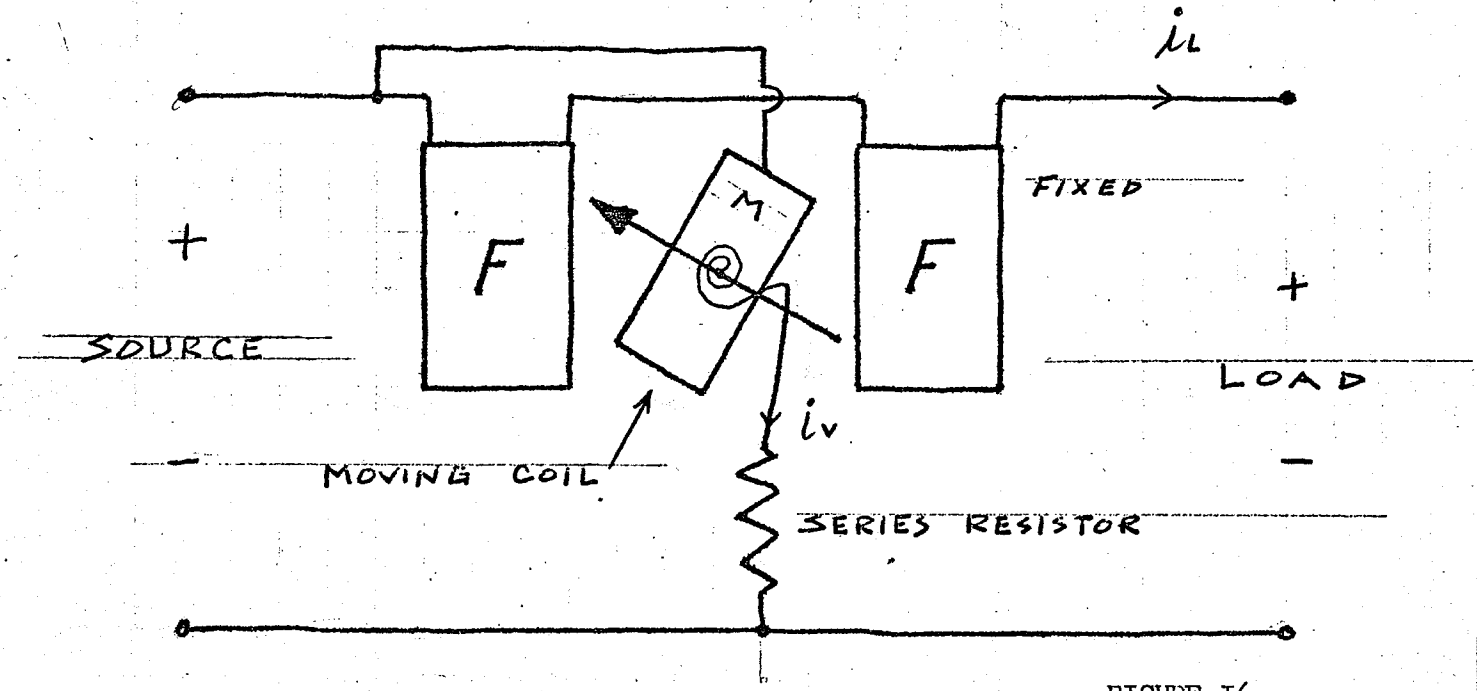

FIGURE I6

DETAILS OF THE ELECTRODYNAMOMETER MOVEMENT

$$I_L \times I_v \times \cos \theta,$$

where θ is the angle between the RMS phasor line current I_L and the RMS phasor I_v. Extending this, Indication $\propto I_L V_L \cos \theta$, since I_v, the moving coil current, is proportional to V_L. The calibration of the meter will be such that Indication = Watts. Frequency errors have been discussed in Appendix A, in regard to measurements of harmonic components in the excitation current.

If possible, a low impedance source should be used to prevent distortion of the sample applied voltage. An oscilloscope was used during core loss tests to ensure that no voltage distortion occurred. Since, as will be shown in 3.3, core loss may be considered to be a function of both peak voltage (the hysteresis component) and RMS voltage (the eddy current component), if the applied voltage is not sinusoidal, core loss measurements must be converted back to a sine wave basis to be compared and reported. Again, the interested reader may refer to Chapter II of "Transformer Engineering" by Blume.

3.2 Comments on Core Loss Characteristics.

Graphs of core loss in watts as a function of RMS applied voltage are presented in Figure 17. To make a quantitative comparison between the curves would have little meaning, since it was not known that the steels are of the same manufacturers grade. It should be pointed out that the readings included the voltmeter I^2R losses, also the winding copper losses, both of which were considered negligible here. Since the absence of visible source voltage distortion was confirmed, the watts readings contained only fundamental frequency components. Carefully

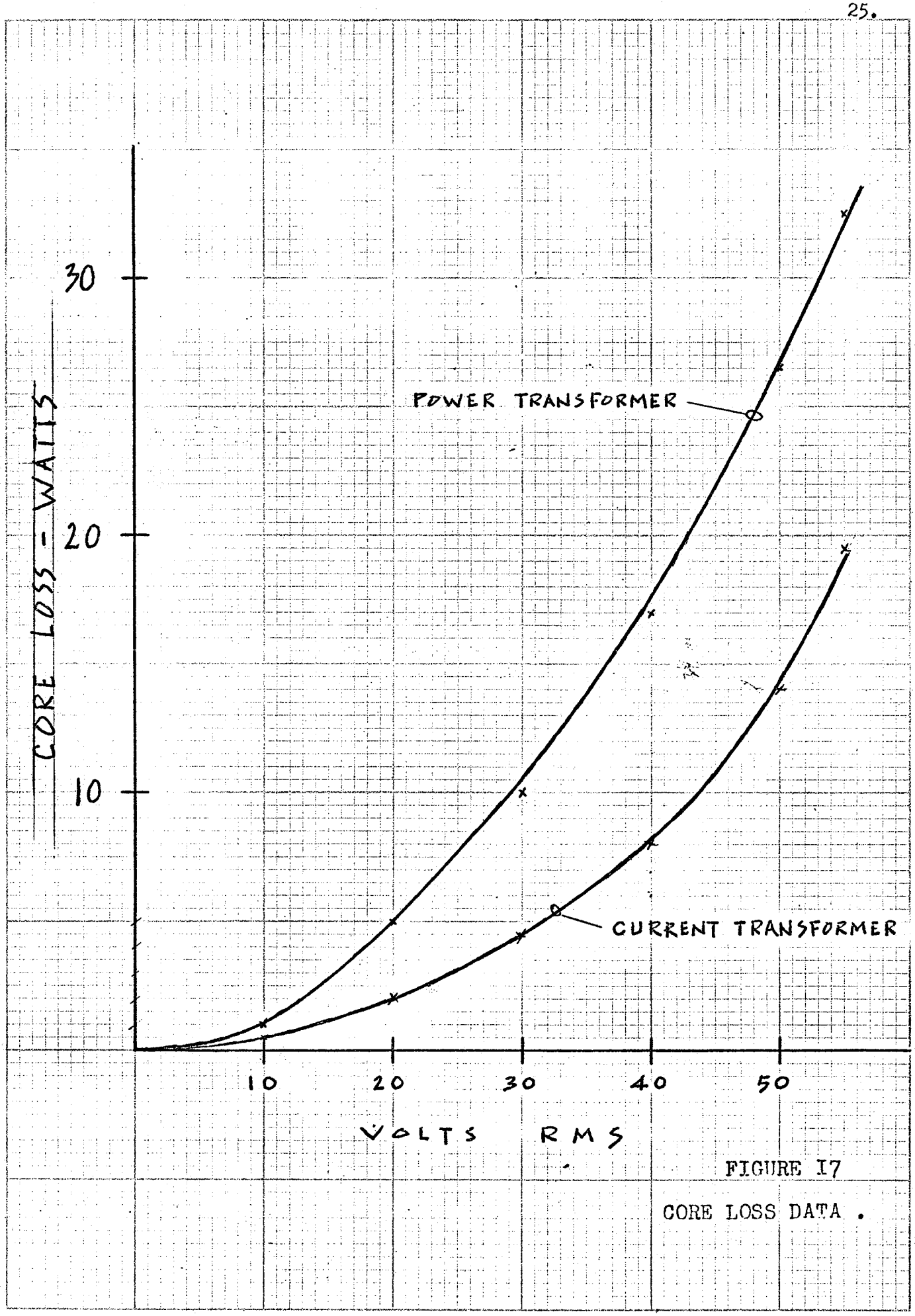

FIGURE I7

CORE LOSS DATA .

controlled core loss tests are important to the transformer manufacturer to aid in developing better core cutting and assembling techniques, among other reasons.

3.3 Mathematical Analysis of Core Losses.

Extrapolation of results is normally made from a formula of the following type:

$$W = k_1 f(B_{max})^n + k_2 f^2(B_{eff})^2 t^2$$

where W = power per unit weight,

k_1, k_2 = constants of the material

f = frequency

B_{max} = peak flux density

B_{eff} = RMS flux density

t = thickness of individual laminations

n = "Steinmetz exponent"

The first term of the loss equation represents the "hysteresis" loss, while the second term is called the "eddy current" loss. In order to show further differences in electrical behavior resulting from the distinct core construction techniques, an attempt was made to evaluate the Steinmetz exponent in the hysteresis term for both the C.T. and the P.T. If the basic loss equation is rewritten in the following manner by dividing by frequency:

$$\frac{W}{f} = k_1 (B_{max})^n + k_2 f(B_{eff})^2 t^2 ;$$

it will be seen that $\frac{W}{f}$ has the dimensions of loss/cycle. If now the frequency is reduced to nearly zero, eddy losses will make a negligible contribution to the right hand side. That is, hysteresis loss/cycle = (constant) $\times (B_{max})^n$.

Thus, if loss/cycle were known, n could easily be evaluated by using logarithms. In the next section, it will be seen that the loss per cycle can be evaluated without too much difficulty, yielding both a loss breakdown and an estimate of the Steinmetz exponent.

3.4 Verification of the Steinmetz Exponent From B-H Curves, and Loss Breakdown.

Appendix B contains a fairly comprehensive discussion of one technique used for obtaining a dynamic B-H curve, that is, B-H traverses taken at non zero frequencies, and illustrates the effects of both hysteresis and eddy currents. It will be considered to be axiomatic that energy loss per cycle is proportional (depending on the system of units) to the area enclosed by the B-H curve. Some of the arguments for proving this are not deemed to be relevant here.

With regard to the Steinmetz exponent, equations presented in the previous section show that

$$\frac{W}{f} \doteq k_1 (B_{max})^n$$

yields loss per cycle at low frequencies. To get "n", B-H photographs were made at about 4 hz for varying (B_{max}). Note that, if

$$k_3 \frac{W}{f} = (B_{max})^n,$$

then

$$\log_{10} [k_3 \frac{W}{f}] = n \log_{10} [B_{max}].$$

If $[B_{max}]$ is plotted vs $[k_3 \frac{W}{f}]$ on log-log paper, then the slope of the line is "n". It was not necessary to know k_3, since relative areas were being plotted, and B_{max} could be in per unit terms. The author used a planimeter to get the relative areas under the B-H curves. Figure 18 shows a tracing of a set of photographs taken at 4 hz for the C.T. sample. Results of this investigation were

C.T. core; n = 2.0

P.T. core; n = 1.6

With regard to the breakdown of losses: B-H curves of the type traced in Figure 19 were photographed for both samples. Figure 20 shows plots of relative loss/cycle vs frequency from tests done on the C.T. and P.T. Extrapolation of these curves to zero frequency allowed a loss analysis to be made for the 60 hertz case.

For the C.T. sample, percent hysteresis loss was 41%: percent eddy current loss was 59%. For the P.T. sample, the proportions were much the same: 46% hysteresis loss and 54% eddy loss.

3.5 Comments and a Discussion of Ferromagnetism and Losses in Magnetic Materials.

Magnetic properties of materials are considered to be due to the magnetic moment created by the electrons orbiting and spinning around the

Voltages set at 60 hz . The input frequency was then reduced to 4 hz , with flux density held fixed .

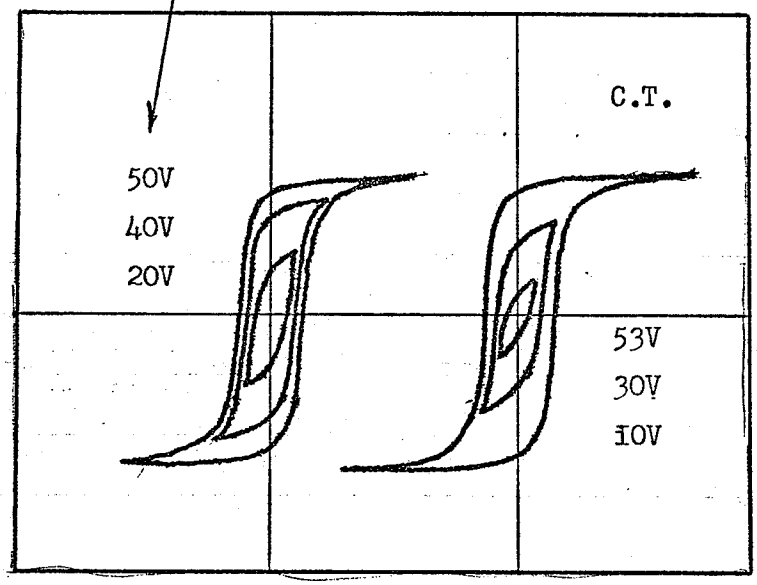

Frequency was 4hz for all photos .

FIGURE I8

TRACING OF THE CT BH CURVES .

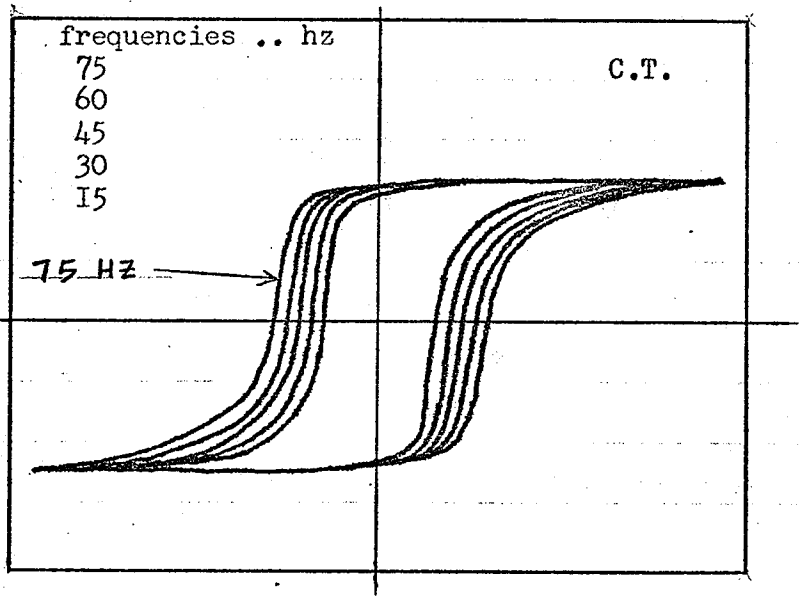

FLUX DENSITY WAS FIXED AT 106 % FOR ALL TESTS .
(53 V RMS)

FIGURE I9

TRACING OF THE CT BH CURVE PHOTOS FOR A FIXED FLUX DENSITY AND A RANGE OF FREQUENCIES .

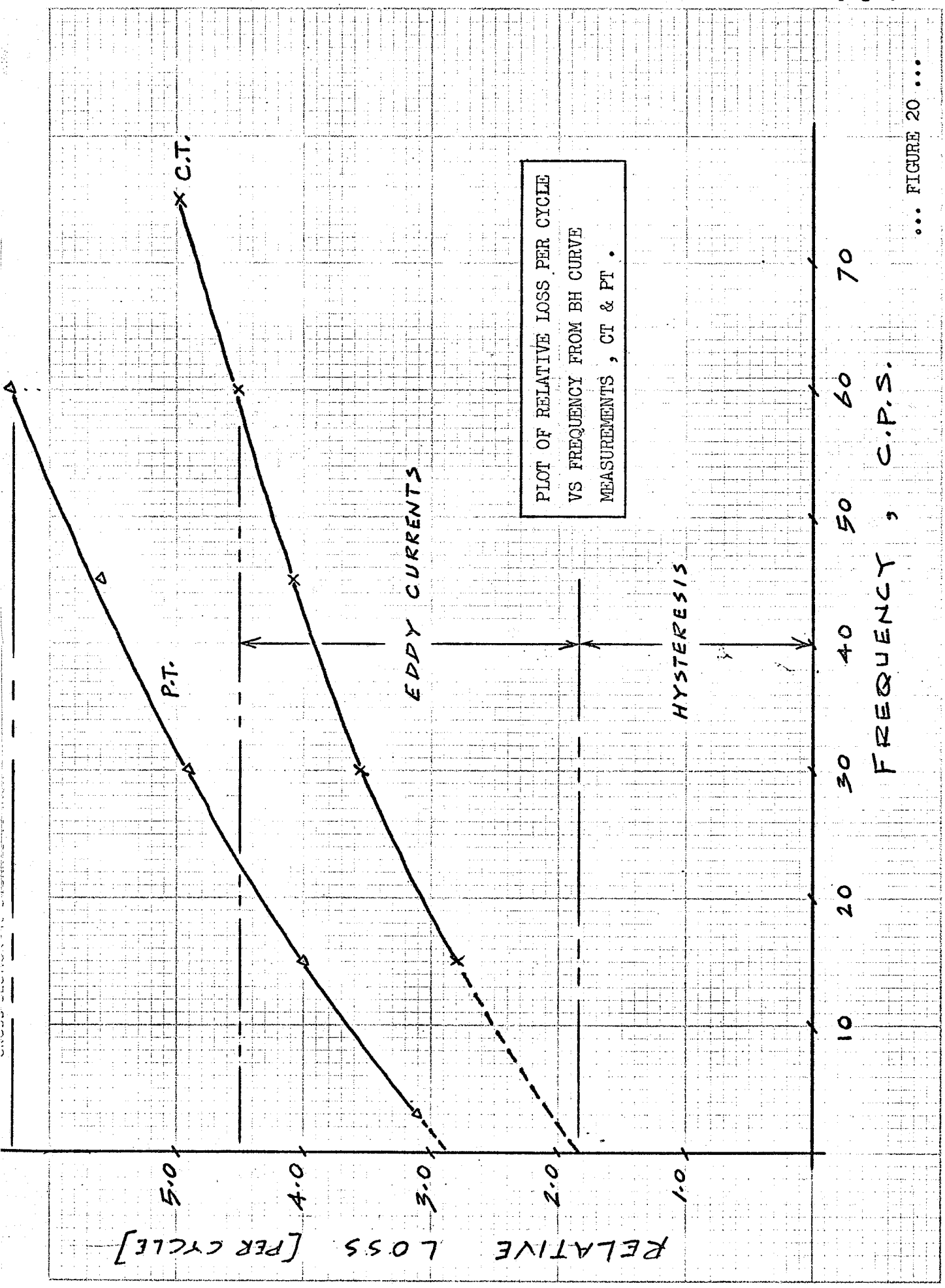
PLOT OF RELATIVE LOSS PER CYCLE
VS FREQUENCY FROM BH CURVE
MEASUREMENTS , CT & PT .
C.T.
P.T.
EDDY CURRENTS
HYSTERESIS
RELATIVE LOSS [PER CYCLE]
5.0
4.0
3.0
2.0
1.0
10
20
30
40
50
60
70
FREQUENCY , C.P.S.

... FIGURE 20 ...

nucleus of the atom. A ferromagnetic material such as iron is considered to be composed of "domains", separated by complex acting domain walls. In a domain, alignment of the magnetic moments of the atoms has taken place. (This implies that iron crystals, since they are formed from symmetrical arrays of iron atoms, are uniformly oriented within the domain). As produced for commercial electrical machines, iron contains microscopic impurities, irregularities, or strain regions in the crystal. These imperfections can occur within a domain, or at the boundary between two.

When no external field has been applied, the random magnetization of the domains in the iron will ensure that a transformer core, for example, exhibits no macroscopic magnetic characteristics. If a magnetic field intensity H (created by current flowing in turns of wire around the core) is now applied, the domain walls are caused to move such that those domains whose orientation direction is near that of the H vector grow in size, while those oppositely oriented decrease in size. We call saturation the macroscopic electrical condition that exists when the domain size is maximized.

Hysteresis is the name given to the energy required to produce the motion of the domain walls past crystal boundaries, non magnetic impurities, or strained regions within a crystal structure. This loss appears as heat and noise in the material.

Eddy current losses result only when time varying fluxes are caused to exist in the core. (It should be noted that the "static" hysteresis loop often referred to is also obtained by applying a time varying current, but the rate of change is very slow i.e. less than 1 hz). Rapidly changing fluxes will induce an emf within a magnetic or

nonmagnetic material which will cause a circulating current to flow, the magnitude of which is dependent upon the resistivity of the material in the case of the transformer core, and of course causes heating.

Modern electrical machine steels are specially processed to minimize hysteresis and eddy losses within the limits dictated by economics. Eddy currents in machine cores are controlled by the use of thin laminations which have a surface insulation to restrict current flow to one layer. In addition, silicon is added to increase the resistivity of the metal.

Hysteresis losses are lowered at the raw manufacturing stage by "cold rolling", which causes the iron crystals to align more nearly in one direction, that direction being taken advantage of by equipment manufacturers. Also, strains caused in the crystal structure due to the basic core shaping procedure, which can also add to hysteresis loss, are removed by a process of high temperature heating and slow cooling in an annealing oven.

CHAPTER IV

FLUX DENSITY vs MAGNETIC FIELD INTENSITY CHARACTERISTICS

The initial purpose of this chapter is to compare the B-H characteristics for the C.T. and the P.T. After introducing the ℓ (flux linkages) and i (current) variables, and relating these to the B-H curves, the functional relationship $i = f(\ell)$ will be deduced from the average of the $\ell - i$ curves. Using the polynomial $i = f(\ell)$, the RMS currents and harmonic components flowing under sinusoidal excitation will be calculated and compared to the actual magnetization and harmonic data. Discrepancies will be explained. It will then be shown that a three segment approximation to the $\ell - i$ curve is a good approximation, and that similar RMS values and harmonics result to those obtained by starting from the polynomial approximation.

Finally, the possible uses of a simple $\ell - i$ relationship will be suggested and reference will be made to the findings of other authors.

4.1 Presentation of B-H Characteristics.

Figures 21 and 22 are tracings of enlarged B-H curve photos. In both, the arithmetic average of the top half has been indicated. The bottom portion has been shown by dashed lines. The photos were taken at rated voltage, and frequency, 50 v RMS for the C.T. and 30 v RMS for the P.T., but they are meaningful in terms of shape only, since the horizontal and vertical scales, while close, were not exactly equal.

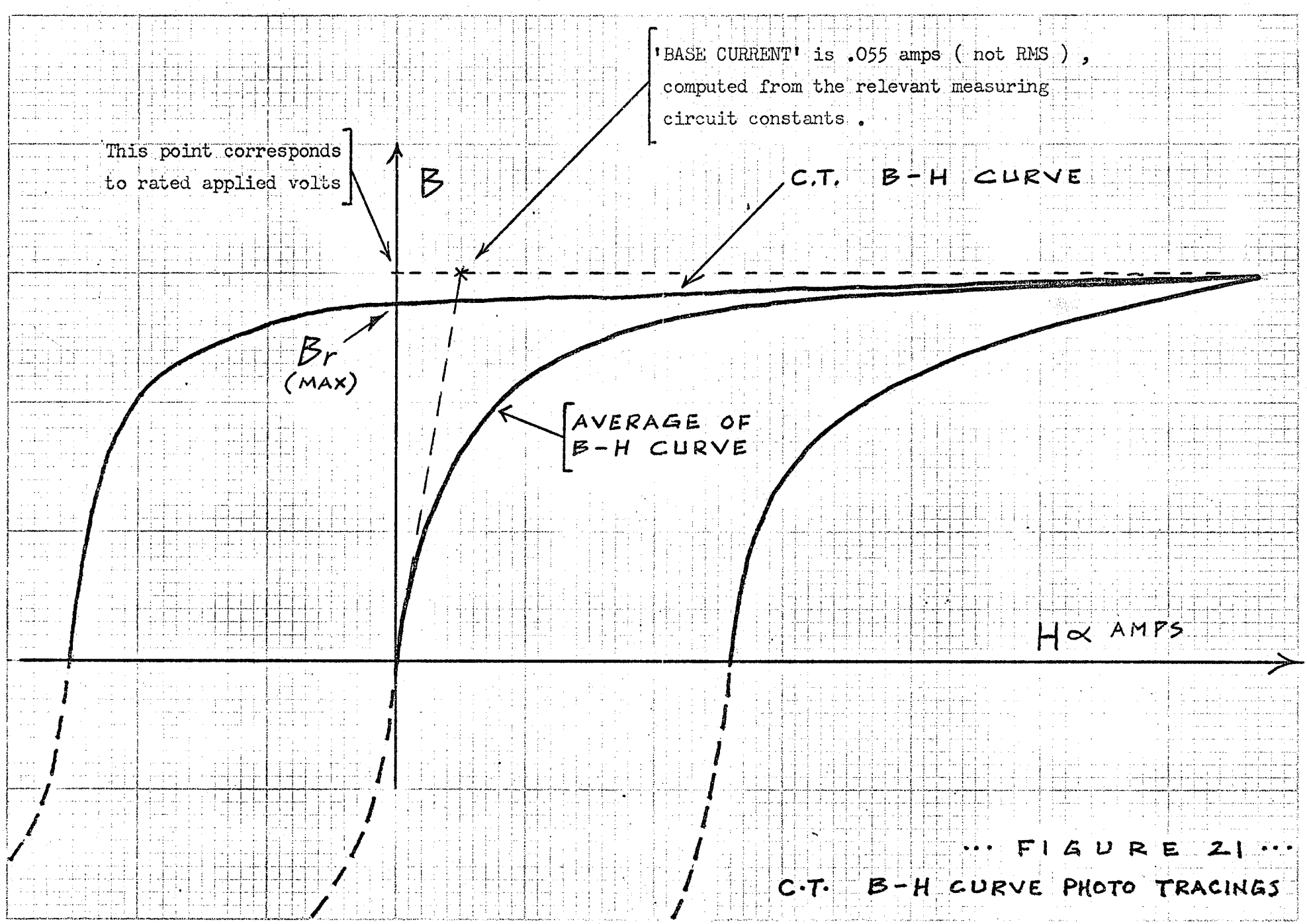

... FIGURE 21 ...

C.T. B-H CURVE PHOTO TRACINGS

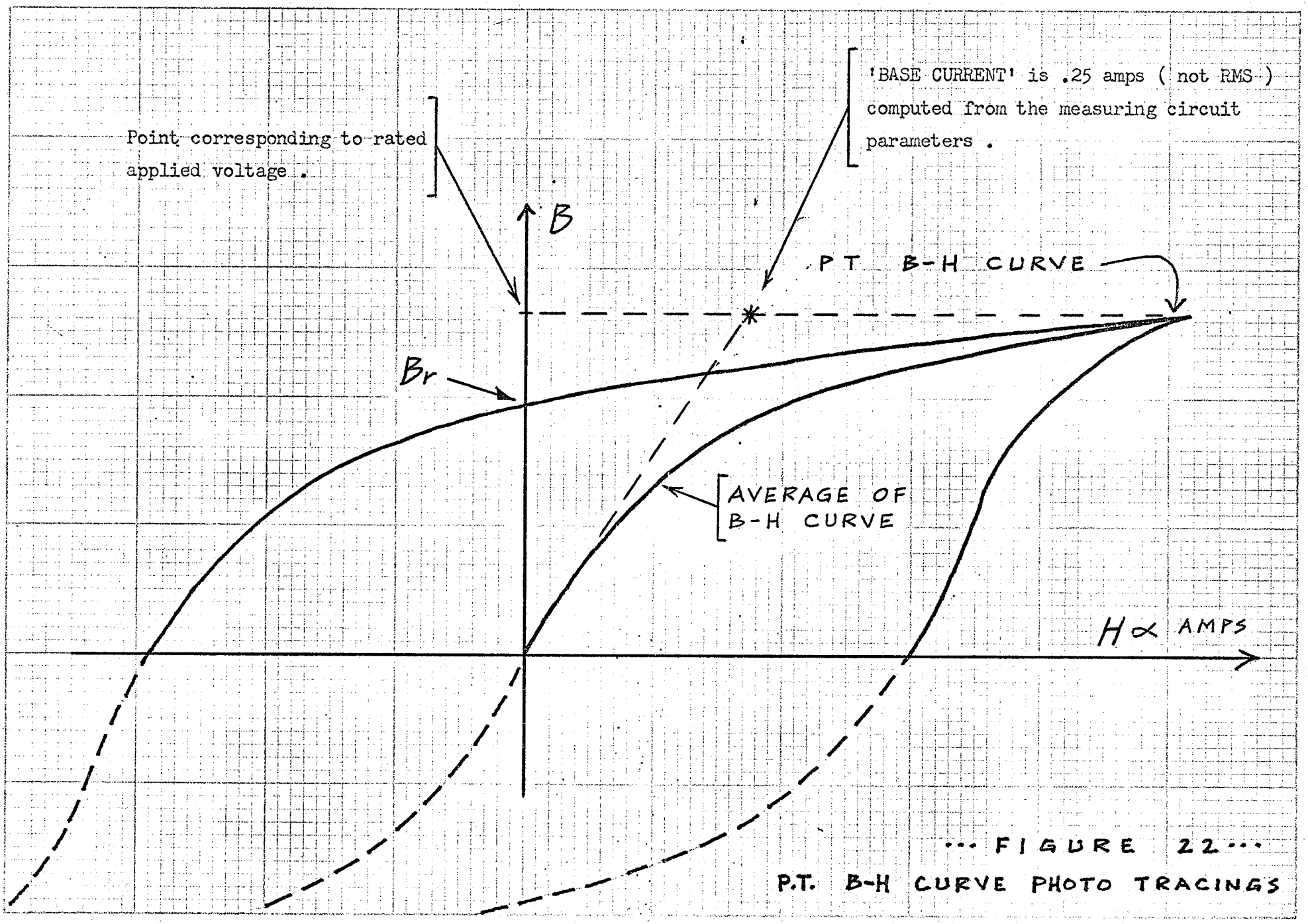

··· FIGURE 22 ···

P.T. B-H CURVE PHOTO TRACINGS

The operational-integrator technique used to display these curves is detailed in Appendix B.

4.2 The Polynomial Relationship Between Flux Linkages and Current.

It is first necessary to show that the relationship between flux linkages and current has the same shape as the B-H curve. By definition:

$$\ell = N\phi \quad ; \quad \text{but since}$$

$$B = \phi / A \quad ; \quad \text{then}$$

$$\ell / B = N\phi / \phi / A = NA = \text{const}$$

Also, since

$$H = Ni / L$$

$$H / i = N / L = \text{constant} \quad , \text{ where}$$

ℓ = flux linkages

N = number of turns

ϕ = flux, lines

B = flux density, lines per unit area

A = net cross sectional area of magnetic circuit

i = current

H = magnetic field intensity.

L = mean length of the magnetic circuit

Figure 23 shows the " average " curves of either figure 2I or 22 rearranged in a form convenient for further analysis.

However , since the property of odd symmetry is required

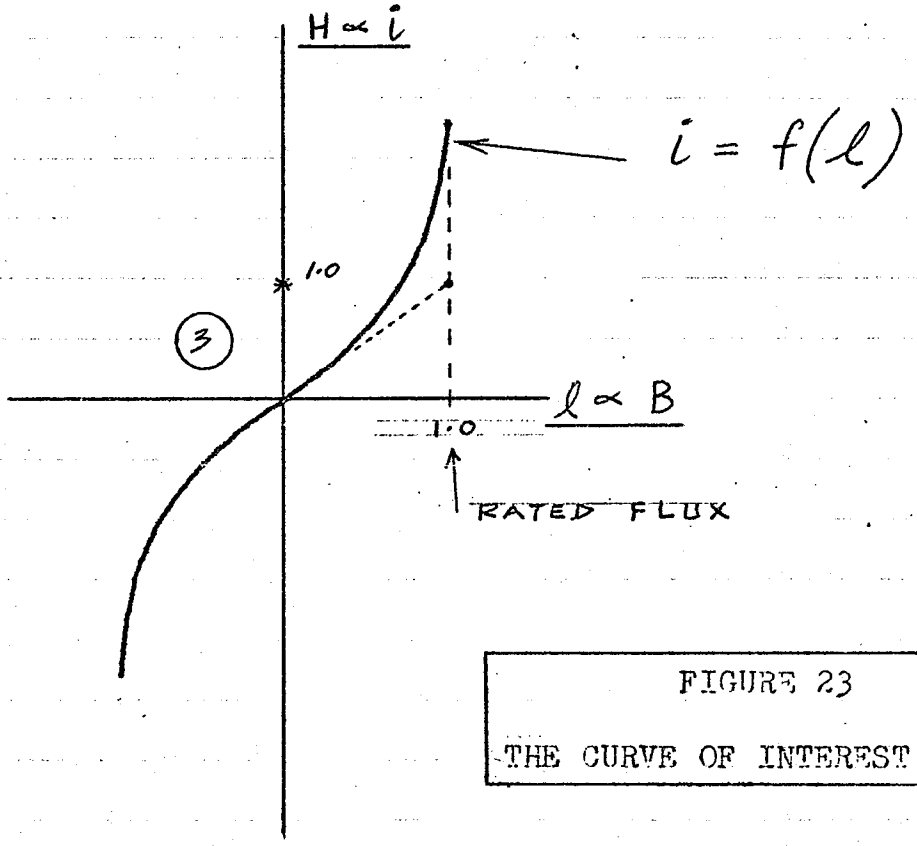

FIGURE 23

THE CURVE OF INTEREST

around the ℓ axis, a binomial with an odd power was chosen as the starting point, that is:

$$i = C_1 \ell + C_n \ell^n$$

Here C_1 and C_n are constants.

If variables in Figure 23 were assigned a per unit scale, that is rated voltage corresponded to $\ell = 1.0$ pu, and base current was set equal to the extension of the initial slope of the curve on the "$\ell = 1.0$" vertical line, then it was found that $C_1 = 1.0$. Figures 24 and 25 show that the average ℓ/i curves are represented fairly closely by

$$i = \ell + 1.83\ \ell^5 \quad \text{for the P.T. and}$$
$$i = \ell + 12.0\ \ell^7 \quad \text{for the C.T.}$$

4.3 The Calculation of RMS Currents Resulting from the Binomial i/ℓ Relationship Under Sinusoidal Excitation.

It must be stated at the outset that, if a sinusoidal voltage of the form $e(t) = E_m \cos \omega t$ is applied to an ideal coil having an iron core, since

$$e(t) = N \frac{d\phi}{dt}, \text{ and}$$

$$\ell = N\phi, \text{ then}$$

$$d\ell/dt = e(t) = \dot{\ell}$$

Thus, $$\ell(t) = \int e\ dt$$

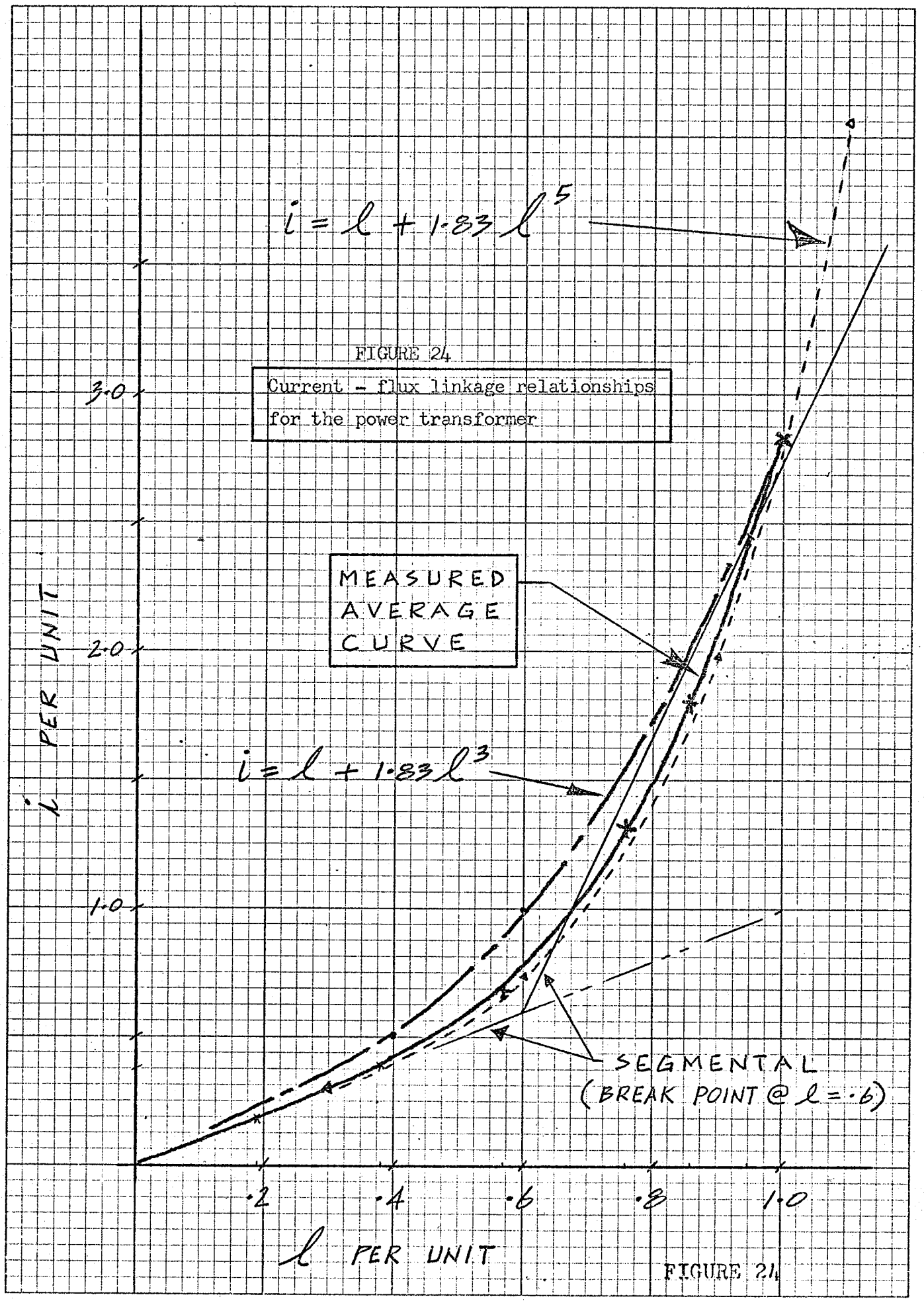

FIGURE 24

Current - flux linkage relationships for the power transformer

FIGURE 21

FIGURE 25.

Current - flux linkage relationships for the current transformer .

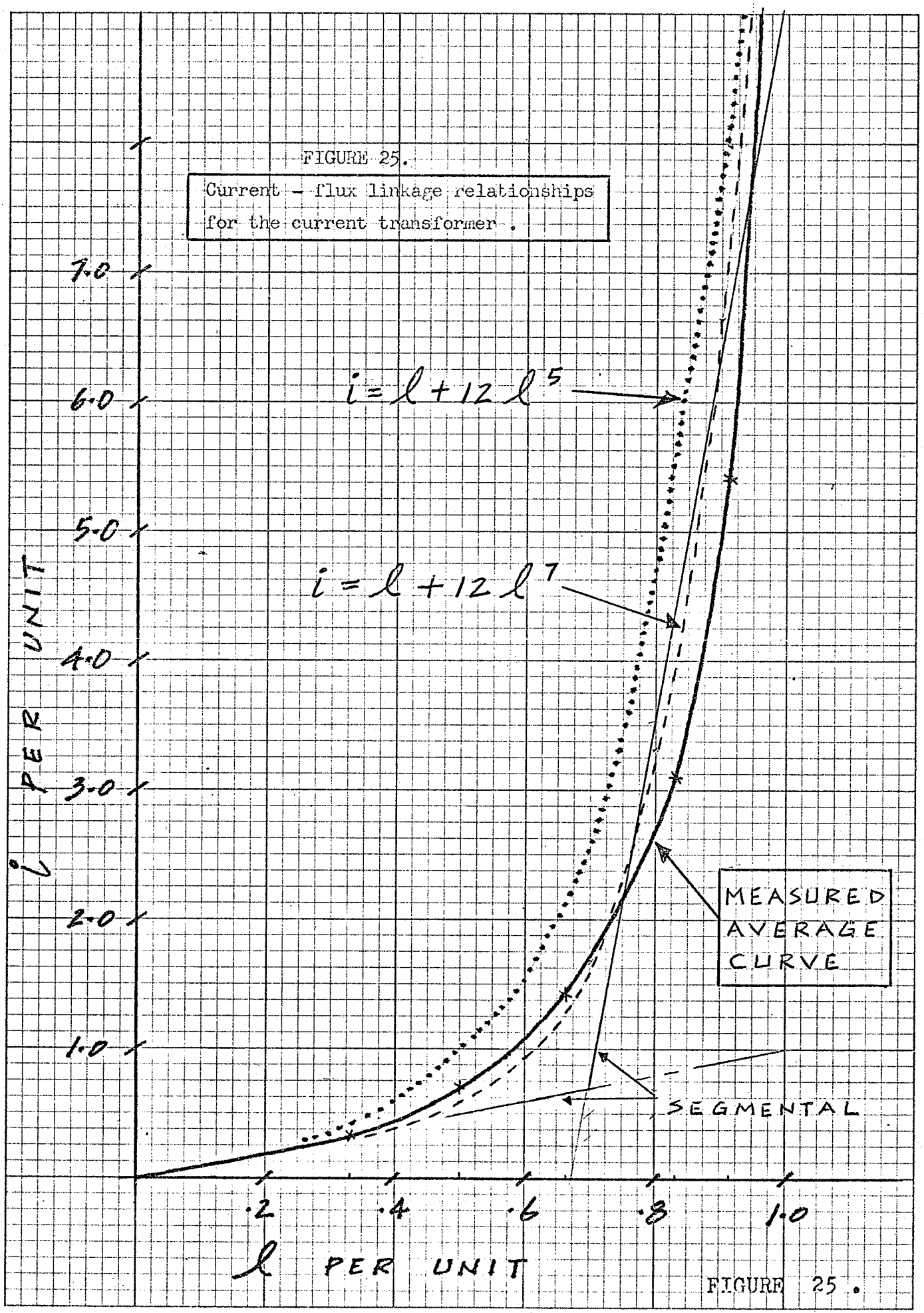

FIGURE 25 .

so $$\ell(t) = + \frac{E_m}{\omega} \sin \omega t,$$

where symbols have all been defined previously.

For the P.T., the binomial $i = \ell + 1.83\ \ell^5$ was deduced. If $\ell = (E_m/\omega) \sin \omega t = (\ell_m) \sin \omega t$; then $i = (\ell_m) \sin \omega t + 1.83\ [(\ell_m) \sin \omega t]^5$.

The RMS value of this function may be evaluated in two ways; the first by applying the basic definition:

$$I[RMS]^2 = \frac{1}{T} \int_0^T [f(t)]^2\ dt$$

where T is the period of the function. Since the integration can become quite cumbersome, it was decided to apply the following theorem:

$$I = \sqrt{(A_1)^2 + (A_2)^2 + (A_3)^2 + \ldots + (A_n)^2}\ .$$

Here $A_1, A_2, \ldots, A_n$ are the RMS values of the individual Fourier coefficients. In addition, A_1 is the "fundamental", A_3 is the "third harmonic", A_5 the "fifth harmonic", that is, this procedure automatically yielded a harmonic analysis.

Consider the original function, and substitute the trigonometric relationships found in Appendix C.

$$\begin{aligned} i &= \ell + 1.83\ \ell^5 \\ &= \ell_m \sin \omega t + 1.83\ \ell_m{}^5 \left[\frac{5}{8} \sin \omega t - \frac{5}{16} \sin 3\omega t \right. \\ &\quad \left. + \frac{1}{16} \sin 5\omega t \right] . \end{aligned}$$

That is, collecting terms;

$$i = \ell_m \sin \omega t + (1.83\, \ell_m^5 \times \frac{5}{8}) \sin \omega t$$

$$- (1.83 \times \frac{5}{16}\, \ell_m^5) \sin 3\omega t + \frac{1}{16} \times 1.83\, \ell_m^5 \sin 5\, \omega t$$

$$= (\ell_m + 1.14\, \ell_m^5) \sin \omega t - (.57\, \ell_m^5) \sin 3\, \omega t$$

$$+ (.11 \ell_m^5) \sin 5\, \omega t \quad .$$

Now, the RMS phasor, I, is given by:

$$I = \frac{1}{\sqrt{2}} \sqrt{(\ell_m + 1.14\, \ell_m^5)^2 + (.57\, \ell_m^5)^2 + (.11\, \ell_m^5)^2} \quad .$$

It is necessary to convert this result back to actual amperes for the sake of comparison and this is done by multiplying by the base current, .25 amps,* and realizing that base voltage is 30 v RMS at $\ell_m = 1.0$. The results of the above equation were compared with test magnetization data in Figure 26.

For the C.T., the polynomial $i = \ell + 12\, \ell^7$ was deduced, with i(base) = .055 amperes* and $\ell = 1.0$ at 50 v RMS. Again since

$$\ell(t) = \ell_m \sin \omega t;$$

$$i = \ell_m \sin \omega t + 12\, \ell_m^7 \sin^7 \omega t \quad .$$

Using Appendix C,

$$i = \ell_m \sin \omega t + 12\, \ell_m^7 \left[\frac{35}{64} \sin \omega t - \frac{21}{64} \sin 3\, \omega t \right.$$

$$\left. + \frac{7}{64} \sin 5\, \omega t - \frac{1}{64} \sin 7\, \omega t \right] .$$

* See figures 2I and 22 .

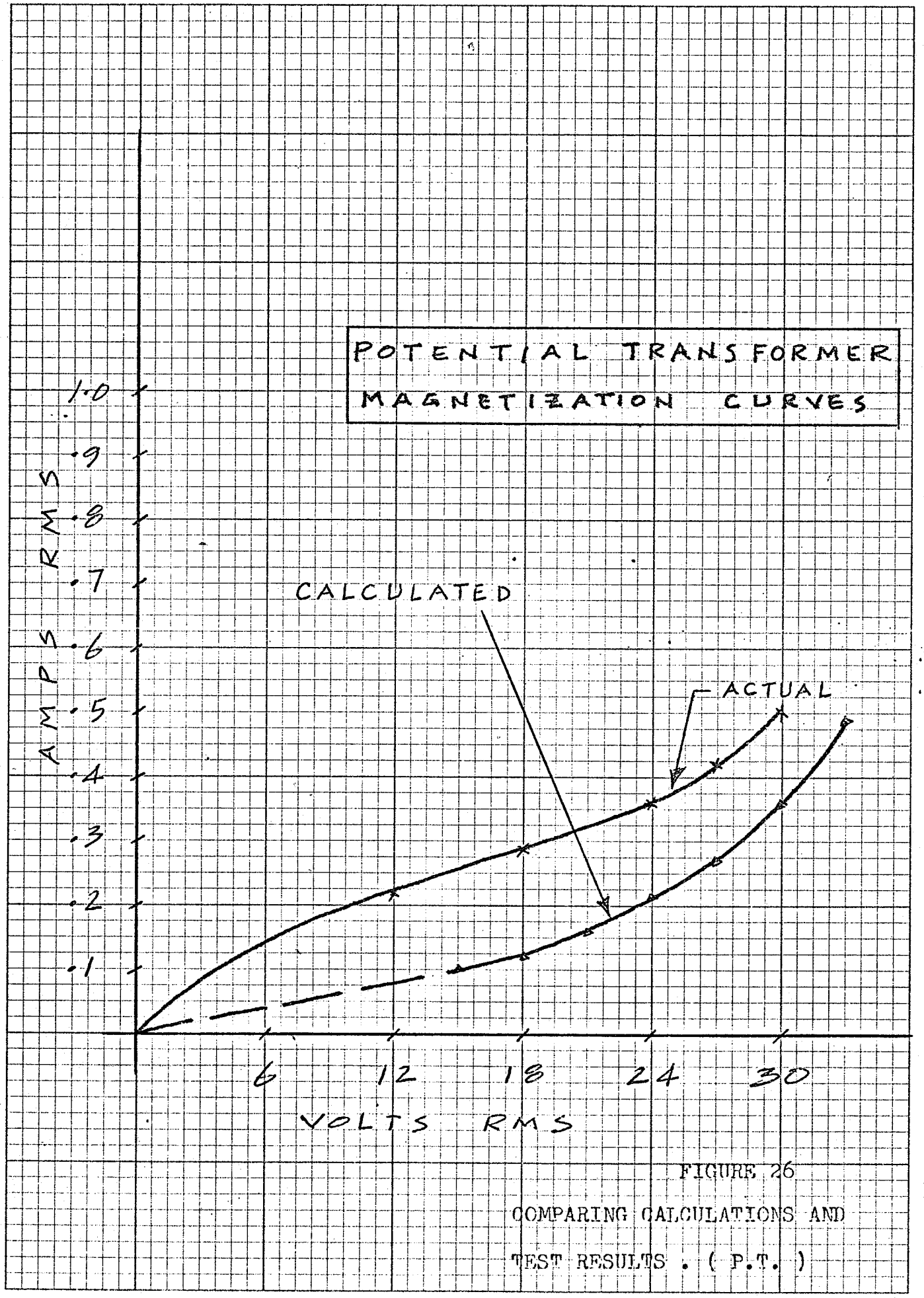

FIGURE 26

COMPARING CALCULATIONS AND

TEST RESULTS . (P.T.)

Collect the coefficients of sine terms of the same order, that is:

$$i = (\ell_m + 12 \times \frac{35}{64} \ell_m^7) \sin \omega t - (\frac{21}{64} \times 12 \ell_m^7) \sin 3 \omega t$$

$$+ (\frac{7}{64} \times 12 \ell_m^7) \sin 5\omega t - (\frac{12}{64} \ell_m^7) \sin 7\omega t.$$

Simplifying,

$$i = (\ell_m + 6.56\ell_m^7) \sin \omega t - (3.94 \ell_m^7) \sin 3 \omega t$$

$$+ 1.31 \ell_m^7 \sin 5 \omega t - .19 \ell_m^7 \sin 7 \omega t.$$

Here, the RMS value of the fundamental is $\frac{1}{\sqrt{2}} (\ell_m + 6.56 \ell_m^7)$ the RMS value of the third harmonic is $\frac{3.94}{\sqrt{2}} \ell_m^7$, while the RMS value of the fifth is $\frac{1.31}{\sqrt{2}} \ell_m^7$.

Now,

$$I = \frac{1}{\sqrt{2}} \sqrt{(\ell_m + 6.56 \ell_m^7)^2 + (3.94 \ell_m^7)^2 + (1.31 \ell_m^7)^2}.$$

Harmonics higher than the fifth order will contribute only a negligible amount to this expression. Figure 27 shows the comparison of actual magnetization data to the results of the above equation.

Since the equation as derived was in per unit, it was converted to amperes by multiplying by the base current, found from the linear extension of the initial part of the $i - \ell$ curve. For the C.T., this was .055 amperes.

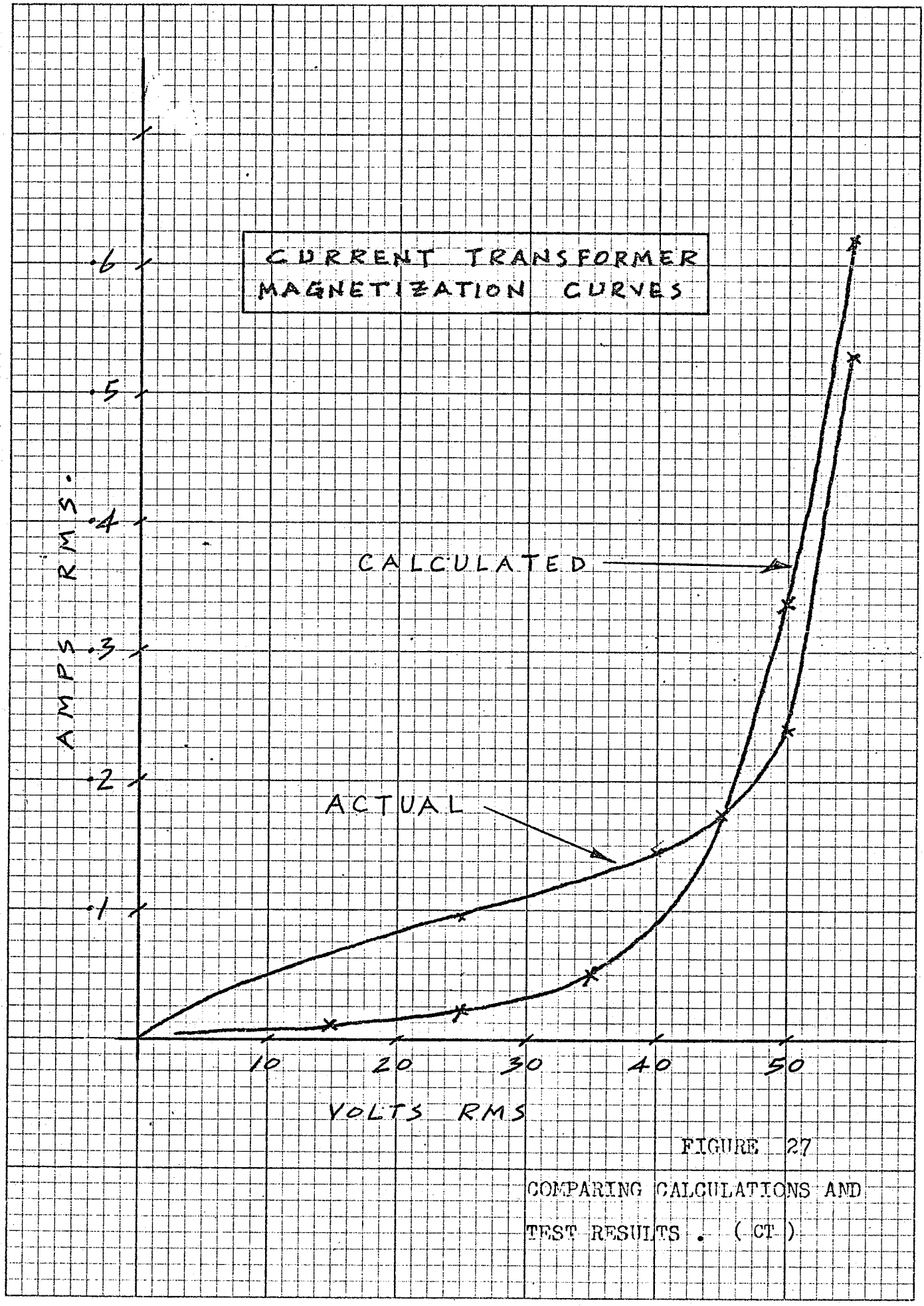

FIGURE 27

COMPARING CALCULATIONS AND TEST RESULTS . (CT)

4.4 RMS Currents Resulting From a Segmental Approximation to the Binomial i/ℓ Relationship.

Figures 24 and 25 show the i/ℓ relationship and a three segmental approximation for the P.T. and the C.T. respectively. A generalized harmonic analysis will be made, based on symbols shown in Figure 28. The following equations are apparent, if $\ell(\theta) = \ell_m \sin\theta$ and $\ell_m > \ell_c$.

$$i = A\,\ell_m \sin\theta; \quad 0 < \theta < \alpha \quad \text{and} \quad (\pi - \alpha) < \theta < \pi$$

$$i = B\,\ell_m \sin\theta - C; \quad \alpha < \theta < (\pi - \alpha).$$

Since $i(\theta)$ is an odd function, it can be written:

$$i(\theta) = \sum_{n=1}^{\infty} b_n \sin n\theta; \quad \text{where}$$

$$b_n = \frac{2}{\pi} \int_0^{\pi} i(\theta) \sin n\theta \, d\theta$$

Thus the fundamental RMS value was calculated as follows

$$I_1 = \frac{2}{\sqrt{2}\pi} \int_0^{\pi} i(\theta) \sin\theta \, d\theta = .45 \int_0^{\pi} i(\theta) \sin\theta \, d\theta$$

$$I_1 = .45 \int_0^{\alpha} A\,\ell_m \sin^2\theta \, d\theta + .45 \int_{\alpha}^{(\pi-\alpha)} (B\,\ell_m \sin\theta - c) \sin\theta \, d\theta$$

$$+ .45 \int_{(\pi-\alpha)}^{\pi} A\,\ell_m \sin^2\theta \, d\theta$$

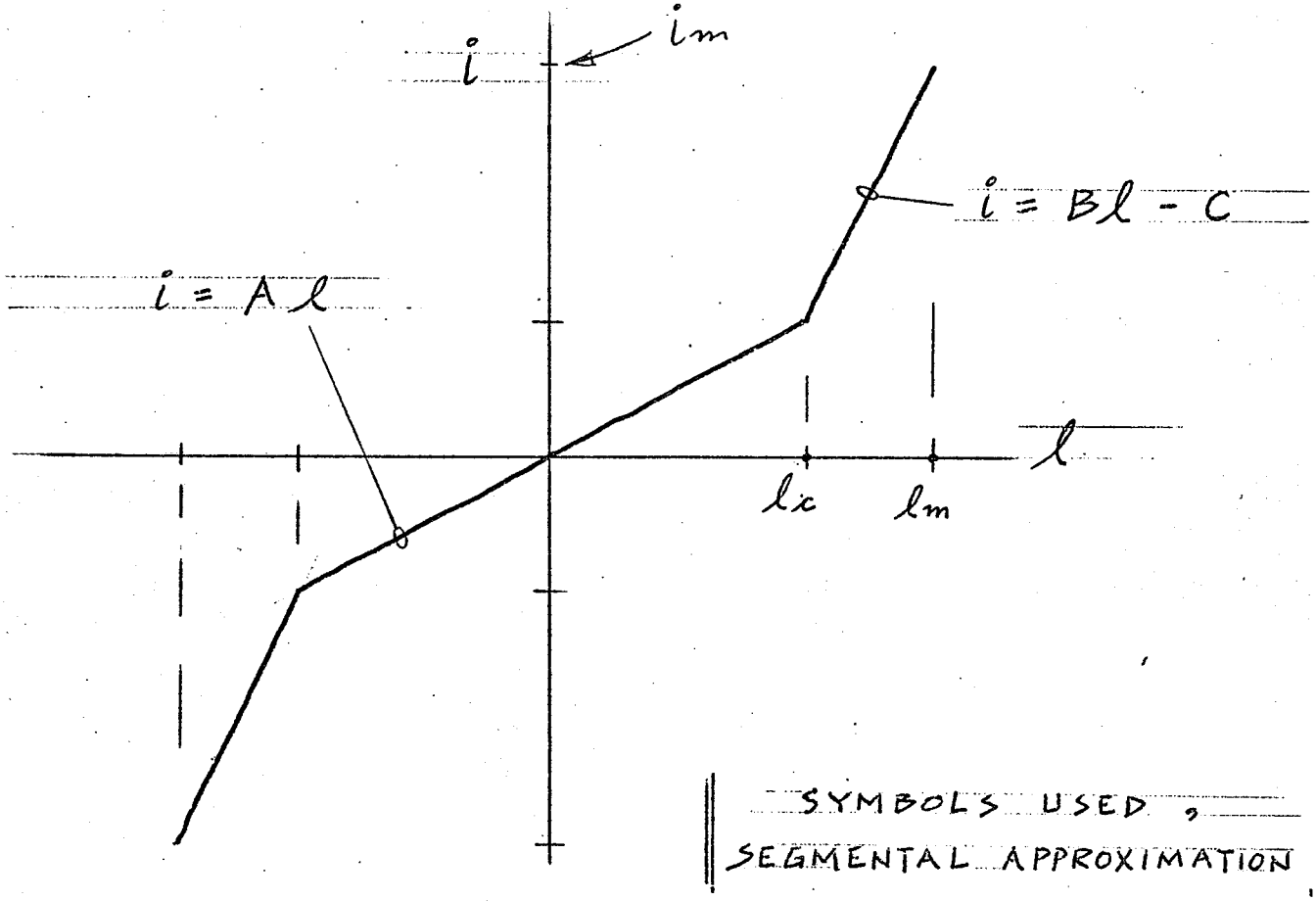

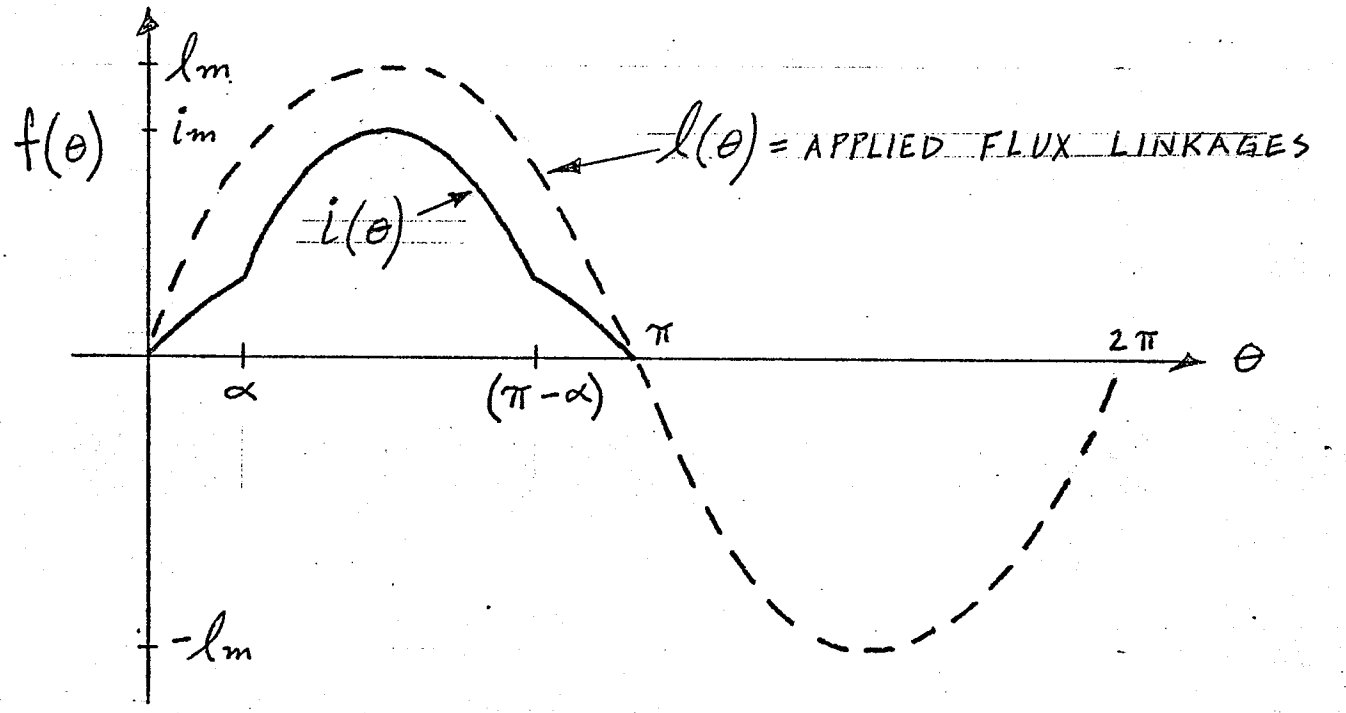

FIGURE 28

symbols and waveforms

$$= .9 \int_{o}^{\alpha} A\, \ell_m \sin^2\theta \, d\theta + .45 \int_{\alpha}^{(\pi-\alpha)} B\, \ell_m \sin^2\theta \, d\theta - .45 \int_{\alpha}^{(\pi-\alpha)} c \sin\theta \, d\theta .$$

Since $\int \sin^2\theta \, d\theta = \frac{\theta}{2} - \frac{1}{4} \sin 2\theta$;

$$I_1 = .9\, A\, \ell_m \left[\frac{\theta}{2} - \frac{1}{4} \sin 2\theta \right]_{o}^{\alpha} + .45\, B\, \ell_m \left[\frac{\theta}{2} - \frac{1}{4} \sin 2\theta \right]_{\alpha}^{(\pi-\alpha)}$$

$$+ .45\, C \cos\theta \Big|_{\alpha}^{(\pi-\alpha)}$$

$$= .9A\, \ell_m \left[\frac{\alpha}{2} - \frac{1}{4} \sin 2\alpha \right] + .45\, B\, \ell_m \left[\frac{\pi}{2} - \frac{\alpha}{2} - \frac{1}{4} \sin 2(\pi - \alpha) \right.$$

$$\left. - \frac{\alpha}{2} + \frac{1}{4} \sin 2\alpha \right] + .45\, C \left[\cos(\pi - \alpha) - \cos\alpha \right] .$$

Using the relationships;

$$\cos(\pi - \alpha) = -\cos\alpha; \quad \text{and}$$

$$\sin 2(\pi - \alpha) = -\sin 2\alpha;$$

$$I_1 = .9\, A\, \ell_m \left[\frac{\alpha}{2} - \frac{1}{4} \sin 2\alpha \right] + .45\, B\, \ell_m \left[\frac{\pi}{2} - \frac{\alpha}{I} + \frac{1}{2} \sin 2\alpha \right] - .9\, C \cos\alpha$$

$$I_1 = .45\, \ell_m\, \alpha[A - B] + .225\pi\, B\, \ell_m - .225\, \ell_m \sin 2\alpha\, [A - B] - .9C \cos\alpha.$$

Consider now the third harmonic

$$I_3 = \frac{b_3}{\sqrt{2}} = \frac{2}{\sqrt{2}\pi} \int_{o}^{\pi} i(\theta) \sin 3\theta \, d\theta$$

$$= 2 \times .45 \int_{o}^{\alpha} A\, \ell_m \sin\theta \sin 3\theta \, d\theta$$

$$+.45 \int_{\alpha}^{(\pi-\alpha)} (B\, \ell_m \sin\theta - C) \sin 3\theta \, d\theta$$

$$\therefore \quad I_3 = .9\, A\, \ell_m \int_{o}^{\alpha} \sin\theta \sin 3\theta \, d\theta$$

$$+ .45\, B\, \ell_m \int_{\alpha}^{(\pi-\alpha)} \sin\theta \sin 3\theta - .45\, C \int_{\alpha}^{(\pi-\alpha)} \sin 3\theta \, d\theta$$

But $\int \sin 3\theta \sin\theta \, d\theta = \frac{\sin 2\theta}{2 \times 2} - \frac{\sin 4\theta}{2 \times 4}$

Thus, in the above expression;

$$\int_{o}^{\alpha} \sin 3\theta \sin\theta \, d\theta = \frac{1}{4} \sin 2\alpha - \frac{1}{8} \sin 4\alpha$$

and $$\int_{\alpha}^{(\pi-\alpha)} \sin 3\theta \sin\theta = \frac{1}{4} \sin 2 (\pi - \alpha) - \frac{1}{8} \sin 4 (\pi - \alpha)$$

$$- \frac{1}{4} \sin 2\alpha + \frac{1}{8} \sin 4\alpha \, .$$

$$= \frac{1}{2} \sin 2\alpha + \frac{1}{4} \sin 4\alpha$$

$$\therefore I_3 = .9A\, \ell_m \left[\frac{1}{4} \sin 2\alpha - \frac{1}{8} \sin 4\alpha \right] + .45B\, \ell_m \left[- \frac{1}{2} \sin 2\alpha + \frac{1}{4} \sin 4\alpha \right]$$

$$- .3C \cos 3\alpha \, .$$

$$I_3 = (.225)\, \ell_m (A - B) \sin 2\alpha - .112\, \ell_m (A - B) \sin 4\alpha - .3C \cos 3\alpha$$

And finally, considering the fifth harmonic,

$$I_5 = \frac{b_5}{\sqrt{2}} = \frac{\sqrt{2}}{\pi}\int^{\pi} i(\theta)\sin 5\theta\, d\theta$$

$$= .9\int_o^{\alpha} A\,\ell_m \sin\theta \sin 5\theta\, d\theta + .45\int_{\alpha}^{(\pi-\alpha)} (B\,\ell_m \sin\theta - C)\sin 5\theta\, d\theta$$

Therefore,

$$I_5 = .9\,A\,\ell_m\int_o^{\alpha} \sin 5\theta \sin\theta\, d\theta + .45\,B\,\ell_m\int_{\alpha}^{(\pi-\alpha)} \sin 5\theta \sin\theta\, d\theta$$

$$- .45\,C\int_{\alpha}^{(\pi-\alpha)} \sin 5\theta\, d\theta$$

But $$\int \sin 5\theta \sin\theta\, d\theta = \frac{\sin 4\theta}{2\times 4} - \frac{\sin 6\theta}{2\times 6}$$

And so, in the above expression

$$\int \sin 5\theta \sin\theta = \frac{1}{8}\sin 4\alpha - \frac{1}{12}\sin 6\alpha$$

and $$\int_{\alpha}^{(\pi-\alpha)} \sin 5\theta \sin\theta = \frac{\sin 4(\pi-\alpha)}{8} - \frac{\sin 6(\pi-\alpha)}{12} - \frac{1}{8}\sin 4\alpha$$

$$+ \frac{1}{12}\sin 6\alpha$$

$$= -\frac{1}{4}\sin 4\alpha + \frac{1}{6}\sin 6\alpha\ .$$

Therefore,

$$I_5 = .9A\,\ell_m\left[\frac{1}{8}\sin 4\alpha - \frac{1}{12}\sin 6\alpha\right] + .45B\,\ell_m\left[-\frac{1}{4}\sin 4\alpha + \frac{1}{6}\sin 6\alpha\right]$$

$$-.18\,C\cos 5\alpha$$

$$= .112\,\ell_m\,[A - B]\sin 4\alpha - .075\,\ell_m[A - B]\sin 6\alpha \; -.18C\cos 5\alpha.$$

In figures 29 A and 30 A are found the results of calculating the harmonics of , and the total RMS current flowing to the CT and the PT , the i/ℓ characteristics having been represented by straight line segments . In figures 29 B and 30 B , the harmonics generated by a segmental core model are compared to the actual figures obtained from tests. (Figures 2I and 22 define the base quantities used for the conversion of per unit to actual quantities). The I80 Hz and 300 Hz curves indicate a fair degree of agreement , while the fundamental curves do not compare well .

4.5 Use of the Average i/ℓ Relationship.

The variables i and ℓ are very often used because of their convenience in many analytical situations. Quantities of interest, currents and voltages, are easily determined if $i = f(\ell)$, rather than, say $H = f(B)$ or $B = f(H)$ is used. The use of the average of the B/H or ℓ/i curves rather than the actual relationship showing hysteresis as in Figures 21 and 22 has the obvious advantage of relative mathematical simplicity. In fact it has been indicated by Swift that, for a ferro-resonant study at least, it is not necessary to model hysteresis or eddy currents, but only saturation where transformer cores are encountered in

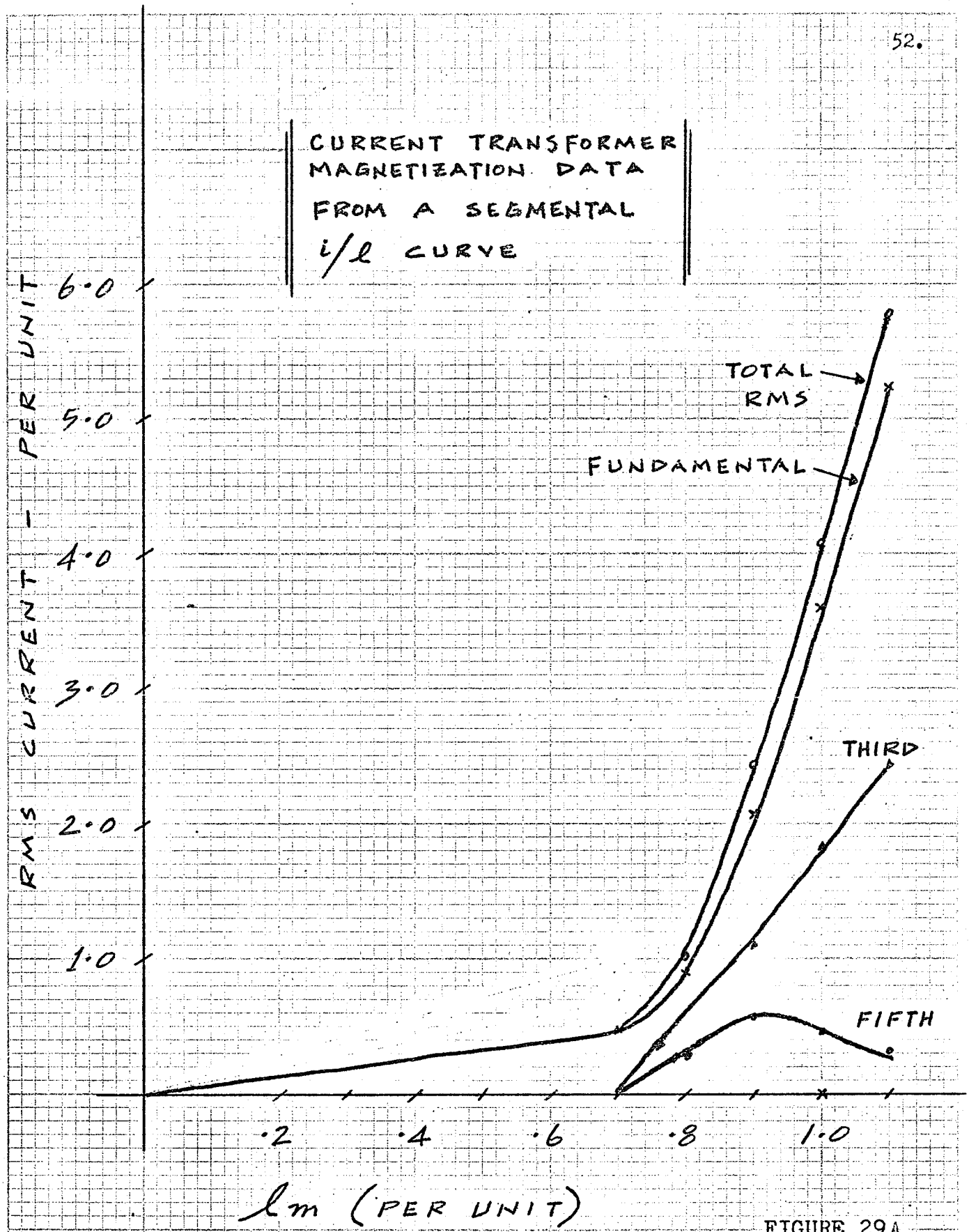

FIGURE 29A

CALCULATED MAGNETIZING AMPS .. (PER UNIT)

FIGURE 29 B

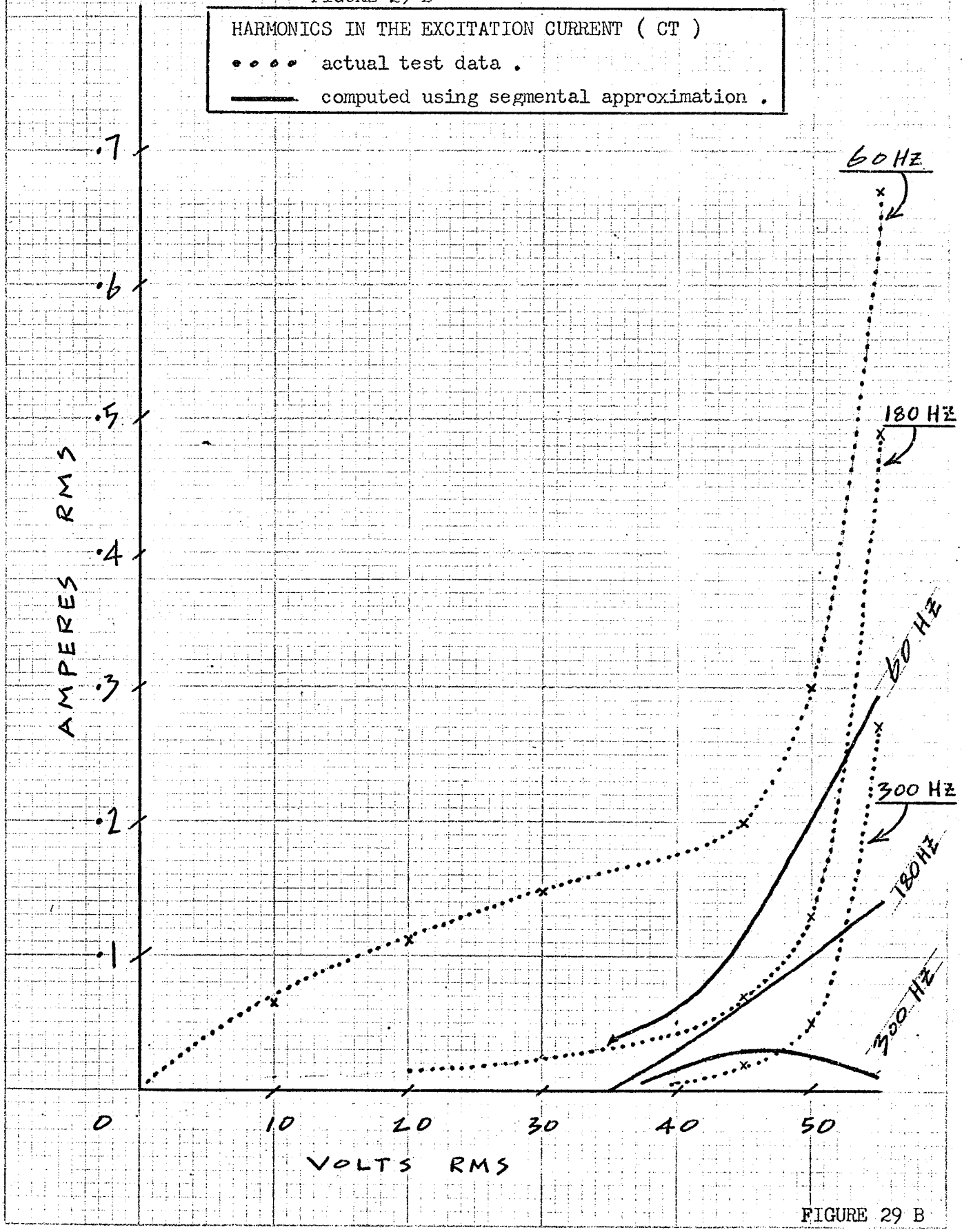

FIGURE 29 B

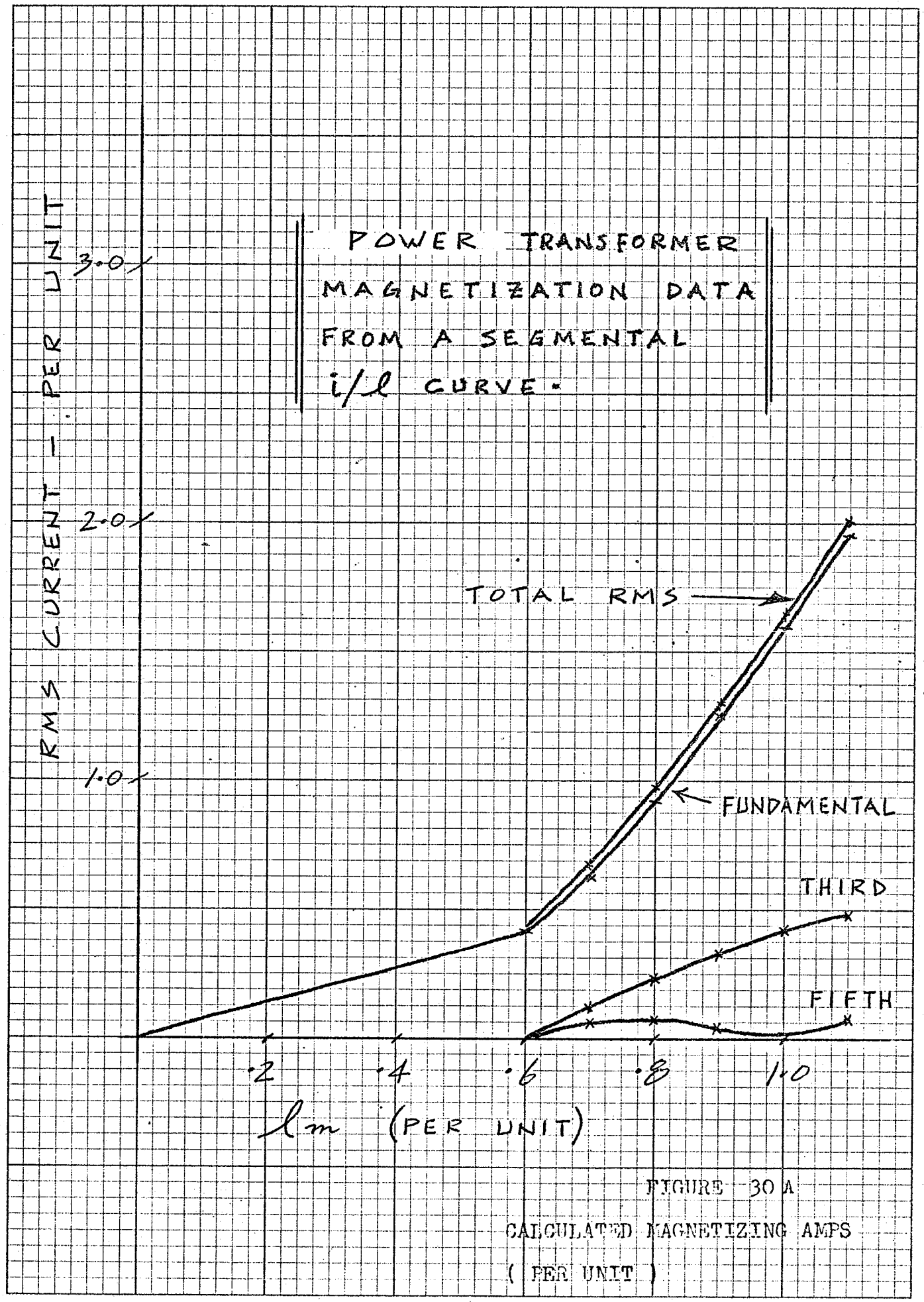

FIGURE 30 A

CALCULATED MAGNETIZING AMPS

(PER UNIT)

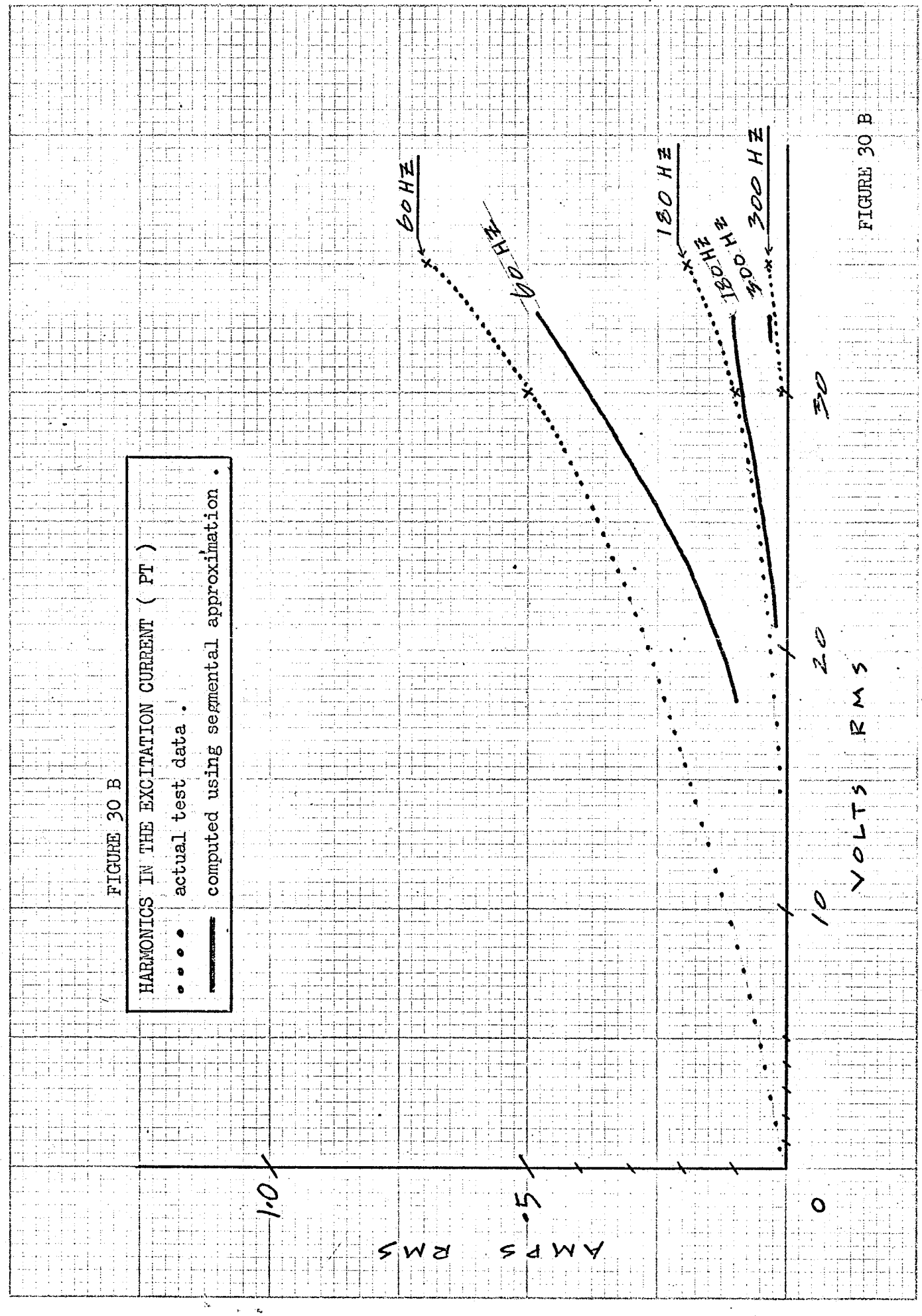

FIGURE 30 B

FIGURE 30 B

a problem. As has been indicated thus far in this thesis, neither real RMS excitation current nor harmonic magnitudes can be accurately predicted from the average of the i/ℓ curves in Figures 21 and 22. Essentially, the reason for this is that the real magnetization current is made up of hysteresis, eddy current, and wattless magnetization components. Even though it is true that the binomial i-ℓ relationship does generate a non zero fundamental current component if a sinusoidal flux linkage is established, (90° out of phase with the ideal coil voltage) , the hysteresis property is not represented, since the i-ℓ equation has zero width. In addition, since the actual B-H curve width is dependent on both hysteresis and eddy current losses, with only the latter being frequency dependent, eddy current losses are improperly modelled.

In the literature, a Russian author named Shankman, (Bibliography, no. 7), has recognized that a binomial of the form $i = A\ell + B\ell^5$ "is sufficiently accurate in practice to approximate the magnetization curve of the transformer", although no reference to core types or sizes was given.

Swift, (Bibliography, No. 10), has established that the binomial $i = \ell + 4\ell^5$ is a good approximation for a typical air cooled, 1.5 kvA, 110v - 110v distribution transformer.

CHAPTER V

THE B-H CURVE DURING AN INRUSH TRANSIENT

The object of this Chapter is to present the results of B-H curve measurements showing transients which resulted when the transformer was switched on when a condition of residual magnetism existed in the core. In addition, no load current component was permitted to flow, i.e., an open circuit transformer existed. The theoretical inrush situation will also be discussed, with the limited use of mathematics.

5.1 Inrush measurements.

The essential elements of the circuit used to obtain these results are shown on Figure B.1, Appendix B. To obtain transient measurements, a switch was placed in series with the winding, the input voltage was preset to some appropriate value, and residual magnetism was established in the core. The closing of the switch must be synchronized with the recording camera's shutter trip, unless the CRO has a beam blanking feature. The film was exposed to the first few cycles of the transient B-H curve. The author took the approach that, after energizing the core, residual flux could be established by opening the switch at some random time, and also that a representative transient could be photographed after very few trials of closing the switch at random. Results seemed to bear this out.

Figure 31 shows tracings of two inrush transient photos for the C.T. It is evident that residual magnetism does cause a very

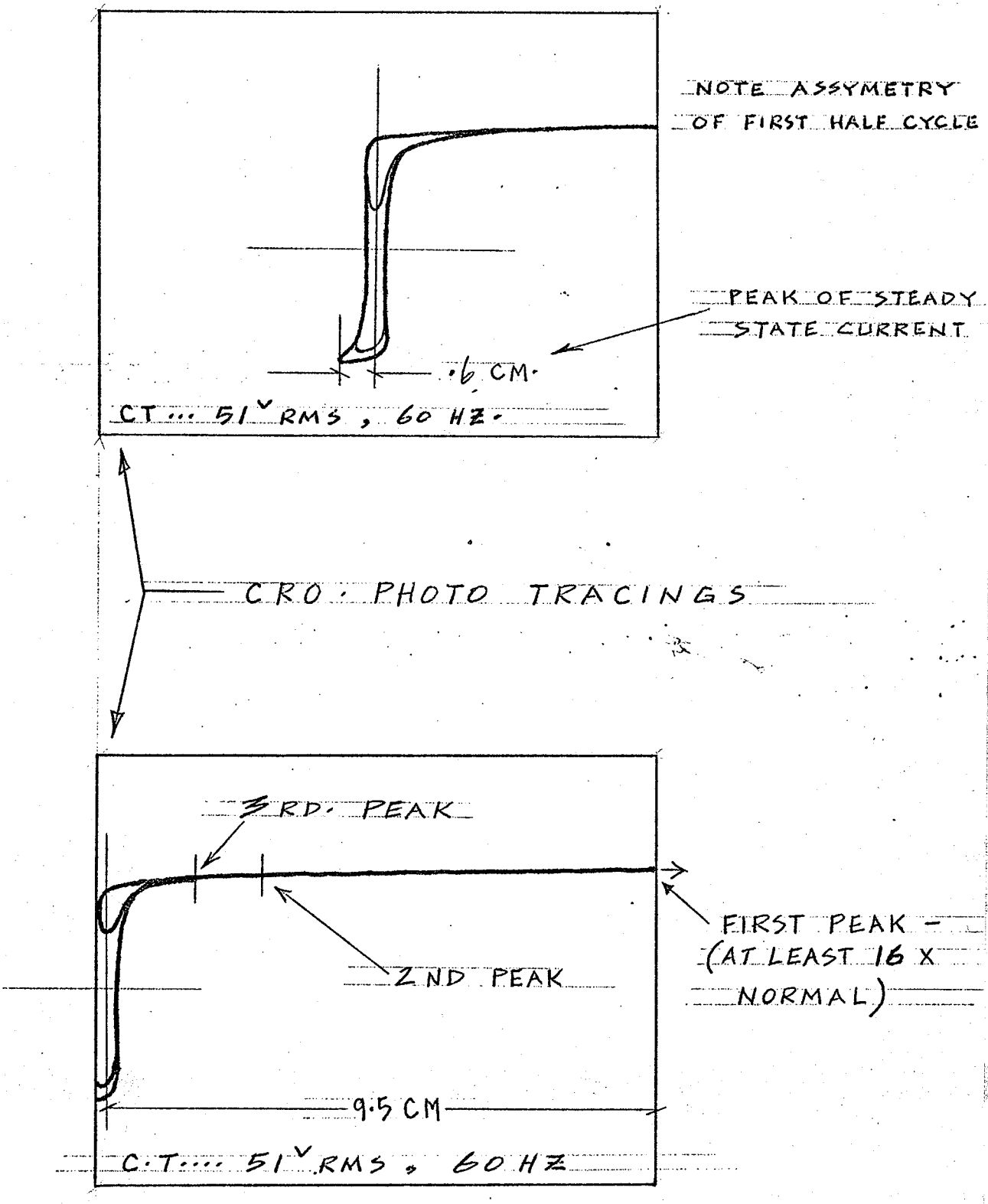

FIGURE 3I

C.T. INRUSH TRANSIENTS

assymmetrical B-H waveform under certain switching conditions. From these particular photos, it is evident that the peak inrush during the first half cycle is at least 16 times the steady state peak for that applied voltage (rated). While it is not implied that this is the maximum possible condition, the photos show that the two peaks which follow are about three, and about two times as large as the steady state value, the rapid decrease attributable to the presence of resistance in the circuit.

In Figure 32, tracings showing the transient B-H curve for the P.T. are presented. Although several photos were taken, the peak measurable inrush was found to be approximately double the steady state value. This seems to indicate that the core residual magnetism was much lower for the P.T. than the C.T. An idea of the possible range for the "residual" flux density may be obtained by referring to Figures 21 and 22. In both of these, maximum residual occurs at the intersection of the B-H curve and the $H = 0$ axis, but its value may lie between $\pm B_r(max)$. It is evident that, relative to the maximum flux density shown in the separate figures, the residual is much higher for the C.T.

5.2 Simplified Analysis of the Most Severe Inrush condition.

The most onerous condition occurs when switching occurs at a voltage zero, so that the increasing flux and the residual have the same direction and therefore add up. For example, assume the functional relationship between current i and flux linkages ℓ shown in Figure 33.

If $e(t) = E_m \sin \omega t$, and since $\ell = N\phi$, and

$$e(t) = N\frac{d\phi}{dt} = \dot{\ell}, \quad \text{thus}$$

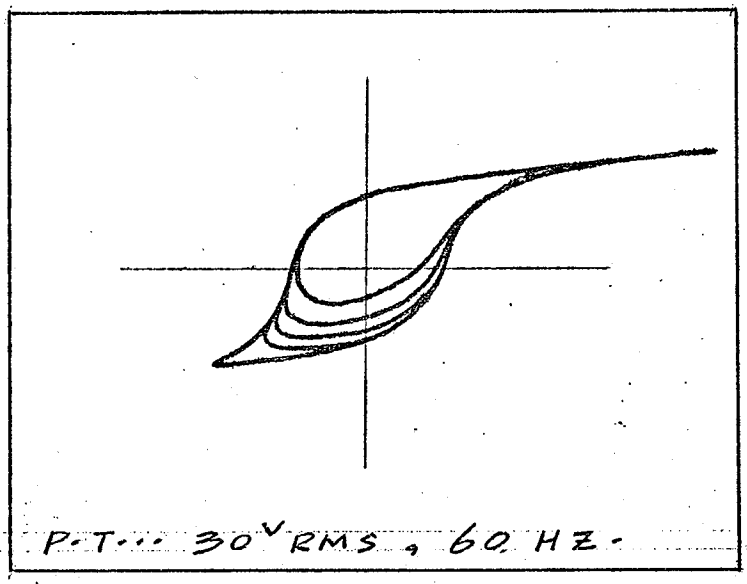

P.T... 30^{V} RMS, 60 HZ.

C.R.O. PHOTO TRACING

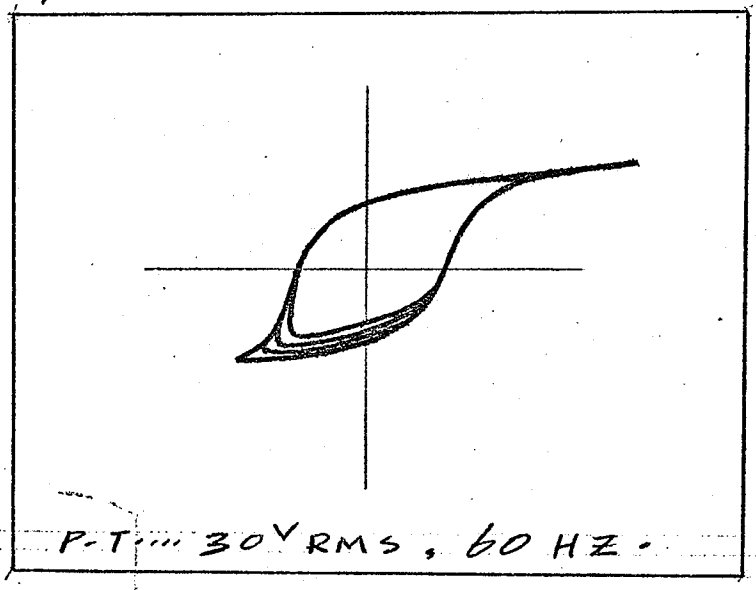

P.T... 30^{V} RMS, 60 HZ.

FIGURE 32

PT INRUSH TRANSIENTS

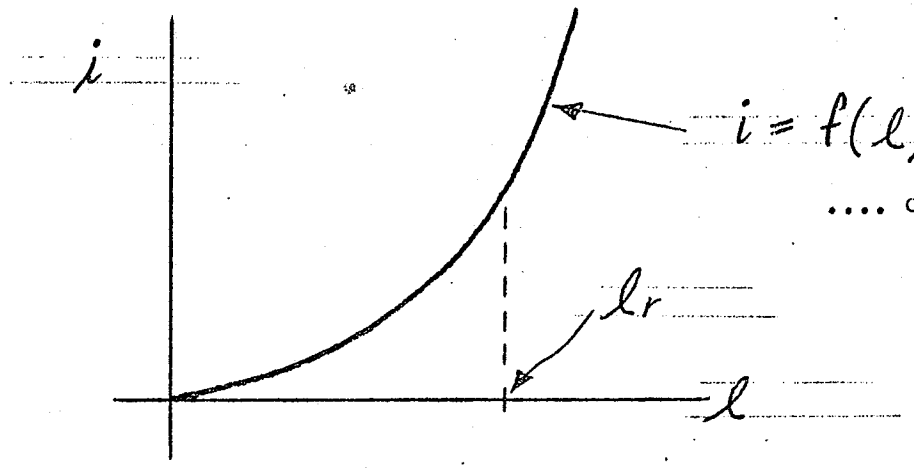

..input voltage..

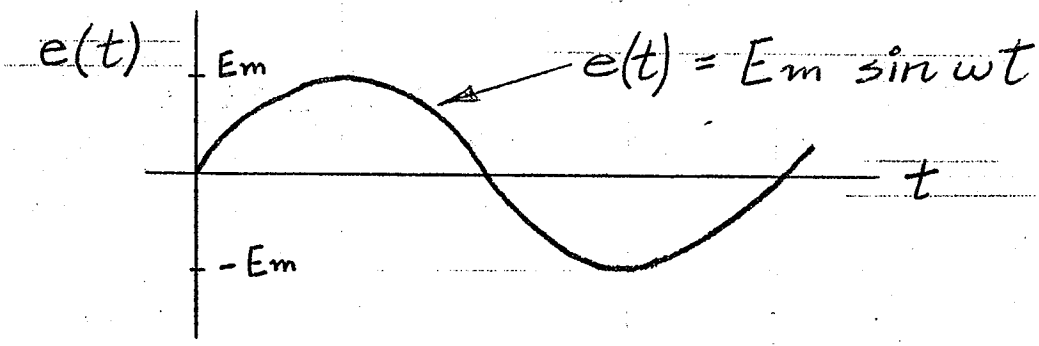

..flux linkages..

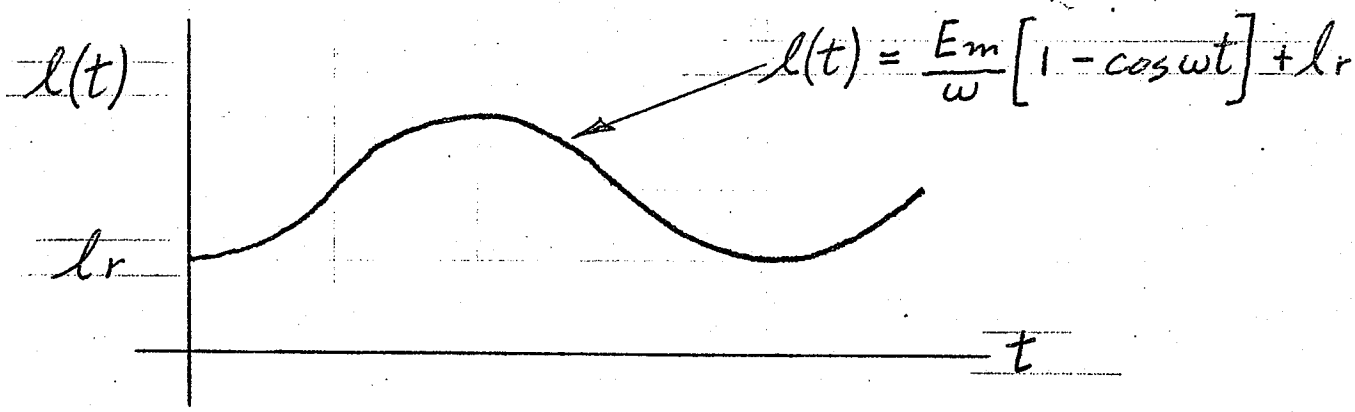

..current..

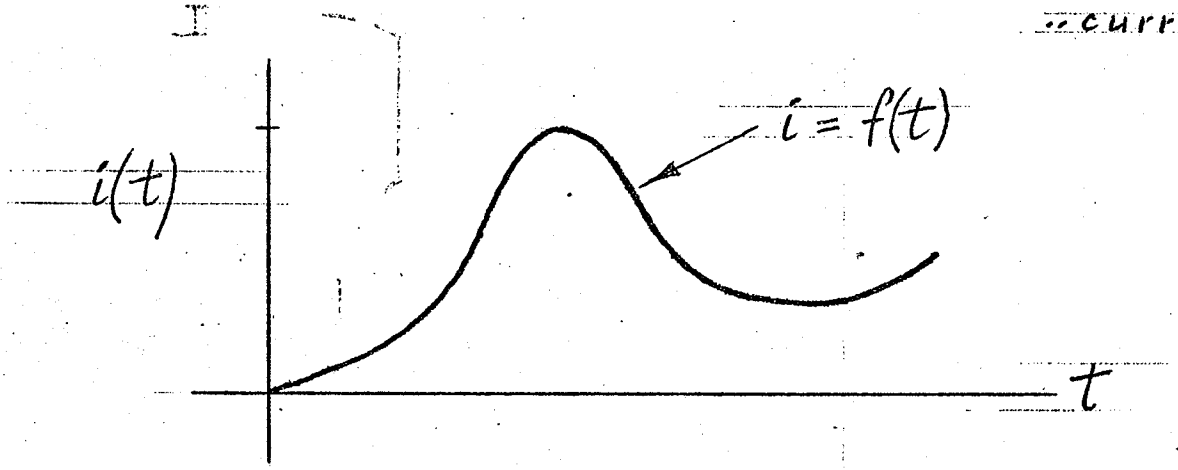

FIGURE 33

SIMPLIFIED INRUSH ANALYSIS

$$\ell = \int e(t)\, dt$$

$$= \int E_m \sin \omega t\, dt$$

$$= \frac{-E_m}{\omega} \cos \omega t + \text{constant}$$

Assume that, for $t = 0$, $\ell = \ell_r$,

thus $$\ell_r = \frac{-E_m}{\omega} (1) + \text{constant}$$

$$\text{Constant} = (\ell_r) + \left(\frac{E_m}{\omega}\right)$$

So, $$\ell = \frac{-E_m}{\omega} \cos \omega t + \frac{E_m}{\omega} + \ell_r$$

or, $$\ell = \frac{E_m}{\omega} [1 - \cos \omega t] + \ell_r$$

This result is shown graphically in Figure 33. More practically, the relationship $i = f(\ell)$, which can be shown to be binomial to a fair degree of closeness, might now be used to find $i(t)$, in particular the peak inrush. It may be appreciated then, why such a large inrush surge may result, for the core may be driven very far into its saturated state on one half cycle. It is the circuit resistance which eventually damps out the assymmetry of the magnetization current.

CHAPTER VI

SUBHARMONIC RESPONSE OF AN OPEN CIRCUIT TRANSFORMER IN SERIES WITH CAPACITANCE AND RESISTANCE

The object of Chapter VI is to present the results of experiments performed to excite subharmonics in the above mentioned series circuit. This will include a description of circuit elements, reproduction of waveforms of voltage and current, as well as the B-H curves when subharmonics exist.

6.1 Second Subharmonic.

In the circuit sketched in Figure 34, it was found that the second subharmonic could be excited by briefly shorting the inductor L, while switch S1 was closed and input voltage V_1 was set to 17 $\pm$ .5 volts RMS, 60 hz. (The reader is referred back to Figure 7 A for magnetization characteristics). It was found that L must be the open circuit C.T., that is, the P.T. did not produce a similar behaviour. Attention is drawn to the fact that this phenomenon occurred at 17 volts, which was only 30% of the assigned C.T. voltage rating. It was not found possible to excite the 30 hz component by closing S1 only, with source voltage set to 17.0 volts and S2 open. In addition, the range of input voltages over which it was possible to excite the subharmonic was very small, in this instance, 1 volt. If the series resistor of Figure 34 was increased by as much as 1 ohm, the subharmonic could not be sustained.

Figure 35 shows a tracing of the voltage across the C.T. while the subharmonic existed in the series circuit. Figure 36 shows the

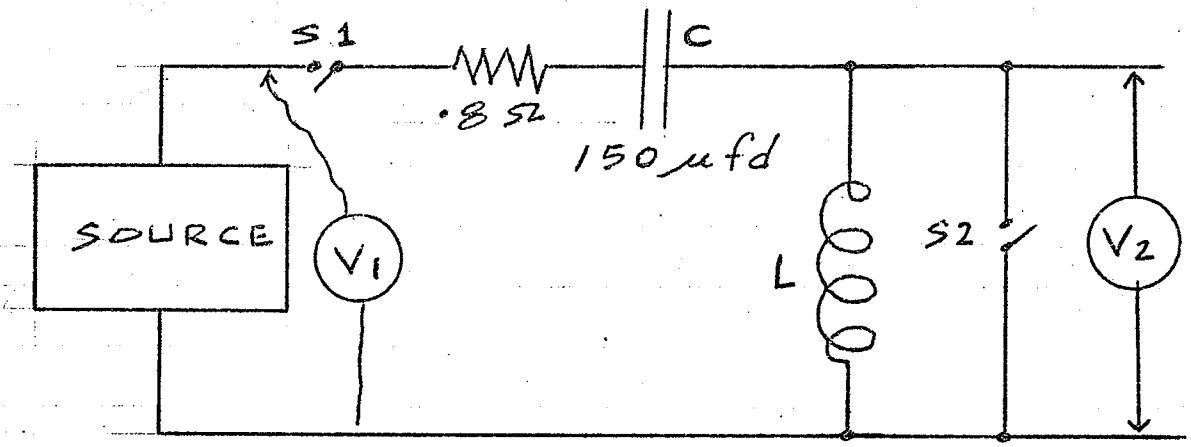

FIGURE 34

THE CIRCUIT OF INTEREST

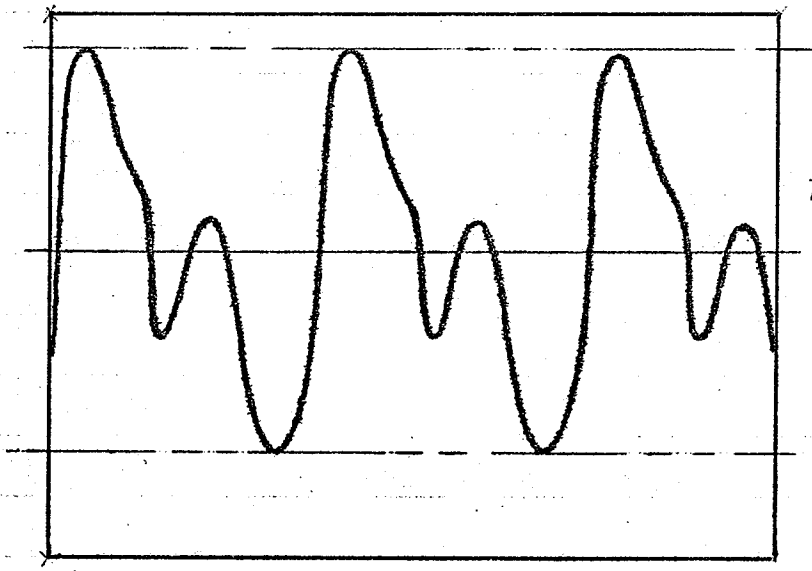

FIGURE 35

INDUCTOR VOLTAGE WHILE THE SECOND SUBHARMONIC EXISTED :

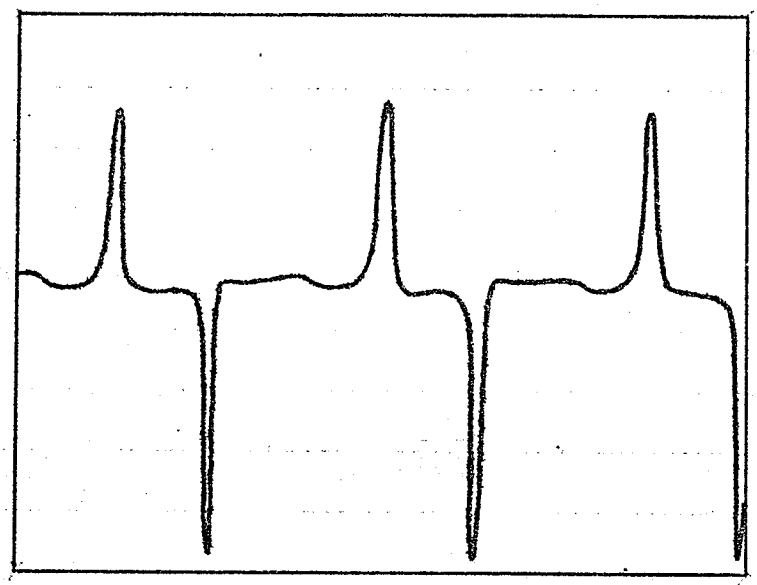

FIGURE 36

CIRCUIT CURRENT , SHOWING

THE SECOND SUBHARMONIC .

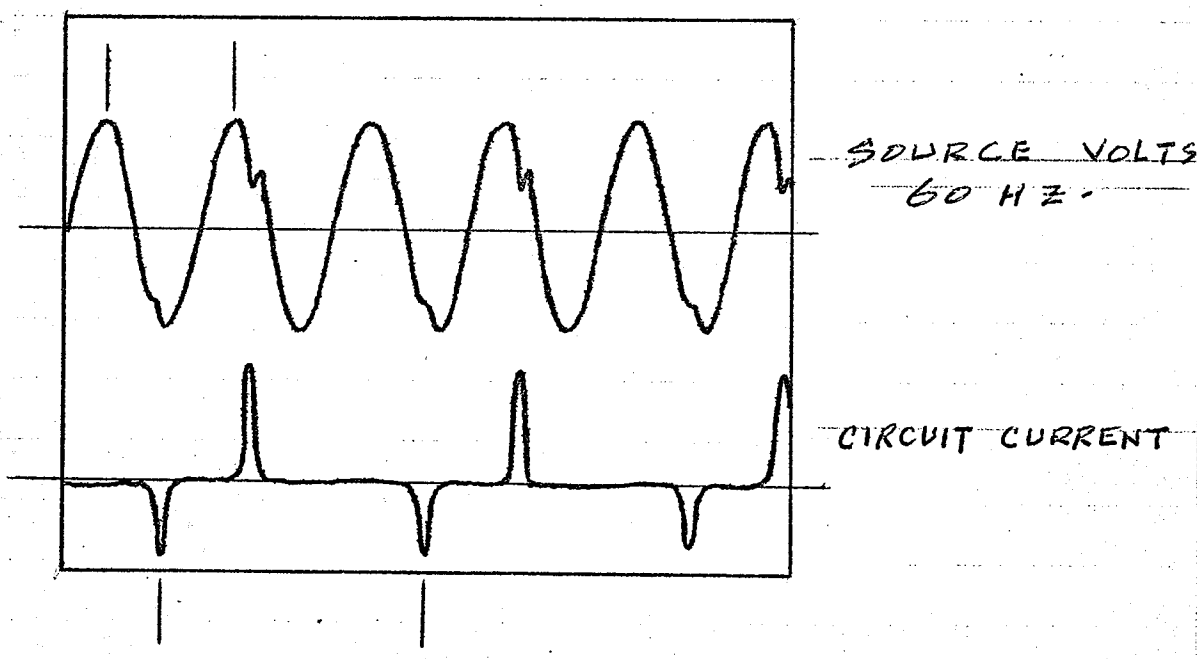

FIGURE 37

MAINS VOLTAGE AND CURRENT

assymmetry in the circuit current waveform, while Figure 37 shows the circuit current at 30 hz against the 60 hz input voltage. Notice that this current caused the main voltage to distort slightly. This was due to voltage drop across the source impedance.

Finally, Figure 38 is a tracing of a B-H curve taken using techniques described in Appendix B. This also shows the assymmetry existing in the C.T. dynamic response. Also in Figure 38, the other stable state of the circuit, that is, the B-H curve at 60 hz, is shown at the same level of input voltage.

6.2 Third Subharmonic.

In the circuit of Figure 34, with the C.T. as the inductance the third subharmonic, at 20 hz, could be excited by briefly closing S2, with the input voltage in the range 20 to 22 v RMS, and C changed to 75 mfd. Again it was found that increasing the series resistance eliminated the possibility of sustaining the 20 hz component after its initiation by the switching transient, and that the critical input voltage was in a very narrow range.

A tracing of the B-H curve plot, taken when the third subharmonic existed is given in Figure 39, in addition to the "normal" 60 hz B-H curve taken at the same input voltage magnitude. The relationship between the voltage waveform and the resulting B-H curve shape may be discussed from the following viewpoint. With reference to Figures 39 and 40, recalling that the integrated C.T. voltage applied as the vertical scope drive has the same waveshape as the actual C.T. voltage, point No. 1 is considered to be the start. As voltage increases from 1 to 2, the B-H curve increases from point 1 to point 2. Voltage decreases from 2 to 3,

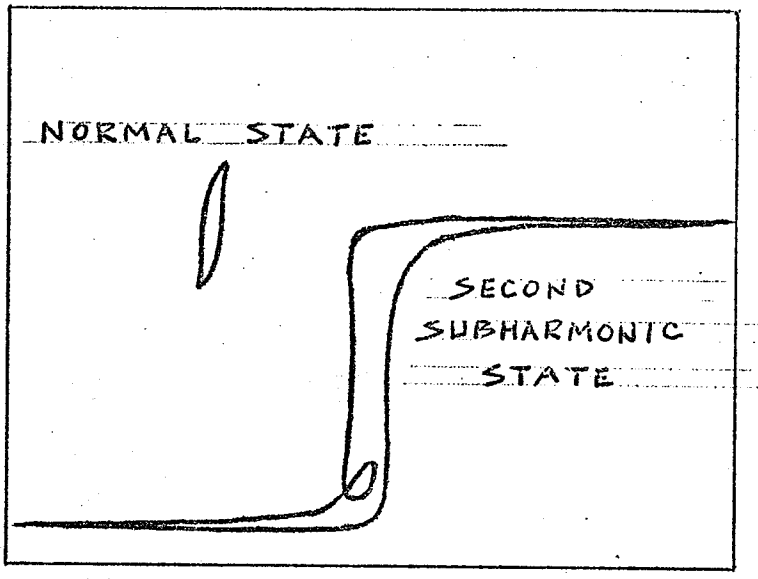

FIGURE 38

BH CURVE WHEN THE SUBHARMONIC EXISTS

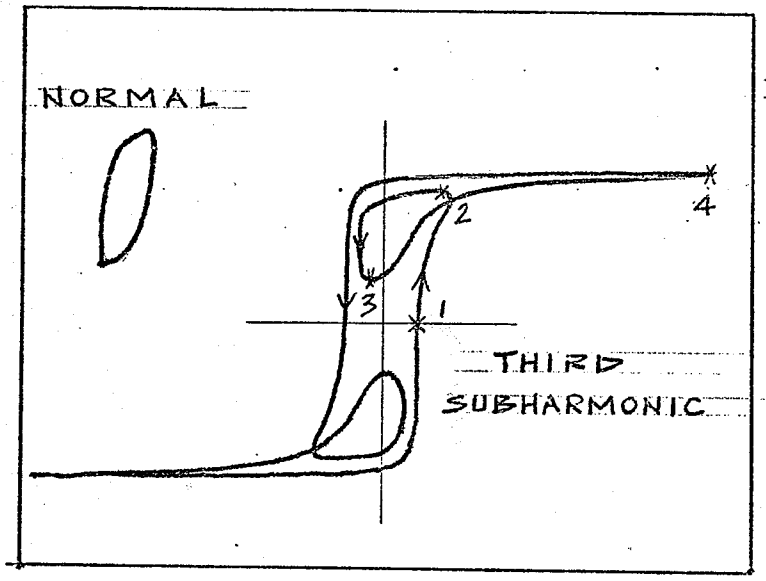

FIGURE 39

BH CURVE WHEN THIRD SUBHARMONIC EXISTS

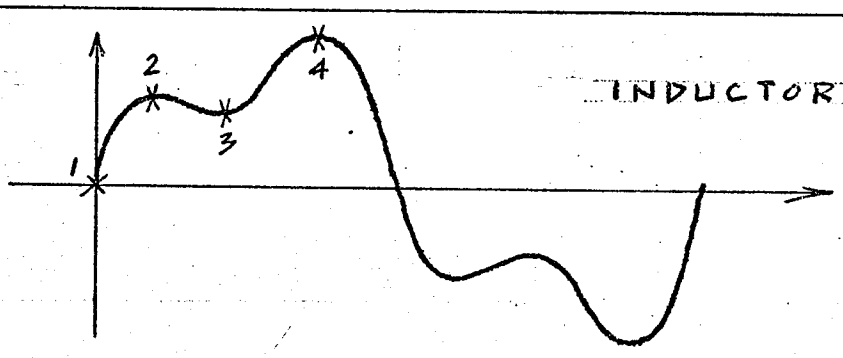

FIGURE 40

the CT voltage

and causes the B-H trace to start through a minor loop from 2 to 3. From 3 to 4, voltage increases to a maximum, causing the B-H curve to go to its extreme right hand limit at 4. At 4 the voltage then begins to drop and quickly goes negative. The B-H loop then follows a normal path as shown by arrows, and the sequence repeats during the negative half cycle of voltage.

It should be noted that although Figure 39 is a photo tracing, Figure 40 (which verifies the waveforms seen on the CRO) was obtained by adding the 60 hz waveform to a 20 hz waveform (with a small phaseshift). The circuit current waveform, of no particular interest, is not shown here.

The writer considers that an attempt at mathematical analysis when circuit subharmonics exist is far beyond the scope and intent of this thesis.

CHAPTER VII

FERRORESONANT RESPONSE OF AN OPEN CIRCUIT TRANSFORMER IN SERIES WITH CAPACITANCE AND RESISTANCE

The various objects of Chapter VII follow. Firstly, the RMS voltage-current characteristics for a specific circuit are presented, showing the ferroresonant condition. Next the analytical problem of predicting ferroresonance is attempted. The technique, taken from the Ph.D. thesis of Swift, requires the reformulation into control system form of equations describing the circuit, then the introduction of the "incremental describing function" and graphical data derived therefrom. The author attempts some original mathematical generalization on the latter topic, before comparing the predicted results to the actual circuit characteristics, thus concluding the thesis.

7.1 R.M.S. Volt-Ampere Characteristics.

The circuit shown in Figure 34 was used to obtained the volt-ampere characteristics shown in Figure 41. The series resistance was .8Ω, the capacitance was 150 mfd, and the inductance was either the C.T. or the P.T. For a slowly increasing input voltage V_1, when the inductor was the C.T., the circuit current was very small until the input voltage reached 47.5V, when the current spontaneously jumped to 10 amps RMS. At the same time, the C.T. voltage jumped 30%, from 47 to 62 v RMS. Here, 47V was defined to be the "critical voltage". If the input voltage was increased further*, current increased almost linearly as indicated in the figure. When the input voltage was decreased, the path of the

* Beyond 47.5 V

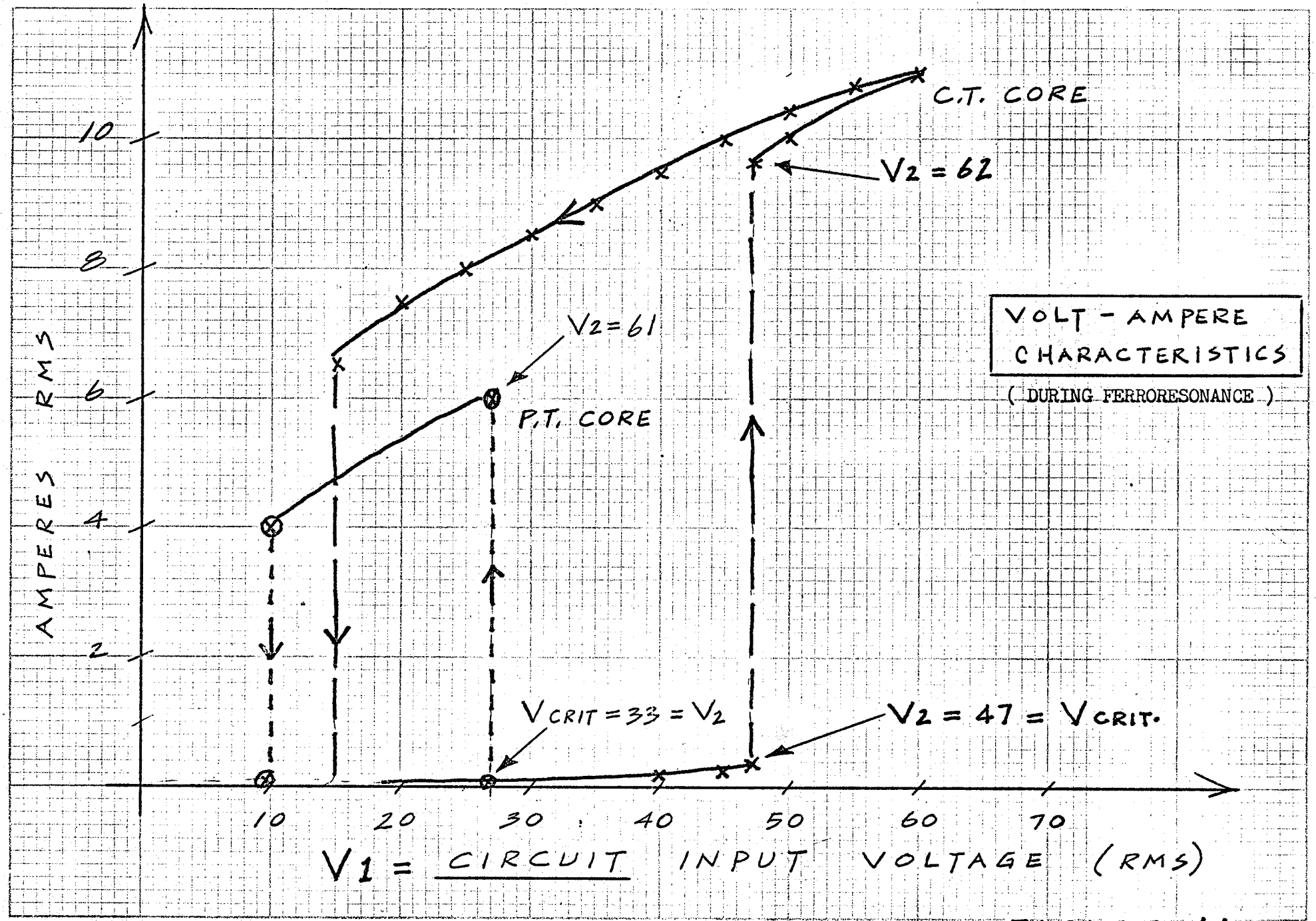
C.T. CORE
$V_2 = 62$
$V_2 = 61$
P.T. CORE
VOLT - AMPERE CHARACTERISTICS
(DURING FERRORESONANCE)
$V_{CRIT} = 33 = V_2$
$V_2 = 47 = V_{CRIT.}$
AMPERES RMS
10
8
6
4
2
10
20
30
40
50
60
70
V_1 = CIRCUIT INPUT VOLTAGE (RMS)

... FIGURE 41 ...

characteristic was not the same as for the increasing voltage. In effect, the circuit had "latched" into the ferro-resonant state. When V_1 had decreased to 15 volts, the ferroresonant condition abruptly ceased, or the circuit returned to the more stable state. The circuit behavior when the P.T. was used as the inductor is also shown on Figure 41. Of interest is the fact that the P.T. voltage jumped 88% from a critical value of 33 to 61 V RMS. Referring back to Figure 7A, it is seen that the critical voltages for both cores were located on the "knee" of the magnetization curves, and were very close to the defined voltage ratings for both cases.

As the data of Figure 41 would indicate, two stable states for the circuit containing the C.T. existed as long as the input voltage was higher than about 15, and lower than about 47 V RMS. Experiments were done to force the circuit to jump from the stable state denoted by the lower line to the ferroresonant state on the higher line, within the previously mentioned voltage limits. This jump could be initiated by briefly shorting the inductance, as in the subharmonic experiments, or by closing switch S1 of Figure 34 with the input voltage V_1 set to certain values, and under certain initial circuit conditions. The latter procedure was taken over a number of trials and it was found that the lowest input voltage that would initiate ferroresonance was 32.5 V RMS with no residual magnetism permitted. When residual magnetism was created, the ferroresonant condition could be caused by as low as 24 V RMS, on about 30% of the switching trials.

It is noteworthy that, if the C.T. is the circuit inductance, it is possible, on a certain number of trials, to initiate the second subharmonic for an input of 17 $\pm$ .5 V RMS, while the third subharmonic

can be caused with an input of 21 ± 1 V RMS, and ferroresonance can result from 24 V RMS up to the circuit limit, subject to the proper switching procedures.

In a more general sense, it was determined experimentally that the "critical voltage", the voltage existing across the iron cored coil just prior to a jump into ferroresonance, increased as the capacitance was increased. This was experimentally indicated for capacitance ranging from 25 to 300 mfd, and the C.T. inductance. For example, for C = 300 mfd, the critical voltage was 53 V RMS, while for C = 25 mfd, it was 45 V RMS.

7.2 Analytical Prediction of Ferroresonant Behavior in the Series R-L-C Circuit.

Although it was demonstrated by experiment that the likelihood of ferroresonance was increased if residual magnetism existed, in the following discussion, no initial condition will be considered. The circuit of interest is redrawn for convenience in Figure 42. The problem involves predicting the "critical voltage" V_2 across the transformer winding, and also the final voltage attained once ferroresonance has occurred. Knowing the critical voltage, the circuit input voltage which would cause ferroresonance could be found using phasor techniques if magnetization data were available for the transformer. The author appreciates that the likelihood of finding a series R-L-C circuit in a practical power circuit is very small, but his wish at this point is to examine a suggested analytical technique.

The normal analytical techniques for finding voltages in the series RLC circuit are complicated by the extremely non-linear relationship between voltage (or flux density) and current (or MMF) in the iron

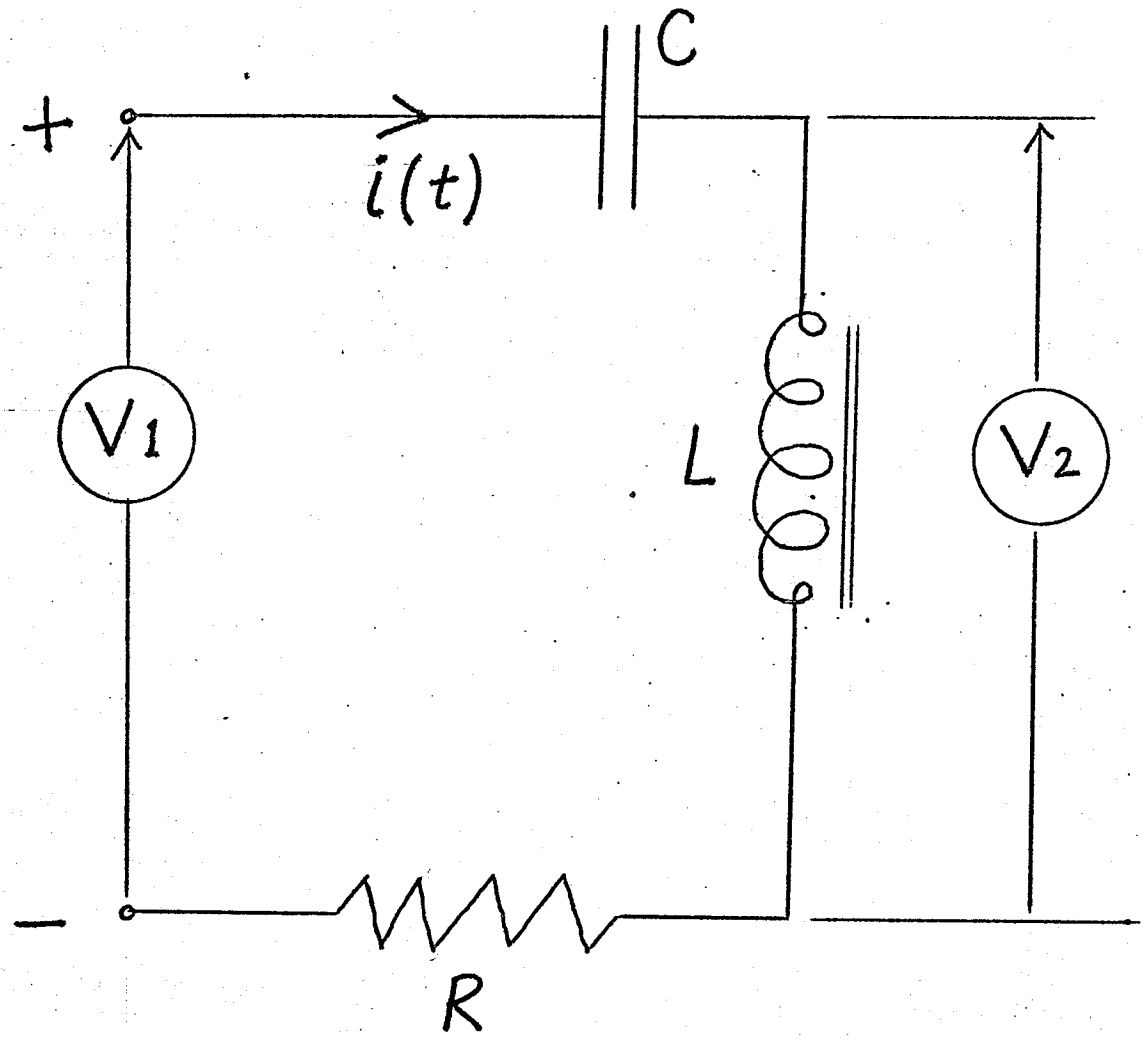

THE CIRCUIT OF INTEREST

FIGURE 42 ..

cored inductance. In fact we know that, to be strictly rigorous, saturation, eddy current losses, and hysteresis must all be considered. A nonlinear analytical approach, using certain simplifications, will be presented.

7.2.1. Reformulation Into Control System Configuration.

This analysis has as its basis the assumption of a binomial relationship between current and flux linkages in the iron cored inductor. The relationships between V_1, I, R, C and flux linkages (ℓ) in Figure 42 can be expressed as follows, in the time domain.

$$V_1 = i\,R + \frac{1}{C}\int i\,dt + N\frac{d\phi}{dt}$$

This may be rewritten in the Laplacian domain, and the flux linkages variable (ℓ) introduced by recalling that $\ell = N\phi$, thus

$$\frac{d(\ell)}{dt} = N\frac{d\phi}{dt} = V_2(t)$$

$$V_1(s) = IR + \frac{I}{sC} + sL$$

So
$$L = \frac{V_1(s)}{s} - I\,\frac{R + \frac{1}{sC}}{s}$$

To be expressed in a block diagram form, the relationship between current and flux linkages,

$$i = \ell + C_5\,\ell^5.$$

must be put into the Laplacian domain:

$$I = L + C_5 L^5$$

Figure 43 is the result, in block form, of relating the previous two Laplacian equations. It remains now to show how this reformulation can lead to an analytical solution.

7.2.2. The Incremental Describing Function.

Nonlinear control system analysts have developed techniques involving the incremental describing function to examine the stability of a system which is driven, i.e., a forced system. (Reference # I9)

Referring to Figure 43, notice that L_1 is sinusoidal (since V_1 is thus), and it may be shown that L_2 is essentially sinusoidal due to the low pass filter properties of G. The difference $L = L_1 - L_2$ may be said, therefore, to be sinusoidal. The nonlinearity input, L, is then expressed in the following form, as a time function.

$$\ell = \ell_m \cos(\omega t + \phi) + u \cos \omega t$$

Expressed thus, ℓ_m is assumed constant, and $u << \ell_m$ (the second term is called the disturbance, and can have any phase relationship with the first term). To linearize the problem, we require the ratio of that part of the nonlinearity output phasor involving the disturbance to the magnitude of the disturbance itself, and this ratio we call the "incremental describing function".

In order to generalize the discussion, assume that the nonlinearity can be expressed in the following polynomial form:

$$i = C_1 \ell + C_3 \ell^3 + C_5 \ell^5 + \ldots + C_n \ell^n$$

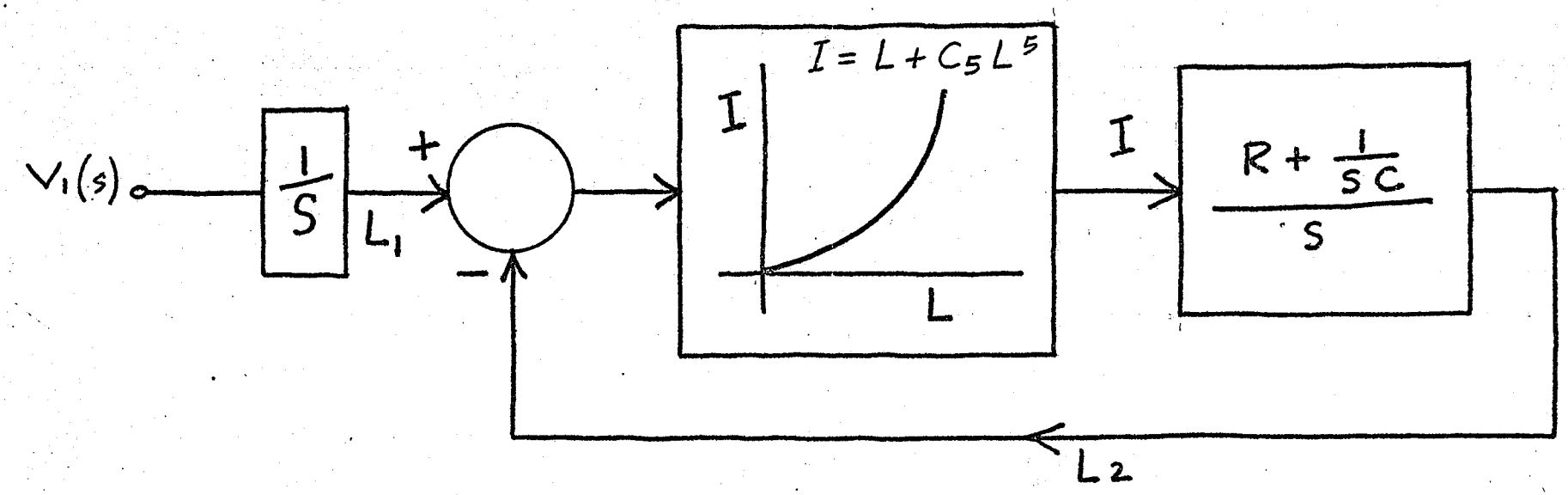

BLOCK DIAGRAMS

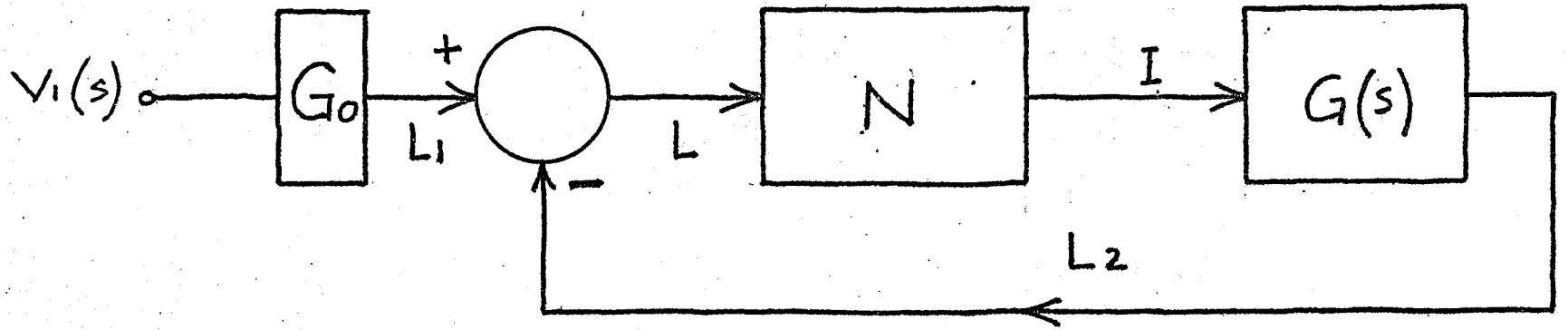

FIGURE 43

REFORMULATION INTO CONTROL SYSTEM FORM

Since the general term $C_n \ell^n$ involves a binomial expansion, the input to the nonlinearity will be expressed in the following way:

$\ell = a + b$, where

$a = \ell_m \cos(\omega t + \phi)$, and

$b = u \cos \omega t$, thus

$$\ell^n = (a + b)^n = a^n + n a^{n-1} b + \frac{n(n-1)}{2!} a^{n-2} b^2$$

$$+ \frac{n(n-1)(n-2)}{3!} a^{n-3} b^3 + \ldots \text{ etc.}$$

This series will converge for $b^2 < a^2$, this requirement being met by the stipulation that $n \ll \ell_m$, and the assumption that ϕ is a small angle, that is, the disturbance <u>will</u> occur at the peak of the input voltage, since we say it <u>can</u>. We are concerned only with the second term of the series expansion, because the first term does not involve $b = f(u)$ and the third and succeeding terms involve only higher powers of u, which are neglected. Thus, in terms of the increment

$$C_n \ell^n (u) = C_n [n a^{(n-1)} b]; \text{ and}$$

substituting for a and b;

$$C_n \ell^n(u) = [n \ell_m^{n-1} \cos^{n-1} (\omega t + \phi) u \cos \omega t] C_n$$

$$= [n u \ell_m (n-1)][C_n] \cos^{(n-1)} (\omega t + \phi) \cos \omega t.$$

Since n must be odd (a requirement of the ℓ/i relationship is odd symmetry), (n - 1) is even. It may be shown by Fourier analysis that, if (n - 1) is even;

$$\cos^{(n-1)}(\omega t + \phi) = A_1 + A_2 \cos 2(\omega t + \phi)$$

$$+ A_4 \cos 4(\omega t + \phi) + \ldots + A_{(n-1)} \cos (n-1)(\omega t + \phi),$$

where A_1, A_2, A_4 etc. are Fourier coefficients associated with the expansion of $\cos^{(n-1)}(\omega t + \phi)$. But the following product is required:

$$[\cos^{(n-1)}(\omega t + \phi)] \cdot [\cos \omega t] = A_1 \cos \omega t + A_2 \cos 2(\omega t + \phi) \cos \omega t$$

$$+ A_4 \cos 4(\omega t + \phi) \cos \omega t + \ldots$$

$$+ A_{(n-1)} \cos [(n-1)(\omega t + \phi)] \cos \omega t.$$

In the last expression, only fundamental frequency terms will be retained, since the incremental describing function is based on a phasor ratio, the fundamental frequency part of the output phasor divided by the input (both numerator and denominator being expressed in terms of the increment u). That is, only the first two terms of the last expression are retained, or

$$[\cos^{(n-1)}(\omega t + \phi)] \cos \omega t \doteq A_1 \cos \omega t + A_2 \cos 2(\omega t + \phi) \cos \omega t.$$

This may be further expanded by use of trigonometric relationships.

$$\cos^{(n-1)}(\omega t + \phi)\cos\phi t = A_1 \cos\phi t$$

$$+ A_2 \times \frac{1}{2}[\cos(3\omega t + 2\phi) + \cos(\omega t + 2\phi)] .$$

After once again dropping the non fundamental frequency terms,

$$\cos^{(n-1)}(\omega t + \phi)\cos\omega t = A_1 \cos\omega t + \frac{A_2}{2}\cos(\omega t + 2\phi)$$

And finally,

$$C_n \ell^n(u) = (C_n)\, n\, u\, \ell_m^{(n-1)} \cos^{(n-1)}(\omega t + \phi)\cos\omega t$$

$$= C_n\, n\, u\, \ell_m^{(n-1)} \left[A_1 \cos\omega t + \frac{A_2}{2}\cos(\omega t + 2\phi)\right]$$

The only restriction on this last result is that $n > 1$. The coefficients A_1, A_2, etc., may be found in Appendix C. Expressed as a phasor, the last expression becomes

$$C_n\, n\, u\, \ell_m^{(n-1)}\left[A_1 + \frac{A_2}{2}\, e^{j\,2\phi}\right]$$

But the incremental describing function is, by definition, the ratio

$$\frac{C_n \ell^n(u)}{u} = n\, C_n \ell_m^{(n-1)}\left[A_1 + \frac{A_2}{2}\, e^{j\,2\phi}\right]$$

As an example, suppose the non linearity were represented by the binomial $i = C_1\ell + C_5\ell^5$. Expressed as a phasor involving u,

$$C_5 \ell^5(u) = 5\, u\, C_5\, \ell_m^4 \left[\left(\frac{3}{8} \right) + \frac{\left(\frac{1}{2} \right)}{2}\, e^{j\, 2\phi} \right]$$

The first term (n = 1) is treated as follows: If $i = C_1 \ell$; then

$$i = C_1 [\ell_m \cos(\omega t + \phi) + u \cos \omega t]$$

and $i(u) = C_1\, u \cos \omega t$; or as a phasor

$$I(u) = C_1 u = 1 \times C_1\, u$$

Now, considering both terms

$$I(u) = C_1\, u + 5\, u\, C_5\, \ell_m^4 \left[\frac{3}{8} + \frac{1}{4} e^{j\phi 2} \right]$$

$$= u\left[C_1 + 5\, C_5\, \ell_m^4 \times \frac{3}{8} \right] + u \left[\frac{5}{4} C_5 \ell_m^4\, e^{j\, 2\phi} \right]$$

$$+ u\left[C_1 + \frac{15}{8} C_5\, \ell_m^4 + \frac{5}{4} C_5\, \ell_m^4\, e^{j\, 2\phi} \right]$$

Now, applying the definition of the incremental describing function, or "IDF":

K_e = IDF [Quintic binomial] = I(u)/u;

or

$$K_e = C_1 + \frac{15}{8} C_5\, \ell_m^4 + \frac{5}{4} C_5\, \ell_m^4\, e^{j\, 2\, \phi}$$

For another illustration, suppose the current-flux linkages relationship were

$$i = C_1 \ell + C_7 \ell^7$$

From the general expression

$$C_7 \ell^7(u) = 7\ u\ C_7\ \ell_m^6\ [A_1 + \frac{A_2}{2} e^{j\ 2\phi}]$$

From the expansion for $\cos^6(x)$ in Appendix C, $A_1 = 10/32$, and $A_2 = 15/32$.

Thus

$$C_7 \ell^7(u) = 7\ u\ C_7\ \ell_m^6 [\ \frac{10}{32} + (\ \frac{15}{64}\ )\ e^{\ j\ 2\phi}]$$

Using an argument previously developed, $C_1 \ell(u) = u\ C_1$

So,

$$I(u) = u[\ C_1 + \frac{70}{32}\ C_7\ \ell_m^6 + \frac{105}{64} C_7\ \ell_m^6\ e^{\ j\ 2\phi}]$$

Again, K_e = IDF [septic Binomial]

= I(u)/u; or

$$K_e = C_1 + \frac{70}{32} C_7\ \ell_m^7 + \frac{105}{64} C_7\ \ell_m^6\ e^{\ j\ 2\phi}$$

Further, given the polynomial relationship between i and ℓ,

$$i = C_1 \ell + C_3 \ell^3 + C_5 \ell^5 + C_7 \ell^7 + \ldots;$$

it may be shown that the IDF has the general form

$$K_e = A + B\, e^{j2},$$

where A and B are constants. This is so since it has been shown that the IDF for the term $C_n \ell^n$ is equal to

$$n\, C_n\, \ell_m^{(n-1)} \left[A_1 + \frac{A_2}{2} e^{j\,2\phi}\right]$$

7.2.3 The Stability Criterion.

Referring to Figure 43, it may be considered that the IDF is the incremental gain of the nonlinearity N for the disturbance 'u'. Since G(s) is a linear block, if the vector $(K_e) \times (G)$ is formed and encloses the (-1, 0) point for any frequency, established stability theory states that the increment is an unstable one. That is, the critical value for the flux linkages ℓ_m may be found by setting

$$(K_e)(G) = -1$$

so

$$G = -1/K_e$$

Now $-1/K_e$ may be plotted for the variable ℓ_m, and $G(j\omega)$ may be plotted on the same coordinates since the circuit to be verified has constant inductance, resistance, and capacitance. Intersections indicate points where ferroresonance should occur. It is shown in Appendix D that $-1/K_e$ produces families of circles for various ℓ_m, with centres at $(A/B^2 - A^2)$, and radii of $(B/B^2 - A^2)$. And since $G(s) = \frac{R}{s} + \frac{1}{s^2 C}$; $G(j\omega) = \frac{R}{j\omega} - \frac{1}{\omega^2 C}$, the locus of which may be plotted for varying ω.

7.2.4. The Real Circuit

The circuit used is shown in Figure 42, with R = 1.0 ohm; C = 150 mfd, and L = power transformer described in Chapter I.

Base quantities were chosen as follows: Base frequency = 60 hz; instantaneous base current = .25 amps (from i/ℓ or B/H photos), therefore RMS base = $.25/\sqrt{2}$ = .177; base voltage = 30 VRMS, since 30 VRMS applied to the P.T. produces ℓ_m = 1.0 pu by definition. Thus a base impedance can be determined:

$$Z_b = V_b / I_b = 170 \text{ ohms}$$

And since $Z_b = 1/\omega_b \times C_b$,

$$C_b = (10^6/377 \times 170) = 15.6 \text{ mfd.}$$

again, $$G(s) = \frac{1 + SRC}{C s^2} = \frac{R}{s} + \frac{1}{s^2 C}$$

$$G(j\omega) = \frac{1 + j\,\omega\, RC}{-\omega^2 C}$$

But $$R_{pu} = 1/170 = .006$$

$$\omega_{pu} = 2\pi \times 60 / 2\pi \times 60 = 1.0$$

$$C_{pu} = 150/15.6 = 9.63$$

So $$G(j1) = \frac{1 + j(.0577)}{-1 \times 9.63} = -.104 - .006\, j$$

The IDF is found from the estimated Binomial relationship between i and ℓ_m for the P.T.

$$i = \ell_m + 1.8\ \ell_m^5; \quad \text{and is}$$

$$K_e = (1 + 3.43\ \ell_m^4) + (2.29\ \ell_m^4)\ e^{j\ 2\phi}$$

$$= A = B\ e^{j\ 2\phi}$$

The family of circles resulting from the inversion of K_e is found in Figure 44, and a particular value of $G(j\omega)$, $\omega = 1.0$ is plotted on this curve. It is seen that $G(J1)$ lies at the intersection of the $\ell_m = 1.1$ & 1.8 pu circles, which indicates that the critical P.T. voltage is $1.1 \times 30 = 33$V and the final voltage is 54V RMS. In the test described in 7.1, voltage jumped from 33V to 61 V RMS. This agreement is creditable, considering all the approximations involved in arriving at an analytical solution.

The analytical technique presented in Figure 41 permits some generalizations to be made, a few of which follow. In the series RLC circuit, with C and L fixed, ferroresonance can exist only for a very narrow range of resistances. In this example, ferroresonance <u>can</u> occur for $0 < R < .08$ pu, or $0 < R < 13$ ohms, although it is evident that, the higher the resistance, the smaller is the possible voltage jump. In addition, for fixed R and L, the critical voltage <u>decreases</u> as C decreases, with a variable lower limit of 80 to 90% of rated voltage (the so called "knee" of the magnetization curve). For example, under test conditions, it was not found possible to excite the ferroresonant state when C was 37.5 mfd or below.

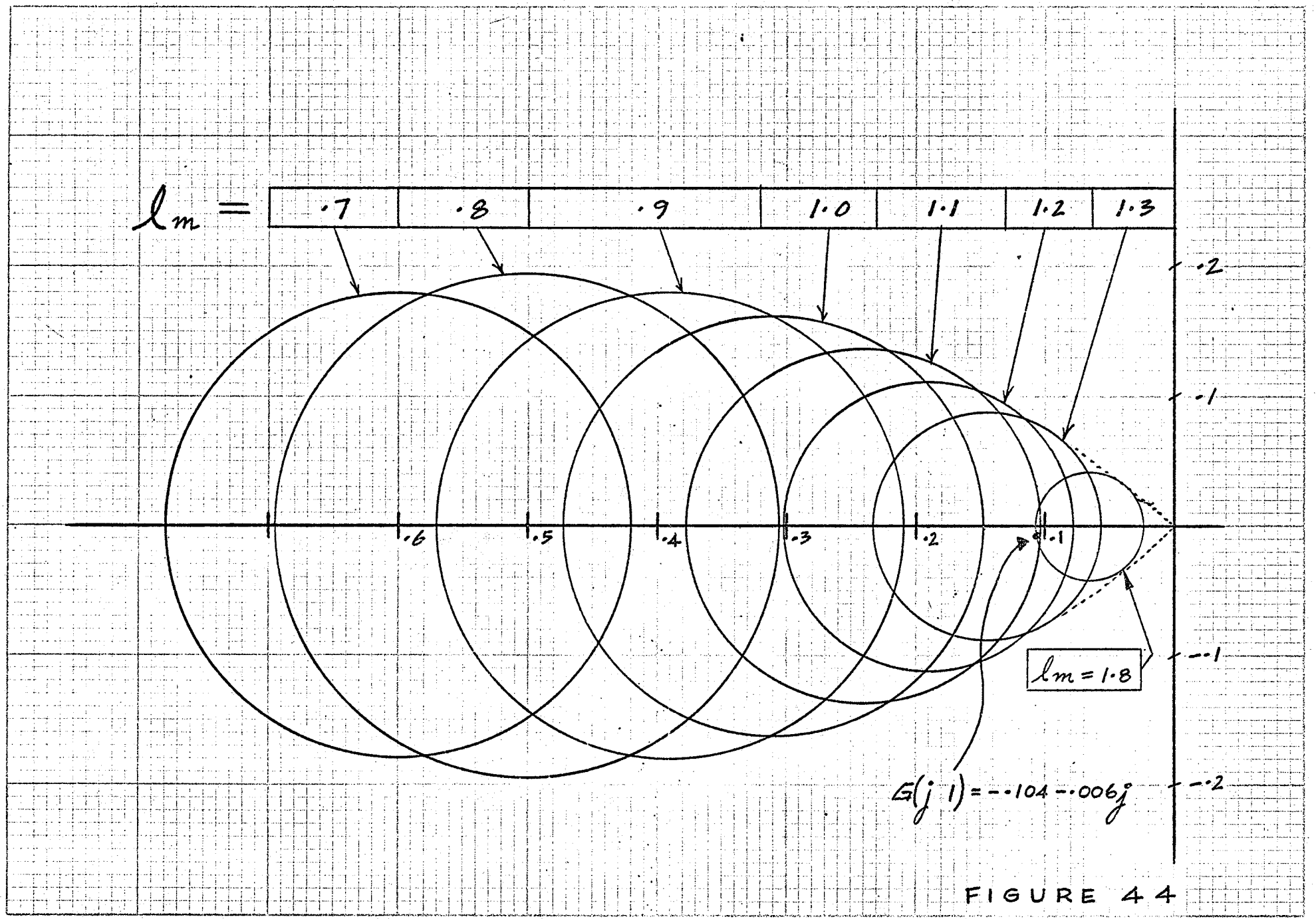

FIGURE 44

DETERMINATION OF CRITICAL VOLTAGE

7.3 Concluding Comments.

The electrical behaviour of two extreme transformer core types has been analyzed, and the relevant measurement techniques have been fairly thoroughly examined. It has been verified that a binomial equation, $i = A\ell + B\ell^n$, will, for these core types, provide a fairly good approximation to the saturation aspect of the fundamental current-flux linkage relationship if $n = 5$ or 7, and with A and B appropriately chosen.

A fairly large discrepancy was shown to exist between the RMS magnetization characteristics as calculated from the i-ℓ relationship above, and the test characteristics.

The second and third subharmonics were experimentally excited and recorded for one of the test transformers in a series R-L-C circuit.

Analytical prediction of ferroresonance was shown to agree fairly closely with test results.

It might be argued that the choice of the rarely encountered series RLC circuit for the various experiments was a poor one, but the intent was to examine the analytical method, not necessarily the practicality of the network.

One fairly obvious extension of this work might be to photograph the B-H loop for a large power transformer in the factory, then to estimate the i-ℓ relationship and compare results to smaller equipment. In the light of the increasing number and complexity of acceptance tests now performed, and as ferroresonant problems become better understood by utilities, it may be that photographs of the B-H relationship become standard test requirements.

APPENDIX A

HARMONIC COMPONENT MEASUREMENT

A schematic diagram of the technique used is found in Figure A.1. Harmonic analysis is accomplished in the following way. If the "current coil" of the wattmeter, which is the higher capacity, fixed member of the electrodynamometer movement, is allowed to carry the excitation current (containing a fundamental & odd harmonics), a torque can be created on the moving coil only when the voltage circuit carries current which has a frequency exactly the same as the fundamental or any of the existing harmonics. In practice, the oscillator frequency is set as close as possible to the component of interest, this being indicated by wattmeter needle motion. Since the wattmeter is calibrated in terms of $V\ I \cos\theta$, if $V = V_2(\text{RMS})$ is known (and is distortionless) and the maximum wattmeter deflection is recorded ($\cos\theta = 1.0$); the harmonic of interest is just $I_n = W(\max)/V_2$. Several sources of error could arise. The pointer motion should be made as slow as possible to prevent overshoot due to the inertia of the movement. Several trials can establish the maximum deflection quite closely.

For higher harmonics, the self inductance of the voltage circuit, found in this instance almost entirely in the series wire wound resistance, could introduce an error in the maximum indication. That is, if V_2 were fixed in magnitude, the increased impedance of the voltage circuit would cause the current in the moving coil to be in error on the low side. The total inductance of the voltage circuit (in the wattmeter used) was measured to be 22 mh, while the total voltage circuit

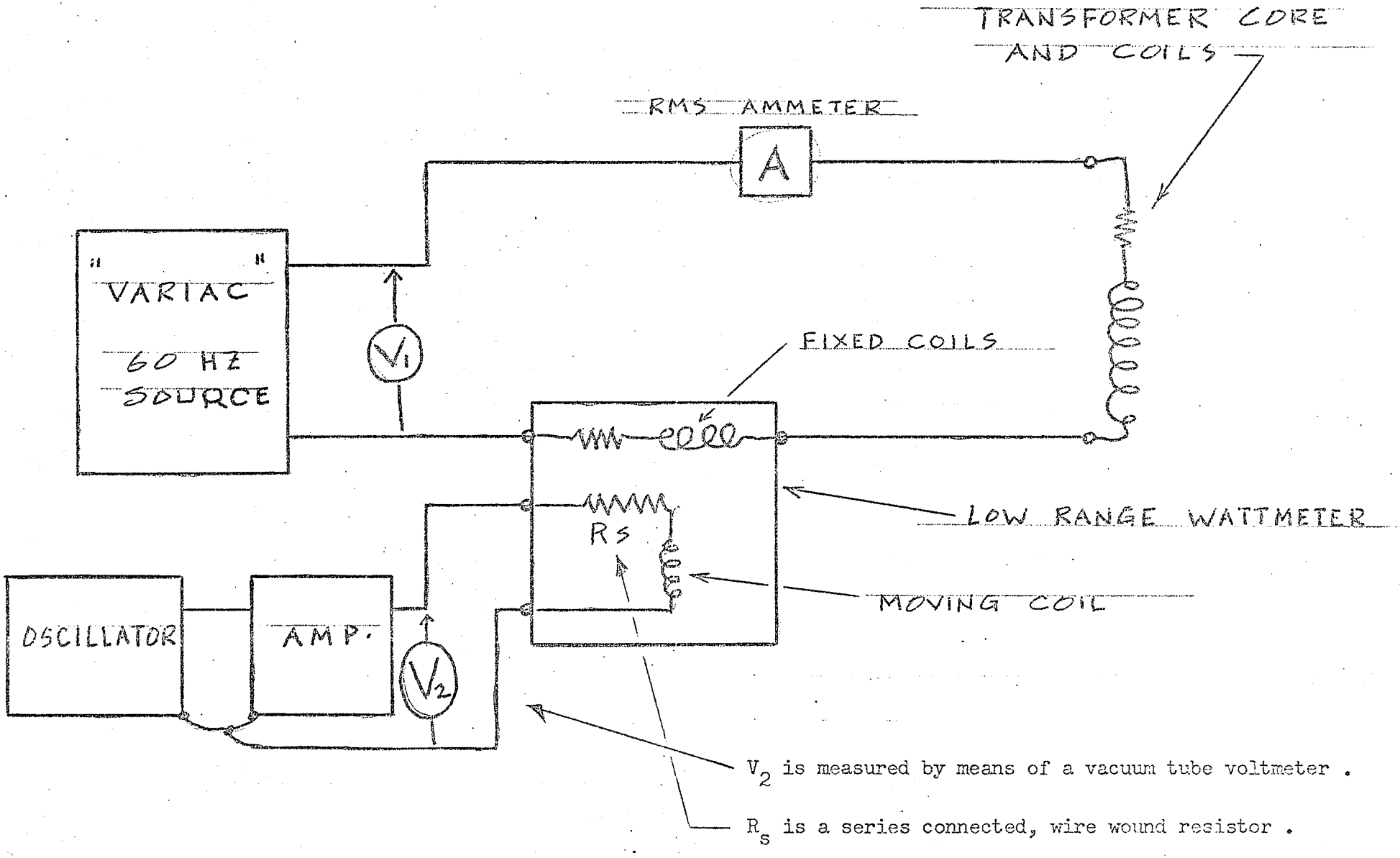

FIGURE A.I

CIRCUIT FOR DETERMINING HARMONIC COMPONENTS OF A TRANSFORMERS EXCITATION CURRENT .

resistance is stated (on the dial) to be 5672.4Ω, for the scale used. For the seventh harmonic, for example, the inductive reactance of the voltage circuit would be $7 \times 377 \times .022 = 58\Omega$, and the voltage circuit impedance would be 5672.4 + j 58 ohms. In other words, negligible error is expected from this source.

Mutual inductance between the fixed and moving coils causes an error in indication which increases linearly with frequency. Since the voltage and current coils are coupled, an electromotive force is induced in each coil due to current flow in the other. In commercial wattmeters, the error due to mutual inductance at 60 hz is so small that a linear extrapolation to 420 hz will result in a negligible error.

Eddy currents can be induced in metal coil supports, in metallic shielding arrangements, or in the wires of the windings themselves, especially if solid wire is employed. For example, in the current coil, the flux produced by load current flow produces eddy currents which themselves create a component of flux lagging the "main" flux, and affecting the resultant angle between fields which react to cause deflection. The error due to eddy current losses increases with the square of the frequency. This error could become important at low power factors, but, as the meter is read at maximum deflection in this case, that is, at that point in time when the angle between current in the voltage coil and load current is zero, it is felt that eddy current errors can be disregarded.

When total RMS current is computed from the harmonic components, it is found that the result is very close to the magnetization data, for high, as well as low current values.

APPENDIX B

DETERMINATION OF DYNAMIC B-H CURVES USING AN OPERATIONAL AMPLIFIER TECHNIQUE.

Figure B.1 shows the equipment and connections necessary to display the B-H curves. That the voltage applied to the horizontal system of the CRO is proportional to 'H' can be shown with the following equations:

$$e_H = R\,i$$

$$H = \frac{Ni}{L} \quad \text{so} \quad i = H\,L\,/\,N$$

$$\therefore \quad e_H = (R\,L\,/\,N)\,H$$

Similarly, the proportionality between e_V and 'B' is shown thusly:

$$e_V = k \int e_S \, dt$$

Since the sample is a 1:1 transformer, the sample applied voltage also equals e_S. But:

$$e_S = N(d\phi/dt)$$

$$\phi = B \times A \quad \therefore \quad d\phi/dt = A\,\frac{dB}{dt}$$

$$\therefore \quad e_S = NA\,(dB/dt)$$

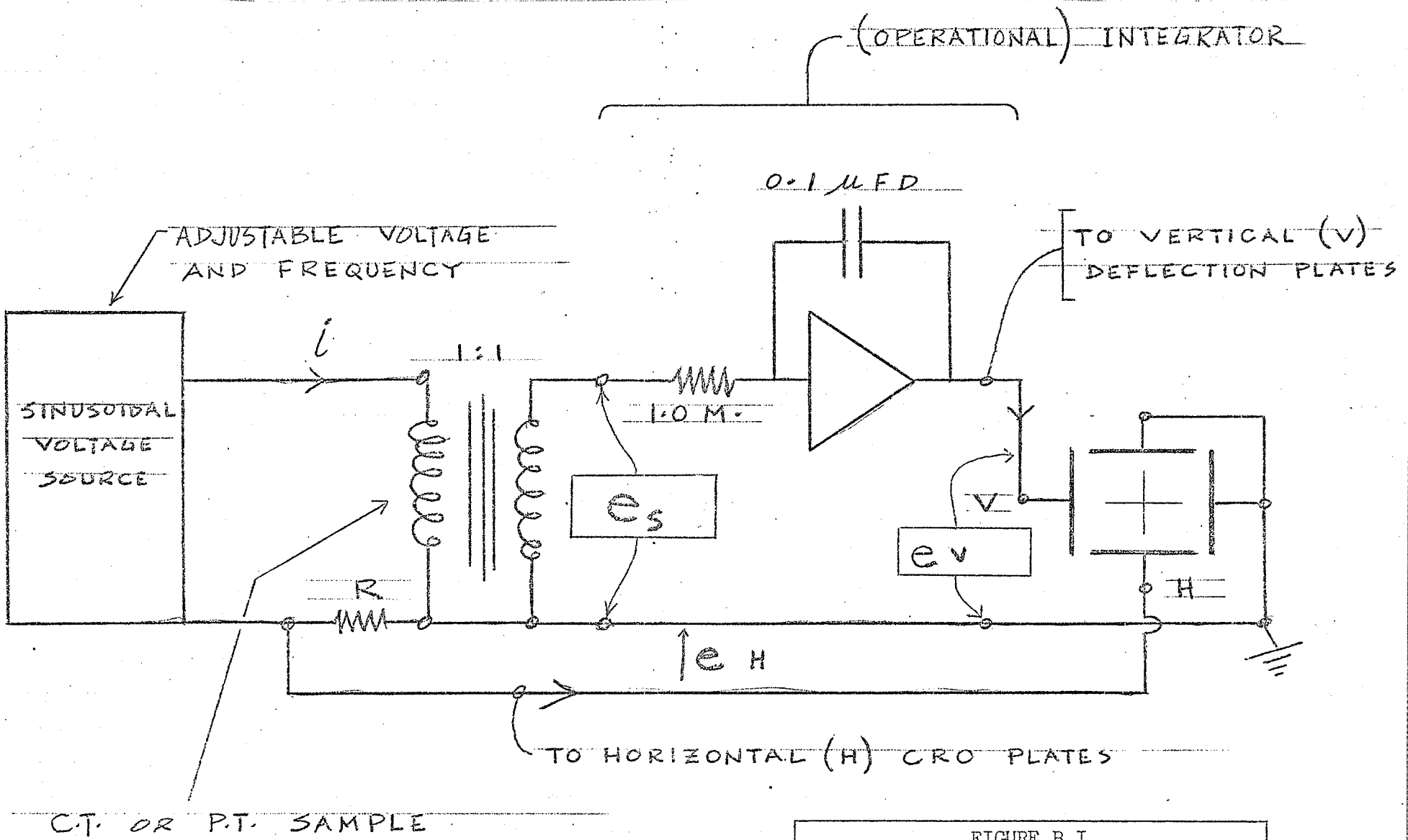

FIGURE B.I

CIRCUITRY NECESSARY TO DISPLAY THE B-H CURVES FOR A TRANSFORMER .

and $$\int e_S \, dt = NAB$$

so $$e_V = (k\,NA)B;$$ where terms are defined as follows:

e_H = voltage applied to horizontal CRO plates

e_V = voltage applied to vertical CRO plates

R = series primary resistor = .81Ω

i = transformer excitation current

H = magnetic field intensity , L = mean length of magnetic circuit

N = number of transformer turns

B = flux density in the core

e_S = sample applied voltage (sinusoidal)

A = net iron cross sectional area

ϕ = flux in the sample core.

It may be apparent that the horizontal and vertical sensitivities of the CRO should be accurately known in order to interpret photographs of the trace. The resistor R should be as small as possible compared with the sample impedance on open circuit. The operational amplifier input resistance must be high to prevent any reflected load component from appearing in the sample primary, thus creating errors in the B-H curve.

The operational amplifier used in tests was modified, in the integrator mode, by a low frequency rejection circuit shown in Figure B.2. This is necessary since normal amplifier drift will also be integrated, forcing the display off the CRO screen. With the network R1, R2, and C1, low frequency changes at the output are fed back to the grid of the input tube, forcing restoration of the trace position on the CRO.

Since some photographic measurements of the B-H curve were done

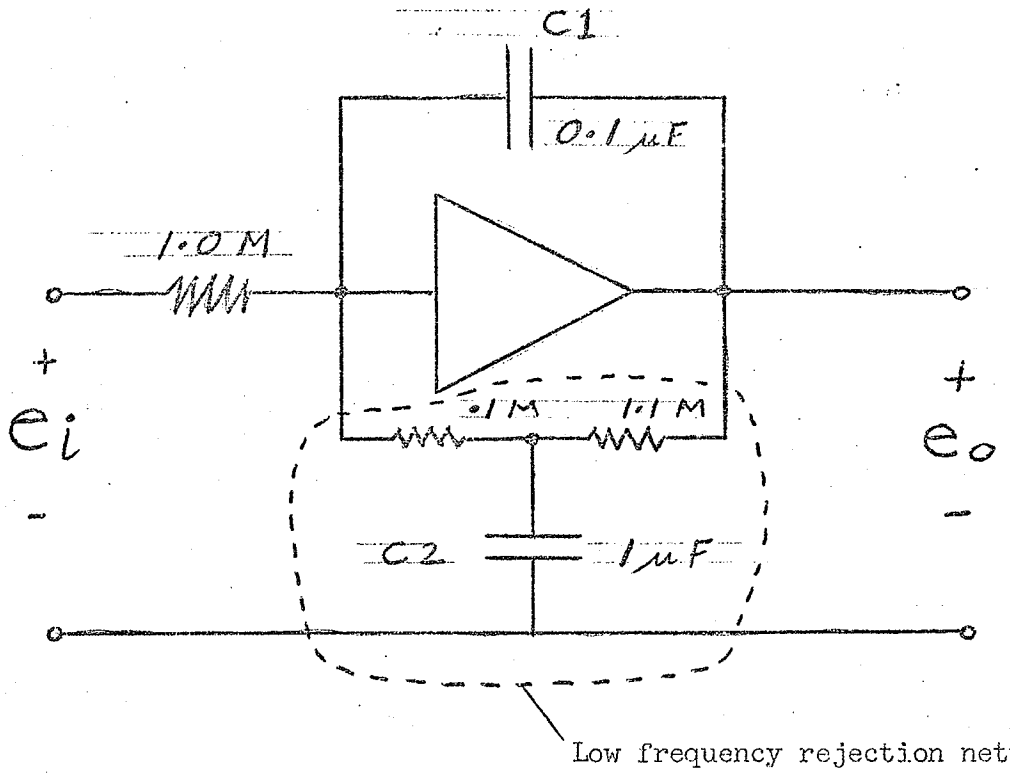

FIGURE B. 2

MODIFIED OPERATIONAL AMPLIFIER NETWORK ,
SHOWING THE INTEGRATOR AND THE LF REJECTION CIRCUIT.

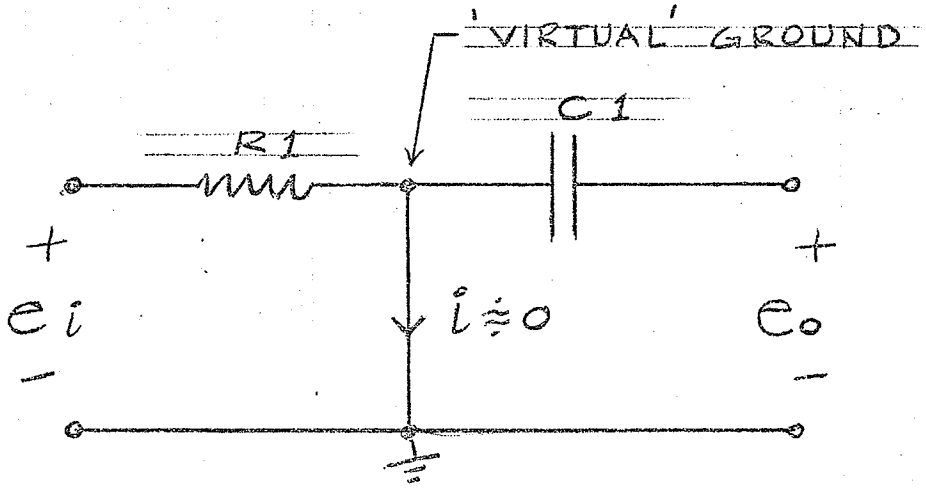

FIGURE B.3

EQUIVALENT CIRCUIT FOR AN UNMODIFIED
OPERATIONAL INTEGRATOR

at 3 hz, it became necessary to determine the low frequency response of the modified integrator.

Figure B.3 is an equivalent circuit for an unmodified integrator using an operational amplifier. The "virtual ground" concept was found especially useful for the more complicated network shown in Figure B.4, that is, all of the input voltage e_i is dropped across R1. For this circuit, $e_o/e_i = 1/s\ R1\ C1$, where 's' is the Laplacian operator.

Figure B.4 shows the first step in the evaluation of the transfer function (the ratio e_o/e_i) for the modified integrator network shown in Figure B.2. A "wye-delta" transformation is performed on the network R2 - C2 - R3. In the resulting delta network, we are concerned only with Z_c, since Z_b is paralleled with a virtual short, and Z_a is across the output, as well as a high impedance amplifier load not shown. Referring to Figure B.5, Z_T is $Z_c // C1$, and $i_1 \times Z_T = e_o$. Since $e_i = i_1\ R1$, $e_o/Z_T = i_1 = e_i/R1$; thus $e_o/e_i = Z_T/R1$. It remains now to evaluate Z_T. In the Laplacian domain,

$$Z_T = \frac{z_C \times 1/s\ C_1}{z_C + (1/s\ C_1)} = \frac{z_C}{1 + sC_1\ z_C}$$

In the wye-delta transformation,

$$z_C = \frac{R2\ R3 + \frac{R2}{s\ C_2} + \frac{R3}{s\ C_2}}{1/s\ C_2}$$

$$z_C = s\ C_2\ R2\ R3 + R2 + R3$$

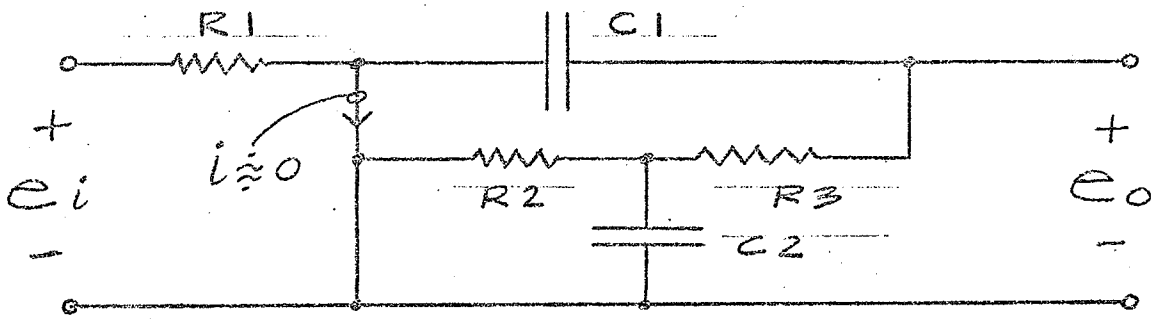

The first step in the evaluation of the network transfer function .

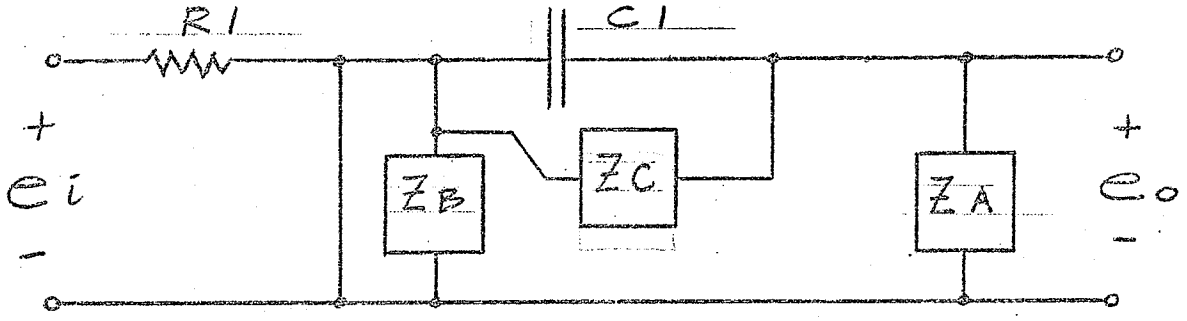

The above network after a WYE - DELTA transformation has been performed

FIGURE B.4

STEPS IN THE EVALUATION OF THE TRANSFER FUNCTION

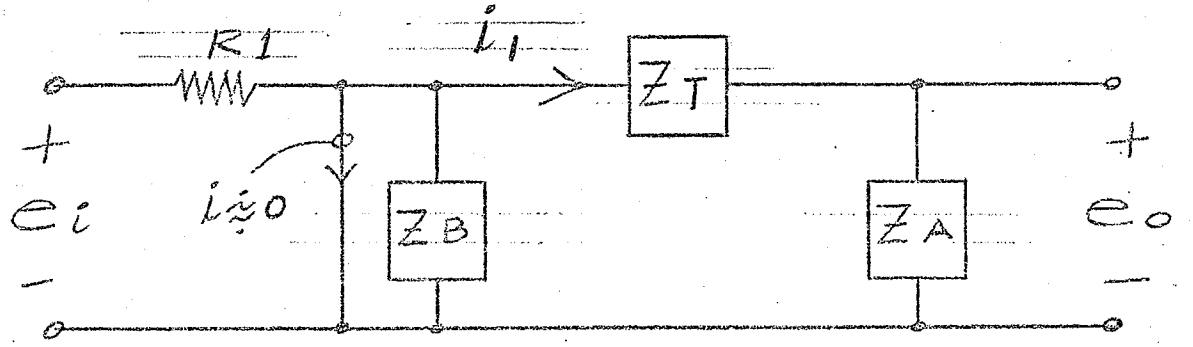

FIGURE B.5

FURTHER STEPS IN THE EVALUATION OF THE TRANSFER FUNCTION

Thus, $e_o/e_i = z_C/(R1 + sC_1 R1 z_C)$

$$= \frac{s C_2 R2 R3 + R2 + R3}{R1 + s^2(R1C_1 R2C_2 R3) + sC_1R1 (R2 + R3)}$$

In Figure B.6 are shown frequency response curves for the unmodified, and the modified integrator circuits, in the range 1 to 10 hz. It is to be noted that the circuit modifications have no effect above about 6 hz. In photos of B-H curves for various frequencies, even if the maximum flux density is carefully held constant, photos taken at 3 hz will appear vertically larger than those shot at 60 hz. In fact, the error introduced by this circuit characteristic in Figures 19 and 20 is not a large one.

It should also be mentioned that a good agreement was found to exist between the computed curves shown in figure B.6 and the actual frequency response tests for this circuitry.

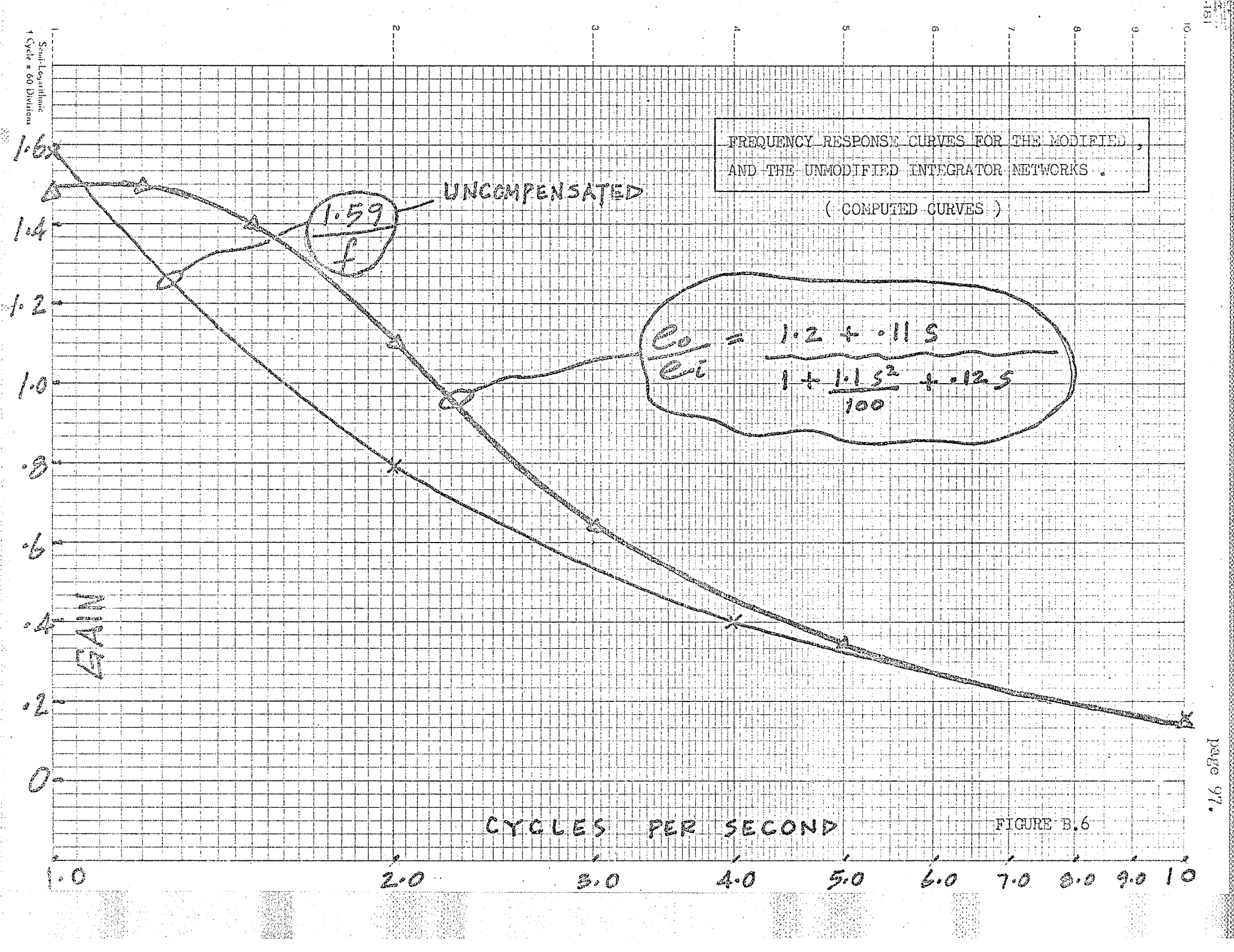
Semi-Logarithmic
1 Cycle x 60 Divisions
FREQUENCY RESPONSE CURVES FOR THE MODIFIED,
AND THE UNMODIFIED INTEGRATOR NETWORKS.
(COMPUTED CURVES)
UNCOMPENSATED
1.59
f
Eo/Ei = 1.2 + .11 S
1 + 1.1 S² + .12 S
100
Eo/Ei
CYCLES PER SECOND
1.0
2.0
3.0
4.0
5.0
6.0
7.0
8.0
9.0
10
1.6
1.4
1.2
1.0
.8
.6
.4
.2
0

FIGURE B.6

APPENDIX C

FOURIER ANALYSIS OF POWERS OF THE COMMON TRIGONOMETRIC FUNCTIONS, IN TABLE FORM

$$\cos x = \cos x$$

$$\cos^2 x = \left(\frac{1}{2}\right) + \left(\frac{1}{2}\right) \cos 2x$$

$$\cos^3 x = \left(\frac{3}{4}\right) \cos x + \left(\frac{1}{4}\right) \cos 3x$$

$$\cos^4 x = \left(\frac{3}{8}\right) + \left(\frac{1}{2}\right) \cos 2x + \left(\frac{1}{8}\right) \cos 4x$$

$$\cos^5 x = \left(\frac{5}{8}\right) \cos x + \left(\frac{5}{16}\right) \cos 3x + \left(\frac{1}{16}\right) \cos 5x$$

$$\cos^6 x = \left(\frac{10}{32}\right) + \left(\frac{15}{32}\right) \cos 2x + \frac{6}{32} \cos 4x + \frac{1}{32} \cos 6x$$

$$\cos^7 x = \frac{35}{64} \cos x + \frac{21}{64} \cos 3x + \frac{7}{64} \cos 5x + \frac{1}{64} \cos 7x$$

Now for the sine function

$$\sin x = \sin x$$

$$\sin^2 x = \left(\frac{1}{2}\right) - \left(\frac{1}{2}\right) \cos 2x$$

$$\sin^3 x = \left(\frac{3}{4}\right) \sin x - \left(\frac{1}{4}\right) \sin 3x$$

$$\sin^4 x = \left(\frac{3}{8}\right) - \left(\frac{1}{2}\right) \cos 2x + \left(\frac{1}{8}\right) \cos 4x$$

$$\sin^5 x = \left(\frac{5}{8}\right) \sin x - \left(\frac{5}{16}\right) \sin 3x + \left(\frac{1}{16}\right) \sin 5x$$

$$\sin^6 x = \left(\frac{10}{32}\right) - \left(\frac{15}{32}\right) \cos 2x + \left(\frac{6}{32}\right) \cos 4x - \left(\frac{1}{32}\right) \cos 6x$$

$$\sin^7 x = \left(\frac{35}{64}\right) \sin x - \left(\frac{21}{64}\right) \sin 3x + \left(\frac{7}{64}\right) \sin 5x - \left(\frac{1}{64}\right) \sin 7x$$

Any power of the cosine function can be generated from any previous power by using the relationship

$$\cos(nx)\cos(x) = \frac{1}{2}[\cos(n+1)x + \cos(n-1)x]$$

For example:

$$\cos^2 x = \cos(x)\cos(x) \ldots n=1$$

$$= \frac{1}{2}[\cos 2x + \cos 0\, x]$$

$$= \frac{1}{2}\cos 2x + \frac{1}{2}$$

Thus,

$$\cos^3 x = \cos^2 x \cos x$$

$$= \frac{1}{2}\cos 2x \cos x + \frac{1}{2}\cos x$$

$$= \frac{1}{2} \times \frac{1}{2}[\cos 3x + \cos x] + \frac{1}{2}\cos x$$

$$= \frac{1}{4}\cos 3x + \frac{1}{4}\cos x + \frac{1}{2}\cos x$$

$$= \frac{1}{4}\cos 3x + \frac{3}{4}\cos x$$

Similar techniques can be applied for the sine function. The constants multiplying each term are known as "Fourier Coefficients".

APPENDIX D

INVERSION OF THE INCREMENTAL DESCRIBING FUNCTION

It has been shown that the IDF arising from the polynomial representation of the nonlinear element (the i/ℓ relationship) has the form:

$$K_e = A + B\, e^{j\,2\,\phi}$$

This relationship is shown in Figure D.1. K_e is a vector whose tip lies on the circumference of a circle, the centre of which is A units from the origin and with a radius = B units. The stability criterion depends upon plotting $1/K_e$ as ϕ varies.

It will be considered to be axiomatic that the inversion of a circle in the 'z' plane results in a circle on the 'w' plane. With this in mind, two points on the diameter of the 'w' plane circle will be located, thus establishing the size of the circle. In Figure D.1, point x_2 is given by $(A + B)\underline{/0^\circ}$, and this point becomes u_1 in the 'w' plane, since, by definition, $W = 1 / Z$ in figure D.2.

$$u_1 = \left(\frac{1}{A + B} \right) \underline{/0^\circ}$$

Similarly, $x_1 = (A - B)\underline{/0^\circ}$ inverts to

$$u_2 = \left(\frac{1}{A - B} \right) \underline{/0^\circ}$$

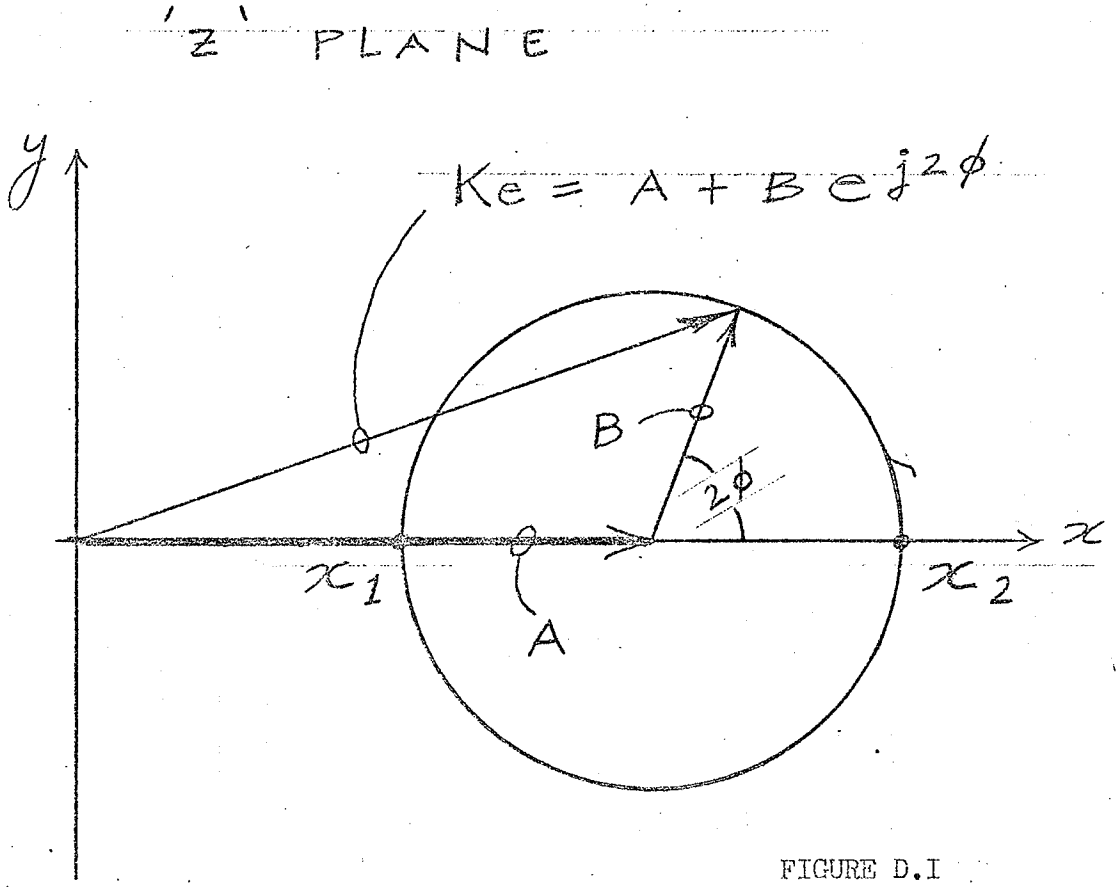

FIGURE D.1

LOCUS OF K_e IN THE 'Z' PLANE

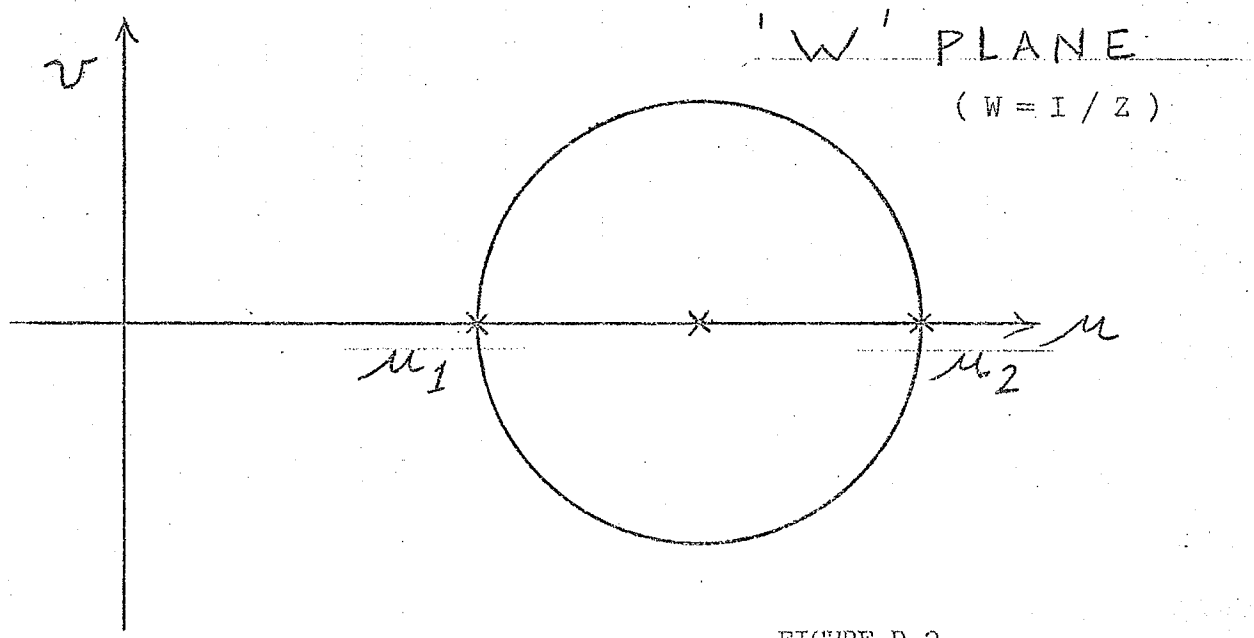

FIGURE D.2

LOCUS OF THE INVERSION OF K_e IN THE 'W' PLANE .

Thus, the 'w' plane circle centre is

$$(u_2 + u_1)/2 = \left[\frac{1}{A + B} + \frac{1}{A - B} \right] \left(\frac{1}{2} \right) = \frac{A}{A^2 - B^2}$$

Also, the radius of this circle is

$$\frac{u_2 - u_1}{2} = \frac{1}{2} \left[\frac{1}{A - B} - \frac{1}{A + B} \right]$$

$$= \frac{1}{2} \left[\frac{A + B - A + B}{A^2 - B^2} \right] = B/A^2 - B^2$$

Finally, $-1/K_e$ has its centre at $A/B^2 - A^2$, with a radius of

$$\left| B/B^2 - A^2 \right|$$

BIBLIOGRAPHY

1) Mathews , Paul ; Protective Current Transformers and Circuits ; Chapman and Hall Ltd ; 1955 ; pp 21 - 39 .

2) Hughes , W.L. ; Nonlinear Electrical Networks ; Ronald Press ; 1960 , pp 68 - 80 .

3) Blume , L.F. ; Transformer Engineering ; Wiley ; 1951 ; pp 20 - 34

4) Mueller , G.V. ; Alternating Current Machines ; McGraw - Hill ; 1952 ; pp 1 - 34 .

5) Rudenberg , R . ; Transient Performance of Electric Power Systems ; McGraw - Hill ; 1950 ; pp 630 - 645 .

6) Swift , G.W. ; An Analytical Approach to Ferroresonance ; IEEE paper 68 - TP - 678 .

7) Shenkman , L.Z. ; Subharmonic Oscillation In A Circuit With an Essentially Non - Linear Inductance ; Electrichestvo ; No 10 ; 23 - 28 , 1967 ; pp 1 - 5.

8) Wright, I, and Morsztyn ; An Improved Method of Simulating The Transient Performance of Power System Transformers ; Journal of Engineering Education , vol. 6 ; p 499 .

9) Harris , F.K. ; Electrical Measurements ; John Wiley and Sons ; 1952 ; pp 400 - 418 .

10) Swift , G.W. ; Transformer Core Simulation In Ferroresonance Studies ; Ph. D. Dissertation ; 1967 ; Illinois Institute of Technology .

II) Turley , S.Q. ; Ferroresonance Oversimplified ; Transmission and Distribution ; Oct. I966 .

I2) Plotkin , S . ; Discontinuous Transition Time Between Stable States In Ferroresonant Circuits ; AIEE Trans. I957 , Vol. 76 , part I ; pp 4I0 - 4I6 .

I3) Kelly , G.E. ; The Ferroresonant Circuit ; AIEE Trans . I958 , Vol. 77 , part I ; pp 843 - 846 .

I4) Brenner , E. ; Subharmonic Response of The Ferroresonant Circuit With Coil Hysteresis ; AIEE Trans. I956 , Vol. 75 , part I ; pp 450 - 5.

I5) Thompson , W.T. ; Similitude of Critical Conditions In Ferroresonant Circuits. ; AIEE Trans. I939 , Vol. 58 ; pp I27 - I35 .

I6) Richardson , F.and Falkowski ; Relation of AC Losses to Hysteresis Losses In Electric Sheet Steels ; IEEE Trans, September I967 , pp I072 - I077 .

I7) Hale , J.W. and Richardson , F.R. ; Mathematical Descriptions of Core Losses ; AIEE Trans. I953 , Vol. 72 , part I ; pp 945 - 498 .

I8) Duckworth , H.E. ; Electricity and Magnetism ; Holt , Rinehart and Winston ; I960 , Chapter I0 .

I9) West, J.C. ; Douce, J.L. ; and Livesley , R.K. : The dual input describing function and its use in the analysis of non - linear feedback systems ; Proc. IEE , Vol. I03 B , pp 463 - 472 , I956 .